

## INFORMATION TO USERS

This material was produced from a microfilm copy of the original document. While the most advanced technological means to photograph and reproduce this document have been used, the quality is heavily dependent upon the quality of the original submitted.

The following explanation of techniques is provided to help you understand markings or patterns which may appear on this reproduction.

1. The sign or "target" for pages apparently lacking from the document photographed is "Missing Page(s)". If it was possible to obtain the missing page(s) or section, they are spliced into the film along with adjacent pages. This may have necessitated cutting thru an image and duplicating adjacent pages to insure you complete continuity.
2. When an image on the film is obliterated with a large round black mark, it is an indication that the photographer suspected that the copy may have moved during exposure and thus cause a blurred image. You will find a good image of the page in the adjacent frame.
3. When a map, drawing or chart, etc., was part of the material being photographed the photographer followed a definite method in "sectioning" the material. It is customary to begin photoing at the upper left hand corner of a large sheet and to continue photoing from left to right in equal sections with a small overlap. If necessary, sectioning is continued again -- beginning below the first row and continuing on until complete.
4. The majority of users indicate that the textual content is of greatest value, however, a somewhat higher quality reproduction could be made from "photographs" if essential to the understanding of the dissertation. Silver prints of "photographs" may be ordered at additional charge by writing the Order Department, giving the catalog number, title, author and specific pages you wish reproduced.
5. PLEASE NOTE: Some pages may have indistinct print. Filmed as received.

**University Microfilms International**

300 North Zeeb Road  
Ann Arbor, Michigan 48106 USA  
St. John's Road, Tyler's Green  
High Wycombe, Bucks, England HP10 8HR

77-4990

BUCK, Warren Wesley, III, 1946-  
CALCULATION OF DEUTERON WAVE FUNCTIONS  
WITH RELATIVISTIC INTERACTIONS.

The College of William and Mary in Virginia,  
Ph.D., 1976  
Physics, nuclear

**Xerox University Microfilms**, Ann Arbor, Michigan 48106

CALCULATION OF DEUTERON WAVE FUNCTIONS  
WITH RELATIVISTIC INTERACTIONS

---

A Dissertation

Presented to

The Faculty of the Department of Physics  
The College of William and Mary in Virginia

In Partial Fulfillment  
Of the Requirements for the Degree of  
Doctor of Philosophy

---

by

Warren Wesley Buck, III

May 1976

APPROVAL SHEET

This dissertation is submitted in partial fulfillment of  
the requirements for the degree of

Doctor of Philosophy

Warren Wesley Buck, III  
Warren Wesley Buck, III

Approved, May 1976

Franz L. Gross  
Franz L. Gross

Carl E. Carlson  
Carl E. Carlson

Charles F. Perdrisat  
Charles F. Perdrisat

Hans C. von Baeyer  
Hans C. von Baeyer

William G. Poole  
William G. Poole  
Department of Mathematics

DEDICATION

To my friends, and to my parents and grandparents.

TABLE OF CONTENTS

DEDICATION . . . . .	iii
ACKNOWLEDGMENTS . . . . .	v
LIST OF TABLES . . . . .	vi
LIST OF FIGURES . . . . .	vii
ABSTRACT . . . . .	x
I. INTRODUCTION . . . . .	2
II. THE WAVE EQUATION . . . . .	6
III. THE RELATIVISTIC INTERACTIONS . . . . .	12
IV. WAVE FUNCTIONS AND OTHER NUMERICAL RESULTS . . . . .	23
V. N-d SCATTERING AT $180^\circ$ . . . . .	65
VI. SUMMARY . . . . .	71
APPENDIX	
A. . . . .	73
B. . . . .	79
C. . . . .	81
D. . . . .	84
REFERENCES . . . . .	91

## ACKNOWLEDGMENTS

I express deep appreciation to Professor Franz L. Gross for his support, encouragement, and insights both as my friend and as my advisor during the entire course of this work. It was my good fortune to have had the opportunity to interact with him.

Discussions with Professors Carl E. Carlson, E. A. Remler, Charles Perdrisat, and my colleagues Etienne Delacroix, John Hornstein, and Mary Vislay are gratefully acknowledged.

I wish to thank both Deborah Damon for an excellent job of typing this manuscript and for enduring the deadlines, and Michael J. Schmidt for doing most of the drafting.

The William and Mary Computer Center is gratefully acknowledged, for without their understanding and assistance this work would have never been completed.

I wish to thank my friends, to whom this work is partially dedicated, for their years of patience and insights, particularly Linda A. Horn, who has touched me significantly.

Finally, I owe a great deal to my parents and grandparents for their undying support and their ability to withstand my often controversial decisions.

Thank you all.

LIST OF TABLES

Table	Page
1. Data for all solutions obtained; $P_D$ is the D state probability, $P_t$ and $P_s$ are the triplet P and singlet P state probabilities respectively; Q, the quadrupole moment, and $M_d$ , the magnetic moment, are measured in units of $e/M_d^2$ and nuclear magnetons respectively. The values of the mixing parameters, $\lambda_4$ , $\lambda_3$ , and $\lambda_\omega$ correspond to $M_R$ 's of 4M, 3M and $M_\omega$ (omega mass) respectively . . . . .	28
2. The normalized dimensionless coefficients $C_{ji}$ for the $\lambda_4 = 1$ interaction . . . . .	50
3. The normalized dimensionless coefficients $C_{ji}$ for the $\lambda_3 = 1$ interaction . . . . .	51
4. The normalized dimensionless coefficients $C_{ji}$ for the $\lambda_3 = .9$ interaction . . . . .	52
5. The normalized dimensionless coefficients $C_{ji}$ for the $\lambda_3 = .6$ interaction . . . . .	53
6. The normalized dimensionless coefficients $C_{ji}$ for the $\lambda_\omega = 1$ interaction . . . . .	54
7. The normalized dimensionless coefficients $C_{ji}$ for the $\lambda_\omega = .8$ interaction . . . . .	55
8. The normalized dimensionless coefficients $C_{ji}$ for the $\lambda_\omega = 0$ interaction . . . . .	56

LIST OF FIGURES

Figure	Page
1. . . . .	7
2. . . . .	12
3. . . . .	13
4. S and D state wave functions (labeled u and w respectively) for $\lambda_3 = 1$ displayed at short distances. The Reid hard and soft core wave functions are shown for comparison . . . . .	29
5. The four relativistic deuteron wave functions for $\lambda_3 = 1$ . The small circles are values of Reid's u and w shown for comparison . . .	31
6. The four relativistic deuteron wave functions for $\lambda_3 = .9$ . . . . .	32
7. The four relativistic deuteron wave functions for $\lambda_3 = .6$ . . . . .	33
8. The quadrupole moment of the deuteron, Q, versus the sigma mass for fixed values of $\lambda_3$ as indicated on each curve. The dotted line is the experimental value for Q . . . .	34
9. The four relativistic deuteron wave functions for $\lambda_\omega = 1$ . . . . .	37
10. The four relativistic deuteron wave functions for $\lambda_\omega = .8$ . . . . .	38
11. The four relativistic deuteron wave functions for $\lambda_\omega = 0$ . . . . .	39
12. The quadrupole moment of the deuteron, Q, versus the sigma mass for fixed values of $\lambda_\omega$ as indicated on each curve . . . . .	40

13.	The short range structure of $u$ for $\lambda_3 = 1, .9, \text{ and } .6$ . . . . .	41
14.	Overall view of $v_t$ for $\lambda_w = 1, .8, \text{ and } 0$ . . . . .	43
15.	The momentum space S state wave functions, $u$ , for $\lambda_3 = 1, .9, \text{ and } .6$ . The right most curves are to be read from the right scale . . . . .	44
16.	The momentum space D state wave functions, $w$ , for $\lambda_3 = 1, .9, \text{ and } .6$ . . . . .	45
17.	The momentum space P state wave functions, $v_t$ and $v_s$ , for $\lambda_3 = 1, .9, \text{ and } .6$ . . . . .	46
18.	The momentum space S state wave functions, $u$ , for $\lambda_w = 1, .8, \text{ and } 0$ . The right most curves are to be read from the right scale. . . . .	47
19.	The momentum space D state wave functions, $w$ , for $\lambda_w = 1, .8, \text{ and } 0$ . . . . .	48
20.	The momentum space P state wave functions, $v_t$ and $v_s$ , for $\lambda_w = 1, .8, \text{ and } 0$ . . . . .	49
21.	The dimensionless momentum space invariant amplitude, $F$ , for $\lambda_3 = 1, .9, \text{ and } .6$ . . . . .	57
22.	The dimensionless momentum space invariant amplitude, $G$ , for $\lambda_3 = 1, .9, \text{ and } .6$ . The right most curves are to be read from the right scale . . . . .	58
23.	The dimensionless momentum space invariant amplitude, $H$ , for $\lambda_3 = 1, .9, \text{ and } .6$ . . . . .	59
24.	The dimensionless momentum space invariant amplitude, $I$ , for $\lambda_3 = 1, .9, \text{ and } .6$ . . . . .	60
25.	The dimensionless momentum space invariant amplitude, $F$ , for $\lambda_w = 1, .8, \text{ and } 0$ . . . . .	61

26.	The dimensionless momentum space invariant amplitude, G, for $\lambda_\omega = 1, .8,$ and 0. The right most curve is to be read from the right scale . . . . .	62
27.	The dimensionless momentum space invariant amplitude, H, for $\lambda_\omega = 1, .8,$ and 0 . . . . .	63
28.	The dimensionless momentum space invariant amplitude, I, for $\lambda_\omega = 1, .8,$ and 0 . . . . .	64
29.	. . . . .	65
30.	The ONE contribution to the differential cross section for N-d scattering at $180^\circ$ with and without $(v_t = v_s = 0), NR,$ the P states for $\lambda_3$ wave functions. The experimental data is found in reference 24 . . . . .	67
31.	The ONE contribution to the differential cross section for N-d scattering at $180^\circ$ with and without $(v_t = v_s = 0), NR,$ the P states for $\lambda_\omega$ wave functions. The experimental data is found in reference 24 . . . . .	68
32.	The ONE contribution to the differential cross section with Q (dashed curves) and P/2 (solid curves) as the arguments of the $\lambda_3 = .6$ wave functions. The data is the same as in figures 30 and 31 . . . . .	70

## ABSTRACT

Deuteron wave functions with a repulsive core are obtained numerically from a fully relativistic wave equation introduced by Gross. The numerical technique enables analytic solutions for classes of interactions composed of the relativistic exchanges of a single pion and a single phenomenological meson, sigma. The pion is chosen to interact as a mixture of pseudoscalar and pseudovector. The amount of mixture is determined by a free mixing parameter,  $\lambda$ , ranging between 1 (pure pseudoscalar) and 0 (pure pseudovector). Each value of  $\lambda$  corresponds, then, to a different interaction. Solutions are found for  $\lambda = 1, .9, .8, .6,$  and 0.

The wave functions for each interaction come in a group of four. Of the four wave functions, two are the usual S and D state wave functions, while the remaining two, arising out of the relativistic prescription, are identified as  $^3P_1$  and  $^1P_1$  wave functions (P state wave functions).

For the interactions solved for, the D state probabilities ranged between 5.1 percent and 6.3 percent, while the total P state probabilities ranged between 0.7 percent and 2.7 percent.

The method of obtaining solutions was to adjust the sigma meson parameters to give the correct binding energy and a good quadrupole moment.

All wave functions obtained are applied to relativistic N-d scattering in the backward direction where the effect of the P states is quite measurable.

CALCULATION OF DEUTERON WAVE FUNCTIONS  
WITH RELATIVISTIC INTERACTIONS

## I. INTRODUCTION

This thesis presents new sets of deuteron wave functions obtained by solving a relativistic wave equation.<sup>1</sup> Each set is composed of four wave functions:

1.  $u$ , the S state wave function
2.  $w$ , the D state wave function
3.  $v_t$ , the triplet P state wave function
4.  $v_s$ , the singlet P state wave function

Of these four wave functions, only  $u$  and  $w$  appear in the usual non-relativistic theories. Non-relativistic wave functions have been obtained by many people. We will compare our results with those of Reid.<sup>2</sup> His  $u$  and  $w$ , which correspond to non-relativistic representations of upper component Dirac wave functions, were the result of solving coupled Schrodinger Equations with potentials that were fit to N-N phase shift data. His analysis did not include the P states,  $v_t$  and  $v_s$ , which are smaller than  $u$  and  $w$  by one order of  $v/c$ , and which correspond to the two additional degrees of freedom of a Dirac particle contained in the lower component wave functions. Furthermore, the overall parity of our P states is the same as for our S and D states in analogy with the Dirac upper and lower component wave functions for the Hydrogen atom.

The P states were first obtained in a semi-relativistic calculation by Hornstein and Gross.<sup>3</sup> The identification of  $v_t$  and  $v_s$  as P states is discussed in Section II. This calculation obtained  $v_t$  and  $v_s$  through the use of an iteration process using the Reid u and w as generators.

In contrast to the above calculations, we calculate, using the three-dimensional wave equation appearing in Section II, all four wave functions numerically from exact relativistic interactions involving a one pion exchange and the exchange of a phenomenological spin-isospin scalar meson, sigma.

To compare with the semi-relativistic model mentioned above, we considered the pion interaction to be a mixture of pseudoscalar ( $\gamma^5$ ) and pseudovector ( $\gamma^\mu \gamma^5$ ) and found solutions for several values of the mixture parameter,  $\lambda$ , ranging between  $\lambda = 1$  (pure  $\gamma^5$ ) and  $\lambda = 0$  (pure  $\gamma^\mu \gamma^5$ ).

The wave functions, u, w,  $v_t$ , and  $v_s$ , were obtained through their relationships with the invariant amplitudes, appearing in the d-NN vertex function, which is tailored to the deuteron's spin channel. The criteria for good solutions were to fit the deuteron's binding energy, B, taken to be 2.22466 MeV, and produce a non-relativistic quadrupole moment, Q, near the experimental value of  $25.5 e/M_d^2$ .

To get the values of the binding energy and quadrupole moment

listed above, the phenomenological mass of the sigma,  $M_\sigma$ , and coupling constant,  $g_\sigma^2/4\pi$ , were adjusted.

Once the solutions were obtained, two deuteron processes were calculated to get a feel for the significance of these new wave functions:

1. pionic disintegration of the deuteron ( $\pi d \rightarrow NN$ )
2. N-d scattering at  $180^\circ$

The first process,  $\pi d \rightarrow NN$ , calculated by E. Delacroix and F. Gross<sup>4</sup>, which is not contained in this manuscript, gives a cross section compatible with the data near threshold which is remarkably higher than previous calculations of the pole term. Delacroix and Gross show that their calculated cross section is very sensitive to  $v_t$  and  $v_s$  (the deuteron's P state wave functions), a fact not known before. Their relativistic calculation of the cross section, with no other mechanisms folded in, shows that relativistic deuteron wave functions have an important effect.

The second process, N-d scattering at  $180^\circ$ , calculated by F. Gross, E. Remler, and this writer,<sup>5</sup> is discussed in Section V. Here, too, we find that the P state wave functions give important contributions to the differential cross section calculated from the one nucleon exchange (ONE). It is pointed out in Section V that other (non-relativistic) attempts to calculate the ONE contribution without other mechanisms have failed.

Good relativistic deuteron wave functions are essential in order to perform calculations in addition to those mentioned above.

It is hoped that the wave functions illustrated in Section IV will give reliable estimates in future calculations.

The examination of other relativistic N-N channels will tell us more about the deuteron's interaction channel and will furnish additional constraints on the choice of interactions. The relativistic triplet N-N scattering phase shifts, important as an additional constraint on our deuteron interactions, can be calculated and at this writing, a program is underway to do just that.

In addition to presenting relativistic deuteron wave functions, this work includes calculations of formulae for Hydrogen-like atoms using our relativistic techniques. These calculations can be found in Appendix D.

## II. THE WAVE EQUATION

We use a three dimensional wave equation to describe the deuteron.<sup>1</sup> The equation is written as:

$$(\vec{r}c)_{\mu\nu}(\vec{q}) = \int \frac{d^3k}{(2\pi)^3} \sum_{\mu\mu', \nu\nu'} G_{\mu\mu', \nu\nu'}(q, k) \gamma_{\mu\mu', \nu\nu'}(k, W) (\vec{r}c)_{\mu''\nu''}(\vec{k}) \quad (1)$$

where the two body Green's Function is

$$G_{12}(k, W) = \frac{[M + \gamma \cdot (\frac{W}{2} + k)]_1 [M + \gamma \cdot (\frac{W}{2} - k)]_2}{2E_k M_d (2E_k - M_d)} \quad (2)$$

and the subscripts 1 and 2 denote the Dirac indices of nucleons 1 ( $\mu\mu''$ ) and 2 ( $\nu\nu''$ ) respectively,<sup>6</sup> where nucleon 1 is on its mass shell and nucleon 2 is off its mass shell so that

$$\left(\frac{W}{2} + q\right)^2 = \left(\frac{W}{2} + k\right)^2 = M^2 \quad (3)$$

$$W = (M_d, \vec{0})$$

$$M_d = \text{mass of deuteron} = 2M + B$$

$$M = \text{nucleon mass} = 936.8 \text{ MeV}$$

$$C = \text{charge conjugation matrix}$$

$$B = \text{deuteron's binding energy} = -2.22466 \text{ MeV} \quad (4)$$

The external nucleon 4-momentum,  $q$ , and the internal nucleon 4-momentum,  $k$ , are defined as:

$$\begin{aligned}
 \delta &= (\delta_0, \vec{\delta}) & \delta_0 &= E_\delta - \frac{M_d}{2} & E_\delta^2 &= M^2 + \vec{\delta}^2 \\
 K &= (K_0, \vec{K}) & K_0 &= E_K - \frac{M_d}{2} & E_K^2 &= M^2 + \vec{K}^2 \\
 \hat{\delta} &= \vec{\delta} / |\vec{\delta}| & \hat{K} &= \vec{K} / |\vec{K}|
 \end{aligned}
 \tag{5}$$

where the interaction kernel,  $\underline{K}$ , is a sum of single particle exchanges, one of which is the pion. The kernel will be discussed in detail in Section III below.

The vertex function of the deuteron,  $\tilde{\Gamma}$ , was first introduced by Blankenbecker and Cook,<sup>7</sup> and for one nucleon on shell and one nucleon off shell takes the form:<sup>8</sup>

$$\tilde{\Gamma}(\delta) = [F - 2H] \gamma_{\hat{\delta}} - \frac{H}{M} \gamma \not{W} - \frac{1}{M} [G - 2H] \delta \cdot \gamma + \frac{I}{M^2} \delta \cdot \gamma \not{W} = \tilde{\Gamma}^M \xi_M \tag{6}$$

where F, G, H, and I are Lorentz invariant amplitudes,  $\xi$  is the deuteron's polarization 4-vector, and the invariants are linearly independent.

In diagrammatic form, equation 1 is:

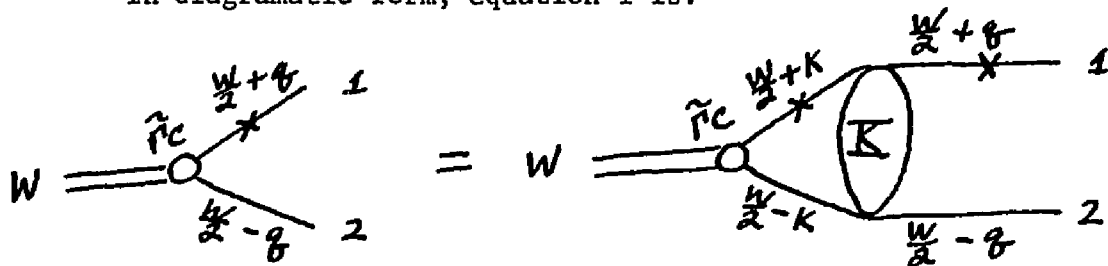


Figure 1

The "x" in figure 1 indicates the on shell nucleon.

If one thinks in terms of the 4-dimensional Bethe-Salpeter Equation,<sup>9</sup> the 3-dimensional nature of equation 1 may be puzzling.

A simple explanation lies in the fourth component integration ( $dK_0$ )

of the Bethe-Salpeter equation.

The Bethe-Salpeter energy denominator (ED) for two propagating internal nucleons is given by:

$$\begin{aligned}
 ED &= [M^2 - (\frac{W}{2} + K)^2 - i\epsilon] [M^2 - (\frac{W}{2} - K)^2 - i\epsilon] \\
 &= (E_K + \frac{M_d}{2} + K_0)(E_K - \frac{M_d}{2} - K_0)(E_K + \frac{M_d}{2} - K_0)(E_K - \frac{M_d}{2} + K_0)
 \end{aligned} \tag{7}$$

The  $K_0$  integration of the Bethe-Salpeter Equation is performed by choosing the pole,  $K_0 = E_K - M_d/2$ , so that the dominant part of the two pion exchange diagram is the first iteration of the one pion exchange diagram.<sup>10</sup> The residue of this pole gives the energy denominator of equation 1:

$$ED = 2E_K M_d (2E_K - M_d) \tag{8}$$

We can define positive ( $\Psi^+$ ) and negative ( $\Psi^-$ ) energy wave functions of the Dirac type, expressible in terms of the d-NN vertex function,  $\tilde{\Gamma}^{1,3}$  as:

$$\Psi_{rs}^+(\vec{q}) = \frac{M}{[2M_d(2\pi)^3]^{1/2}} \frac{\bar{U}_N^{(r)}(\vec{q}) \bar{U}_N^{(s)}(-\vec{q}) (\tilde{\Gamma}^c)_{\mu\nu}(\hat{q})}{E_\delta (2E_\delta - M_d)} \tag{9a}$$

$$\Psi_{rs}^-(\vec{q}) = \frac{-M}{[2M_d(2\pi)^3]^{1/2}} \frac{\bar{U}_N^{(r)}(\vec{q}) \bar{V}_N^{(s)}(-\vec{q}) (\tilde{\Gamma}^c)_{\mu\nu}(\hat{q})}{E_\delta M_d} \tag{9b}$$

where the Dirac spinors,  $\underline{U}$  and  $\underline{V}$ , are defined as:

$$\underline{u}(\vec{q}) = \sqrt{\frac{E_1 + M_1}{2M}} \begin{pmatrix} \chi \\ \frac{\vec{\sigma}_1 \cdot \vec{q}}{E_1 + M_1} \chi \end{pmatrix} \quad \underline{v}(\vec{q}) = \sqrt{\frac{E_2 + M_2}{2M}} \begin{pmatrix} \frac{\vec{\sigma}_2 \cdot \vec{q}}{E_2 + M_2} \chi' \\ \chi' \end{pmatrix} \quad (10)$$

$\chi$  = nucleon spin wave function

Furthermore,  $\Psi^+$  and  $\Psi^-$  can be case into two-component form<sup>3,8,11</sup> and written as:

$$\Psi^+(\vec{q}) = \frac{1}{(2\pi^2)^{1/2}} \left[ u(\vec{q}) - \frac{w(\vec{q})}{\sqrt{3}} (3\vec{\sigma}_1 \cdot \hat{q} \vec{\sigma}_2 \cdot \hat{q} - \vec{\sigma}_1 \cdot \vec{\sigma}_2) \right] \chi_{1M} \quad (11a)$$

$$\Psi^-(\vec{q}) = -\frac{\sqrt{3}}{(2\pi^2)^{1/2}} \left[ \frac{v_t(\vec{q})}{\sqrt{2}} (\vec{\sigma}_1 + \vec{\sigma}_2) \cdot \hat{q} - \frac{v_s(\vec{q})}{2} (\vec{\sigma}_1 - \vec{\sigma}_2) \cdot \hat{q} \right] \chi_{1M} \quad (11b)$$

where  $\chi_{1M}$  are the spin wave functions of two spin 1/2 particles coupled to a spin 1 particle with projection M and where  $\vec{\sigma}_1$  and  $\vec{\sigma}_2$ , the Pauli spin matrices, act on nucleons 1 and 2.

Equation 11b contains the triplet,  $v_t$ , and singlet,  $v_s$ , wave functions which are the coefficients of terms linear in momentum as they should be for P states ( $\ell = 1$ ). In equation 11a,  $u$ , the S state wave function, enters with a term constant in momentum ( $\ell = 0$ ), and the D state wave function,  $w$ , enters with a term quadratic in momentum ( $\ell = 2$ ). A detailed analysis of the spin and angular momentum structure of equations 11, along with how these wave functions behave under the parity operation, has been done by Hornstein.<sup>8</sup>

Using equations 10, one can reduce equations 9 to equations 11. The deviation can be found in reference 8, where relationships connecting the wave functions  $u$ ,  $w$ ,  $v_t$ , and  $v_s$  to the invariant amplitudes  $F$ ,  $G$ ,  $H$ , and  $I$  appearing in equation 6 result. These relationships are:

$$u(\vec{\delta}) = \frac{1}{3\sqrt{4\pi M_d} E_\delta (2E_\delta - M_d)} \left[ \frac{\delta^2}{M} G(\vec{\delta}) + (2E_\delta + M) F(\vec{\delta}) - (2M + E_\delta)(2E_\delta - M_d) \frac{H(\vec{\delta})}{M} \right] \quad (12a)$$

$$w(\vec{\delta}) = \frac{-\sqrt{2}(E_\delta - M)}{2\sqrt{4\pi M_d} E_\delta (2E_\delta - M_d)} \left[ F(\vec{\delta}) - \frac{(E_\delta + M)}{M} G(\vec{\delta}) + (2E_\delta - M_d) \frac{H(\vec{\delta})}{M} \right] \quad (12b)$$

$$v_t(\vec{\delta}) = \frac{|\vec{\delta}|}{\sqrt{4\pi M_d} E_\delta M} \sqrt{\frac{2}{3}} H(\vec{\delta}) \quad (12c)$$

$$v_s(\vec{\delta}) = \frac{-|\vec{\delta}|}{M_d \sqrt{4\pi M_d} E_\delta \sqrt{3}} \left[ F(\vec{\delta}) - G(\vec{\delta}) + \frac{E_\delta M_d}{M^2} I(\vec{\delta}) \right] \quad (12d)$$

normalized so that

$$\frac{2}{\pi} \int \frac{\delta^2 d\vec{\delta}}{\delta} \left[ u^2(\vec{\delta}) + w^2(\vec{\delta}) + v_t^2(\vec{\delta}) + v_s^2(\vec{\delta}) \right] = 1 \quad (13)$$

where  $u$ ,  $w$ ,  $v_t$ , and  $v_s$  correspond to the  $^3S_1$ ,  $^3D_1$ ,  $^3P_1$ ,  $^1P_1$  state wave functions respectively. <sup>1,3,8,11</sup>

Once  $F$ ,  $G$ ,  $H$ , and  $I$  are obtained, equations 12a-d are used to generate the momentum space wave functions.

To obtain the position space wavefunctions, Fourier transform was performed on the momentum space wave functions:

$$\frac{u(r)}{r} = \frac{2}{\pi} \int_0^\infty q^2 dq j_0(qr) u(q) \quad (14a)$$

$$\frac{w(r)}{r} = \frac{2}{\pi} \int_0^\infty q^2 dq j_2(qr) w(q) \quad (14b)$$

$$\frac{v_t(r)}{r} = \frac{2}{\pi} \int_0^\infty q^2 dq j_1(qr) v_t(q) \quad (14c)$$

$$\frac{v_s(r)}{r} = \frac{2}{\pi} \int_0^\infty q^2 dq j_1(qr) v_s(q) \quad (14d)$$

where  $j_l(qr)$  are the Spherical Bessel Functions.

### III. THE RELATIVISTIC INTERACTIONS

We now restrict the interaction kernel,  $\mathbf{K}$ , to be composed of the relativistic exchange of only two mesons, the  $\pi$  meson which has been known for some time to correctly describe the long range nuclear force, and a spin-isospin scalar, or  $\sigma$  meson, which many people employ to describe the intermediate attraction known to be necessary to bind the deuteron.<sup>12</sup>

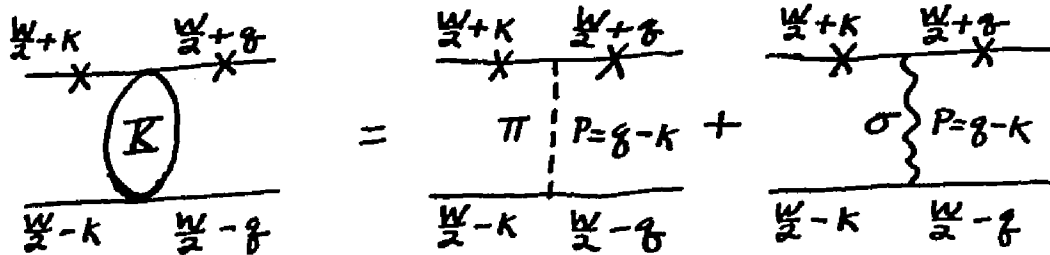


Figure 2

In this initial calculation of relativistic deuteron wave functions, we chose to use the sigma instead of the more exact and harder to calculate two pion exchange contributions. The rho meson, a two pion resonance, together with the omega meson, a three pion resonance, can easily be added to the interaction to give us, perhaps, more information concerning the short range nature of the nuclear force. However, for this work, we chose the simple interaction kernel composed of the one pion and the one sigma exchanges as an initial test of our equation's ability to describe the deuteron's dynamics.

Our sigma exchange represents those two pion exchange diagrams which are not contained in the one pion exchange. Some of these diagrams, represented by the sigma, are illustrated in Figure 3.

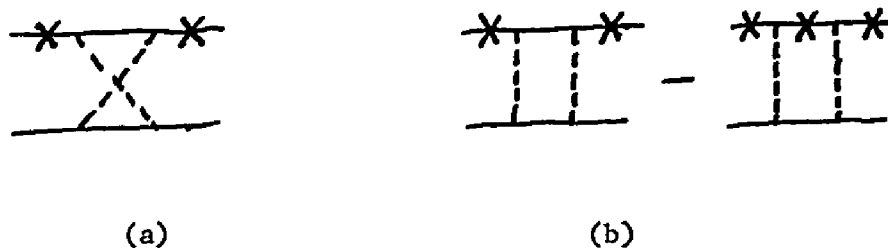


Figure 3

Figure 3b represents the full box diagram minus the first iteration of the one pion exchange, and figure 3a is the crossed box diagram.

The sigma meson, therefore, is a phenomenological representation of the two pion continuum.

Since the  $\sigma$  is a spin-isospin scalar, its  $\sigma$ -NN coupling is simply  $g_{\sigma} \mathbf{1}_2$ , where  $\mathbf{1}_2$  is a unit operation in the Dirac space of nucleon one. The  $\pi$ , being a pseudoscalar, is usually described by a  $\gamma^5$  coupling; but, recently<sup>1</sup> it was shown, using a semi-relativistic approximation of equation 1, that a pure  $\gamma^5$  interaction produced too much repulsion and that when more of the  $\gamma^5 \gamma^{\mu}$  interaction was added, the repulsion was reduced. So, to examine the effect of mixed  $\gamma^5 - \gamma^5 \gamma^{\mu}$  interactions in a fully relativistic framework,

the pion coupling was chosen to be

$$ig_{\pi} \tau_1 \left[ \lambda \gamma_1^5 + \frac{\not{x}}{2M} \gamma_1^5 (1-\lambda) \right] \quad (15)$$

where  $\lambda$  is the mixing parameter for the  $\gamma^5$  and  $\gamma^5 \not{x}$  interactions,  $\tau$  is the nucleon isospin operator, and the subscript  $1$  is a shorthand for the Dirac indices of particle one. Both the mass shell  $\pi$ -NN interaction and the long range part of the nuclear force are independent of  $\lambda$ . The nuclear force's dependence on  $\lambda$  comes from the off mass shell  $\pi$ -NN interaction which affects the short range force only.

In what follows,  $g_{\sigma}^2/4\pi$  and  $g_{\pi}^2/4\pi$  will be referred to as the  $\sigma$ -NN coupling constant and the  $\pi$ -NN coupling constant respectively.

Since a calculation of the two pion exchange kernels have to have a regularized one pion exchange kernel as input,<sup>10</sup> both the one pion exchange and the one sigma exchange kernels are regularized with the same regularization mass.

Two types of regularization were used. One is written as:

$$f(p^2) = \frac{(M_R^2 - \mu_{ex}^2)^2}{(M_R^2 - p^2)^2} \quad (16)$$

and the other is written as

$$f(p^2) = \frac{M_R^4}{(M_R^2 - p^2)^2} \quad (17)$$

where

$M_R$  = regularization mass

$M_{ex}$  = exchanged particle mass,  $M_\pi$  or  $M_\sigma$

$p = q - k$

This regularization procedure is flexible enough not only to guarantee convergence of our equations but to allow the possibility of using it as a form factor (see Section IV).

Hence, the regularized pion kernel is

$$-g_\pi^2(\tau_1 \cdot \tau_2) \left[ \lambda \gamma^5 + \frac{p}{2M} \gamma^5 (1-\lambda) \right]_1 \left[ \lambda \gamma^5 - \frac{p}{2M} \gamma^5 (1-\lambda) \right]_2 \frac{f(p^2)}{M_\pi^2 - p^2} \quad (18)$$

and the regularized sigma kernel is

$$g_\sigma^2(1_1 1_2) \frac{f(p^2)}{M_\sigma^2 - p^2} \quad (19)$$

where  $M_\pi$  and  $M_\sigma$  are the pion and sigma masses respectively.

For the sake of simplifying the discussion below, equation 16 is taken to be the form of the regularization.

So, folding equation 16 and the exchanged particle propagators together and expanding as

$$\frac{f(p^2)}{M_{ex}^2 - p^2} = \frac{(M_R^2 - M_{ex}^2)^2}{(M_{ex}^2 - p^2)(M_R^2 - p^2)} = \frac{1}{M_{ex}^2 - p^2} - \frac{1}{M_R^2 - p^2} - \frac{M_R^2 - M_{ex}^2}{(M_R^2 - p^2)^2} \quad (20)$$

and then substituting into relations 18 and 19, three terms result from each substitution. Considering for the moment terms independent

of  $M_R$ , equation 1 becomes with the  $M_R$  independent interaction kernels,

$$\begin{aligned} \tilde{\Gamma}(\not{q}) = & \frac{-g_\pi^2 (\not{c}_1 \cdot \not{c}_2)}{(2\pi)^3} \int d^3k \frac{[\not{\gamma} \lambda + \frac{\not{p}}{2M} \not{\gamma}^5 (1-\lambda)] (\frac{\not{W}}{2} + K + M) \tilde{\Gamma}(k) (M - \frac{\not{W}}{2} + K) [\not{\gamma} \lambda - \frac{\not{p}}{2M} \not{\gamma}^5 (1-\lambda)]}{2M_d E_k (2E_k - M_d) (\mathcal{M}_d^2 - p^2)} \\ & + \frac{g_\sigma^2}{(2\pi)^3} \int d^3k \frac{(\frac{\not{W}}{2} + K + M) \tilde{\Gamma}(k) (M - \frac{\not{W}}{2} + K)}{2M_d E_k (2E_k - M_d) (\mathcal{M}_\sigma^2 - p^2)} \end{aligned} \quad (21)$$

Since nucleon 1 is on its mass shell,

$$\left(\frac{\not{W}}{2} + K\right)^2 = \left(\frac{\not{W}}{2} + \not{p}\right)^2 = M^2 \quad (22)$$

and  $\not{W}/2 + \not{q} = M$  when acting to the left, then

$$\left[\not{\gamma} \lambda + \frac{\not{p}}{2M} \not{\gamma}^5 (1-\lambda)\right] \left(\frac{\not{W}}{2} + K + M\right) = \not{\gamma}^5 \left(\frac{\not{W}}{2} + K + M\right) \quad (23)$$

Thus, equation 21 reduces to

$$\begin{aligned} \tilde{\Gamma}(\not{q}) = & \frac{3g_\pi^2 \lambda}{(2\pi)^3} \int d^3k \frac{\not{\gamma}^5 \left(\frac{\not{W}}{2} + K + M\right) \tilde{\Gamma}(k) (M - \frac{\not{W}}{2} + K) \not{\gamma}^5}{2M_d E_k (2E_k - M_d) (\mathcal{M}_d^2 - p^2)} \\ & - \frac{3g_\pi^2 (1-\lambda)}{2M (2\pi)^3} \int d^3k \frac{\not{\gamma}^5 \left(\frac{\not{W}}{2} + K + M\right) \tilde{\Gamma}(k) (M - \frac{\not{W}}{2} + K) \not{p} \not{\gamma}^5}{2M_d E_k (2E_k - M_d) (\mathcal{M}_d^2 - p^2)} \\ & + \frac{g_\sigma^2}{(2\pi)^3} \int d^3k \frac{\left(\frac{\not{W}}{2} + K + M\right) \tilde{\Gamma}(k) (M - \frac{\not{W}}{2} + K)}{2M_d E_k (2E_k - M_d) (\mathcal{M}_\sigma^2 - p^2)} \end{aligned} \quad (24)$$

To keep the bookkeeping under control, the first and third terms of equation 24 will be calculated presently and the remaining term, T (the  $1-\lambda$  term), will be calculated afterwards.

Define  $\tilde{N}(k)$  as

$$\begin{aligned}\tilde{N}(k) &\equiv \tilde{\Gamma}(k) \left(M - \frac{W}{2} + K\right) \\ &= -\frac{H}{M}(M^2 - u)\xi - F\xi\psi + 2k \cdot \left\{ (F - G + I \frac{(M^2 - u)}{2M^2}) + \frac{G}{M} k \cdot \xi \right\} \psi\end{aligned}\quad (25)$$

where  $u = (\frac{W}{2} - k)^2$  and  $M^2 - u = M_d(2E_k - M_d)$

Therefore, equation 24 becomes

$$\begin{aligned}\tilde{\Gamma}(g) &= \frac{\lambda}{(2\pi)^3} \int \gamma^5 \left(\frac{W}{2} + K + M\right) \tilde{N}(k) \gamma^5 d^3 k'_\pi \\ &+ \frac{1}{(2\pi)^3} \int \left(\frac{W}{2} + K + M\right) \tilde{N}(k) d^3 k'_\sigma + T\end{aligned}\quad (26)$$

where

$$\begin{aligned}d^3 k'_\pi &= \frac{3 g_\pi^2 d^3 k}{2 M_d E_k (2E_k - M_d) (\mu_\pi^2 - p^2)} \\ d^3 k'_\sigma &= \frac{g_\sigma^2 d^3 k}{2 M_d E_k (2E_k - M_d) (\mu_\sigma^2 - p^2)} \\ d^3 k &= \vec{k}^2 d\vec{k} d\phi_k dz \\ z &= \hat{g} \cdot \hat{k}\end{aligned}\quad (27)$$

Now, substituting for  $\tilde{\Gamma}$  and  $\tilde{N}$ , equation 26 takes the form

$$\begin{aligned}&(F - 2H)\xi - \frac{H}{M}\xi\psi - \left(\frac{G}{M} - \frac{2H}{M}\right)g \cdot \xi + \frac{I}{M^2}g \cdot \xi \psi \\ &= \frac{\lambda}{(2\pi)^3} \int \gamma^5 \left(\frac{W}{2} + K + M\right) \gamma^5 \left[ \frac{H}{M}(M^2 - u)\xi - F\xi\psi + 2k \cdot \left\{ (F - G + I \frac{(M^2 - u)}{2M^2}) \right. \right. \\ &\quad \left. \left. - \frac{G}{M} k \cdot \xi \right\} \psi \right] d^3 k'_\pi + \frac{1}{(2\pi)^3} \int \left(\frac{W}{2} + K + M\right) \left[ -\frac{H}{M}(M^2 - u)\xi - F\xi\psi \right. \\ &\quad \left. + 2k \cdot \left\{ (F - G + I \frac{(M^2 - u)}{2M^2}) + \frac{G}{M} k \cdot \xi \right\} \psi \right] d^3 k'_\sigma + T\end{aligned}\quad (28)$$



$$\begin{aligned}
-\frac{H}{M} &= \frac{\lambda}{(2\pi)^2} \int d^2 k'_\pi \left[ \frac{b'H}{M}(M^2-u) - M(1-a)F + \frac{e}{M}G \right] \\
&+ \frac{1}{(2\pi)^2} \int d^2 k'_\sigma \left[ \frac{b'H}{M}(M^2-u) - M(1+a)F + \frac{e}{M}G \right] \\
-\left(\frac{G}{M} - \frac{2H}{M}\right) &= \frac{\lambda}{(2\pi)^2} \int d^2 k'_\pi \left[ 2M(a-d)(F-G+I\frac{M^2-u}{2M^2}) \right. \\
&+ \left. c'_d M^2 \frac{G}{M} \right] + \frac{1}{(2\pi)^2} \int d^2 k'_\sigma \left[ 2M(a+d)(F-G+I\frac{M^2-u}{2M^2}) \right. \\
&+ \left. c'_d M^2 \frac{G}{M} \right]
\end{aligned} \tag{30b}$$

$$\begin{aligned}
\frac{I}{M^2} &= \frac{\lambda}{(2\pi)^2} \int d^2 k'_\pi \left[ 2c'(F-G+I\frac{M^2-u}{2M^2}) - (a-d)G \right] \\
&+ \frac{1}{(2\pi)^2} \int d^2 k'_\sigma \left[ 2c'(F-G+I\frac{M^2-u}{2M^2}) + (a+d)G \right]
\end{aligned} \tag{30c}$$

The set of equations 30a-d can easily be cast into a compact matrix notation. The  $dZ$  integration can be performed with little effort using Appendix A.

Thus, the final result is written

$$F_\alpha(\beta) = 3\lambda \frac{g^2}{4\pi} \int \frac{kdK G_{\alpha\beta}^\pi(\mu_\sigma, k, \rho, \rho_\ell) F_\beta(k)}{2\pi g M_d E_k (2E_k - M_d)} + \frac{g^2}{4\pi} \int \frac{kdK G_{\alpha\beta}^\sigma(\mu_\sigma, k, \rho, \rho_\ell) F_\beta(k)}{2\pi g M_d E_k (2E_k - M_d)} + T'_\alpha \tag{31}$$

where  $T'_\alpha$  is the contribution to  $T$ , and  $Q_\ell(x)$ 's are the Legendre

Polynomials of the Second kind with

$$X = \frac{M C_k^2 - 2M^2 + 2E_k E_B}{2K_B} \quad (32)$$

and

$$G_{\alpha\beta}^{\pi} = \begin{bmatrix} -2\left[E_{\pi} + \frac{B'_{\pi} M_{\pi}^2}{2} + M^2(A_{\pi} - Q_0)\right] & 0 & -(M^2 - u)(A_{\pi} - Q_0 + 2B'_{\pi}) & -\frac{E_{\pi}}{M^2}(M^2 - u) \\ -4M^2 A_{\pi} + 2M^2(D_{\pi} + Q_0) & -2E_{\pi} - 2\left[\frac{C'_{\pi} M_{\pi}^2}{2} - M^2(A_{\pi} - D_{\pi})\right] & -2B'_{\pi}(M^2 - u) & -(A_{\pi} - D_{\pi})(M^2 - u) \\ -M^2(A_{\pi} - Q_0) & -E_{\pi} & -B'_{\pi}(M^2 - u) & 0 \\ -2M^2 C'_{\pi} & 2M^2\left(C'_{\pi} - \frac{(A_{\pi} - D_{\pi})}{2}\right) & 0 & -\frac{C'_{\pi}}{2}(M^2 - u) \end{bmatrix} \quad (33)$$

$$G_{\alpha\beta}^{\sigma} = \begin{bmatrix} 2\left[E_{\sigma} + \frac{B'_{\sigma} M_{\sigma}^2}{2} + M^2(A_{\sigma} + Q_0)\right] & -4E_{\sigma} & -(M^2 - u)(A_{\sigma} + Q_0 + 2B'_{\sigma}) & \frac{E_{\sigma}}{M^2}(M^2 - u) \\ -2M^2(D_{\sigma} - Q_0) & -2E_{\sigma} - 2\left[\frac{C'_{\sigma} M_{\sigma}^2}{2} - M^2(A_{\sigma} + D_{\sigma})\right] & -2B'_{\sigma}(M^2 - u) & -(A_{\sigma} + D_{\sigma})(M^2 - u) \\ M^2(A_{\sigma} + Q_0) & -E_{\sigma} & -B'_{\sigma}(M^2 - u) & 0 \\ 2M^2 C'_{\sigma} & -2M^2\left[C'_{\sigma} - \frac{(A_{\sigma} + D_{\sigma})}{2}\right] & 0 & C'_{\sigma}(M^2 - u) \end{bmatrix} \quad (34)$$

Both  $\alpha$  and  $\beta$  range from 1 to 4 such that  $F_1 = F$ ,  $F_2 = G$

$F_3 = H$ ,  $F_4 = I$ .

Now,  $T'_\alpha$  is calculated using the very same techniques as described above for the other two terms and is written

$$T'_\alpha = -3(1-\lambda) \frac{\partial^2}{4V} \left( \int K dK \frac{H'_{\alpha\beta}(K, \beta, \beta_0) F_\beta(K)}{2\pi\beta M_\beta E_K (2E_K - M_\beta)} \right) \quad (35)$$

where

$$H'_{\alpha\beta} = \begin{bmatrix} \frac{X}{\pi} - 2M_\beta(E_\beta - E_K) \left[ \frac{B'_\beta}{\pi} + \frac{(A'_\beta - \beta_0)}{2} \right] & \frac{-EM_\beta(E_\beta - E_K)}{M^2} & -\frac{(M^2 - u) X}{2M^2} & 0 \\ \frac{X}{\pi} - 2M_\beta(E_\beta - E_K) \frac{B'_\beta}{\pi} & \frac{Y_\beta - M_\beta(E_\beta - E_K)(A'_\beta - \beta_0)}{\beta} & 2(M^2 - u) \frac{D'_\beta}{\pi} & -\frac{(M^2 - u) Y_\beta}{2M^2} \\ \frac{1}{2} \left[ \frac{X}{\pi} - 2M_\beta \frac{B'_\beta}{\pi} (E_\beta - E_K) \right] & 0 & 0 & 0 \\ -2M^2 \frac{D'_\beta}{\pi} & \frac{1}{2} \left[ \frac{Y_\beta - 2M_\beta(E_\beta - E_K)}{\pi} \right] & -\frac{(M^2 - u)(A'_\beta - \beta_0)}{\pi} & 0 \end{bmatrix} \quad (36)$$

and all variables appearing in  $G_{\alpha\beta}^\pi$ ,  $G_{\alpha\beta}^\sigma$ , and  $H_{\alpha\beta}^\pi$  are defined in Appendix A.

So far, we have only calculated the contribution to equation 1 of the first term in equation 20. That is, we have calculated equation 1 independent of any regularization.

#### First Regularization

First Regularization is defined as the contribution to equation 2 of the second term in equation 20.

As is readily seen from equation 20, the form of First

Regularization is exactly the same as was just calculated above, with the only difference being that the regularization mass,  $M_R$ , replaces the exchanged meson mass.

Therefore, to arrive at First Regularization, we replace the pion mass,  $M_\pi$ , by the regularization mass,  $M_R$ , in equation 31 and subtract this result from the pion contribution in equation 31 (terms with  $\lambda$  dependence). We do a similar operation for the sigma term.

### Second Regularization

We define Second Regularization as the contribution to equation 2 of the remaining term in equation 20, R.

$$R = - \frac{M_R^2 - M_{ex}^2}{(M_R^2 - p^2)^2} \quad (37)$$

We see that by considering first derivatives of the Legendre Polynomials of the second kind, R is easily incorporated into equation 31 in a similar fashion as First Regularization. We replace the  $Q_\ell$ 's in equation 31 by  $-(M_R^2 - M_{ex}^2) Q_\ell' / 2kq$  (see Appendix A).

Thus, with the incorporation of the full regularization procedure, equation 31 represents relativistic interactions dependent upon the mixing parameter,  $\lambda$ , having a range from 0 to 1.

To use equation 17 as the regularization instead of equation 16, it is only necessary to multiply the result just obtained by  $M_R^4 / (M_R^2 - M_{ex}^2)^2$

#### IV. WAVE FUNCTIONS AND OTHER NUMERICAL RESULTS

The process of computing wave functions from equation 30 is a fairly straightforward matter with the help of the numerical techniques described in Appendix C and the relationships between the wave functions and the invariant amplitudes (equations 11a-d). This section's purpose is to display and discuss the wave functions and other numerical results obtained.

Using the expansion

$$F_j(z) = e^{-z/2} \sum_i^n C_{ji} L_i(z) \quad (38a)$$

where  $L_i(z)$  are Laguerre Polynomials and  $F_1 = F$ ,  $F_2 = G$ ,  $F_3 = H$ ,  $F_4 = I$ , and

$$z = \frac{1}{.64} \left[ \sinh^{-1} \left( \frac{g}{M_q + \sqrt{MB'}} \right) \right]^2 \quad (38b)$$

a mapped variable enhancing convergence of our equations, to express the invariant amplitudes appearing in equation 31, and fixing  $M_R$ ,  $\lambda$ , and  $g_\sigma^2/4\pi$ , we obtain a set of coupled algebraic equations from a set of four coupled linear integral equations to be solved with two parameters for the dimensionless coefficients,  $C_{ji}$ . The two parameters are the sigma coupling constant,  $g_\sigma^2/4\pi$ , and mass,  $M_\sigma$ . We set  $M_\sigma$  and solved the equations numerically for the

eigenvalue,  $g_{\sigma}^2/4\pi$ . The requirements for a solution were that the adjusted  $M_{\sigma}$  and  $g_{\sigma}^2/4\pi$  give wave functions corresponding to the correct deuteron binding energy,  $B = 2.22466$  MeV, and a good non-relativistic quadrupole moment,  $Q$ , given by

$$Q = \frac{M_d^2 \sqrt{2}}{10} \int_0^{\infty} r^2 dr \left[ uw - \frac{w^2}{\sqrt{8}} \right] \quad (39)$$

The experimental value of  $Q$  in the above units was taken to be 25.5.

As was stated earlier, the mixing parameter for the  $\gamma^5$  and  $\gamma^5 \gamma^{\mu}$  interactions is denoted as  $\lambda$ . This parameter is free to take on any value between zero and one. Each value of  $\lambda$  corresponds to a different interaction. In this work, solutions were found for  $\lambda$  equal to 1. (pure  $\gamma^5$ ), .9, .8, .6, and 0 (pure  $\gamma^5 \gamma^{\mu}$ ).

#### Convergence of the Numerical Procedure

Convergence criteria are discussed here. The uninterested reader can go directly to the discussion of the solutions.

The parameter,  $n$ , appearing in equation 38a, is determined by the number of integration points,  $n_I$ , necessary for the integrals (equations C.8) to converge. The optimum  $n$  is equal to  $n_I - 1$ , using a numerical quadrature formula of the Gauss Laguerre type. This condition, together with equations 38a-b, was first introduced by Y. Chao and A. D. Jackson.<sup>13</sup> Their techniques were verified and used in the course of this work.

To test the Chao and Jackson criteria for the convergence of  $n$ ,  $M_\sigma$  was given the value of 500 MeV,  $\lambda$  was set at 1,  $g_\pi^2/4\pi$  was taken to be 14.0,  $M_R$  was set equal to  $4M$ , and  $n_I$  was taken to be 8. Using the single pole regularization (First Regularization) and using  $g_\sigma^2/4\pi$  as the convergence parameter, we obtained for  $n = 4$ ,  $n = 7$ ,  $n = 8$ ,  $\sigma$ -NN coupling constants of 25.1, 23.8, 23.8 respectively. It is clear from this data that for  $n_I = 8$ ,  $n$  converges at 7.

The number of integration points,  $n_I$ , was chosen by examining  $g_\sigma^2/4\pi$  as  $n_I$  was increased. For 4, 8, and 12 integration points,  $g_\sigma^2/4\pi$  had the values 16.1, 19.3, and 19.4 respectively, with  $M_\sigma = 450$  meV,  $\lambda = 1$ ,  $M_R = 4M$ ,  $g_\pi^2/4\pi = 15.0$ ,  $n = 4$ , and using First Regularization. This data indicates convergence for  $n = 4$  with  $n_I = 8$ . From these findings and the results obtained above for the determination of  $n$ , the number of integration points was chosen to be 8 and, therefore,  $n$  was chosen to be 7.

Thus far, results have been quoted for the single pole regularization (First Regularization) only. These results were for the  $\lambda = 1$  (pure  $\gamma^5$ ) interaction. When the double pole regularization (Second Regularization) is taken into account for  $\lambda = 1$ ,  $g_\sigma^2/4\pi$  changes by less than 0.02 percent. In fact, for First Regularization and Second Regularization,  $g_\sigma^2/4\pi$  has the values of 53.30 and 53.29 respectively for  $M_\sigma = 625$  MeV,  $n = 7$ , and  $g_\pi^2/4\pi = 14.0$ . It is not expected to obtain these respective values

of the  $\sigma$ -NN coupling constant for  $\lambda \neq 1$  since the  $\gamma^5 \gamma^4$  interaction carries with it an additional power of momentum in the numerator of the pion kernel.

Thus, the number of integration points set equal to 8,  $n = 7$ , the  $\pi$ -NN coupling constant,  $g_\pi^2/4\pi$ , set equal to 14.0 (that of Reid's) and the regularization taken to be Second Regularization is the parameter package used for all solutions obtained. We now turn to a discussion of the solutions themselves.

#### Solutions for High Mass Regularization (Case I)

In this first case of two to be discussed, the regularization used was equation 16, and we required that the regularization mass,  $M_R$ , be large enough so that a further increase of  $M_R$  will not change the dynamics significantly. Measures of the dynamics were taken to be the  $\sigma$ -NN coupling constant and the non-relativistic quadrupole moment. For  $M_R = M, 1.5M, 2M, 3M, 4M$ , the resulting  $g_\sigma^2/4\pi$  had values of 17.16, 15.52, 16.32, 16.20, 16.19 respectively and the corresponding quadrupole moments in units of  $e/M_d^2$  for the  $M_R$ 's cited above had the values of 27.97, 27.61, 27.39, 27.27, 27.26 respectively with  $M_\sigma = 450$  MeV,  $g_\pi^2/4\pi = 15.0$ ,  $n = 4$ ,  $\lambda = 1$ , and the number of integration points being 4. Convergence is clearly obtained at  $M_R = 3M$ .

Thus, for this high mass regularization case  $M_R$ 's were taken to be 3M and 4M. With  $g_\pi^2/4\pi = 14.0$  and  $M_R = 4M$ , a solution was

found for  $\lambda = 1$  (denoted  $\lambda_4 = 1$ ). Table 1 contains the parameter data and the physical quantities associated with this interaction. Table 1 also contains the relativistic quadrupole moment obtained from equation B.3 and the magnetic moment obtained from equation B.4 associated with  $\lambda_4 = 1$ .

Figure 4 illustrates the position space wave functions for  $\lambda_4 = 1$  compared to those obtained by Reid<sup>2</sup> non-relativistically.

Since the interaction is composed of the relativistic exchange of the  $\pi$  and  $\sigma$  mesons, and because in the non-relativistic limit both of these mesons give potentials which are purely attractive, the repulsion exhibited by the wave functions (u and w) in figure 4 are due to the relativistic nature of the wave equation, a "relativistic" effect.<sup>14</sup>

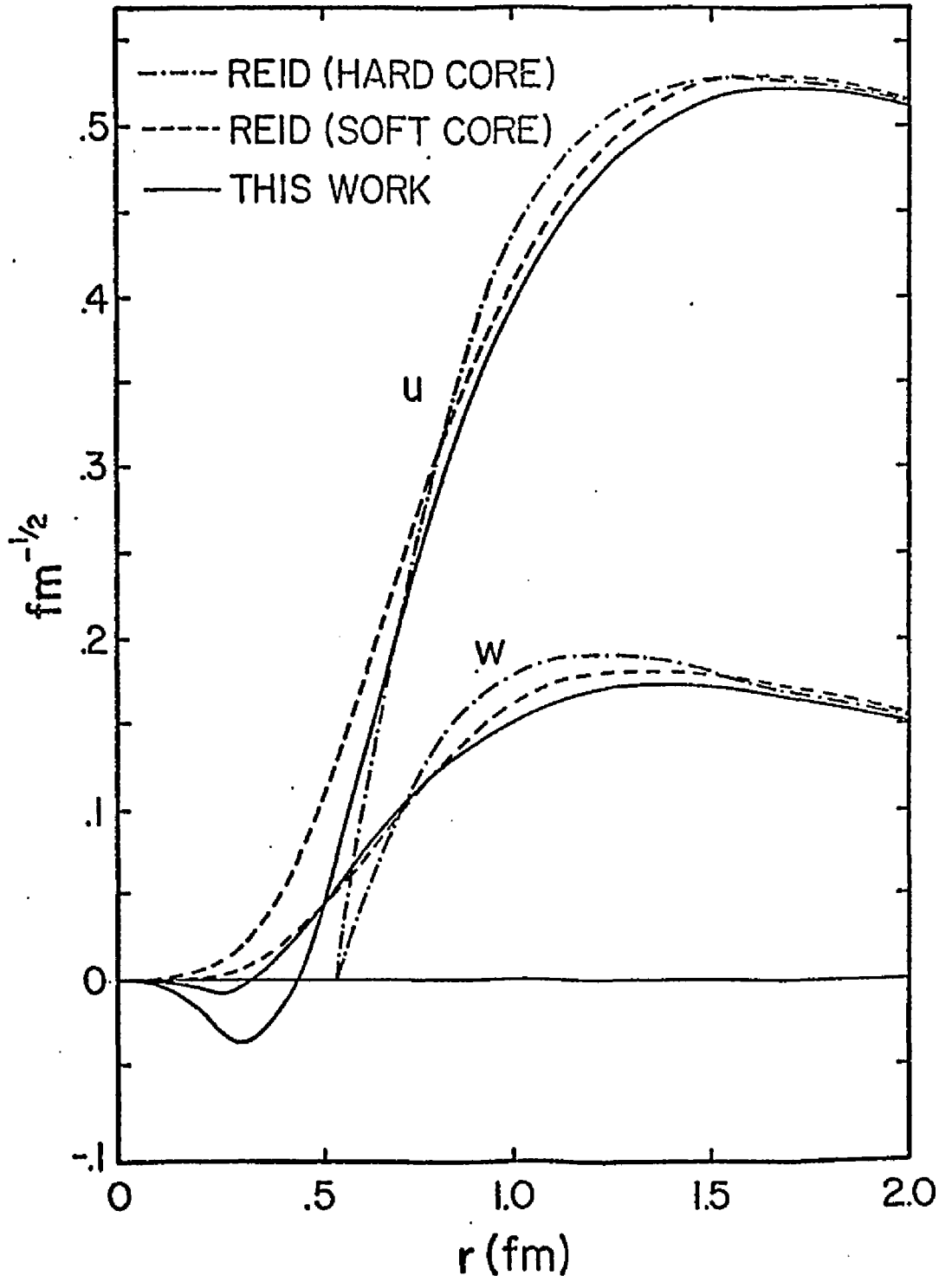
An obvious feature of these wave functions is the oscillation of u and w at short distances. This behavior may partially explain the success of hard core models,<sup>15</sup> and can arise naturally when there are several coupled angular momentum channels even though all of the potentials are regular. Oscillations have also been obtained previously from unitary transformations of potentials, and are associated with the additional non-locality introduced by the transformations at short distances.<sup>16</sup> In our case, the potentials produced by the interaction are both regular and non-local at short distances, and the oscillations are characteristic of the solutions obtained from this model.

Table 1. Data for all solutions obtained;  $P_D$  is the D state probability,  $P_t$  and  $P_s$  are the triplet P and singlet P state probabilities respectively; Q, the quadrupole moment, and  $\mu_d$ , the magnetic moment, are measured in units of  $e/M_d^2$  and nuclear magnetons respectively. The values of the mixing parameters  $\lambda_4$ ,  $\lambda_3$ , and  $\lambda_\omega$  correspond to  $M_R$ 's of 4M, 3M, and  $M_\omega$  (omega mass) respectively.

$\lambda_4 = 1$     $\lambda_3 = 1$     $\lambda_3 = .9$     $\lambda_3 = .6$     $\lambda_0 = 1$     $\lambda_0 = .8$     $\lambda_0 = 0$    HG   EXP.  
 (  $\lambda = .41$  )   RSC   MOM.

	625 MeV	625 MeV	600 MeV	450 MeV	525 MeV	500 MeV	300 MeV	364 MeV	
$M_\sigma$	53.29	53.33	35.68	5.09	11.15	5.92	.56	2.41	--
$\mathcal{D}_{\sigma}^2/4\pi$	6.112	6.115	6.163	6.370	5.101	5.213	6.306	6.380	6.47
$P_D$	2.698	2.686	2.286	1.354	2.000	.886	.696	.530	0
$P_t$	.050	.050	.045	.026	.108	.051	.009	.010	0
Q (N.R.)	25.60	25.60	25.54	25.42	25.43	25.59	25.58		25.5
Q (Re1.)	25.784	25.782	25.673	25.528			25.686		--
$M_d$ (N.R.)	.845	.845	.845	.844	.851	.850	.844	.844	.843
$M_d$ (Re1.)	.844	.844	.844	.841			.899	.852	--
$M_p$	--	--	--	--	--	--	--	789 MeV	--
$M_\omega$	--	--	--	--	--	--	--	789 MeV	--
$\mathcal{D}_p^2/4\pi$	--	--	--	--	--	--	--	1.0	--
$\mathcal{D}_\omega^2/4\pi$	--	--	--	--	--	--	--	9.0	--

Figure 4. S and D state wave functions (labeled u and w respectively) for  $\lambda_3 = 1$  displayed at short distances. The Reid hard and soft core wave functions are shown for comparison.



Solutions were also obtained for  $\lambda = 1, .9, \text{ and } .6$  with  $M_R = 3M$  (interactions denoted  $\lambda_3$ ). Position space wave functions are illustrated in figures 5, 6, and 7 respectively. The two cases  $\lambda_4 = 1$  and  $\lambda_3 = 1$  are identical and confirm the high mass regularization criteria. The repulsion exhibited by the wave functions in figure 5, 6, and 7 noticeably decreases as  $\lambda_3$  is decreased. This is a verification of the semi-relativistic findings predicted by Gross, cited earlier.

Table 1 contains the relevant data associated with the  $\lambda_3$  interactions and figure 8 shows the non-relativistic quadrupole dependence on the sigma mass for a given  $\lambda_3$ . It is shown in figure 8 that physical solutions exist for only a few values of  $\lambda_3$ . It will be an easy matter to find solutions for  $\lambda_3 = .8$  and  $.7$  using the same parameters as in the  $\lambda_3$  interactions previously obtained. However, our inability to find solutions in the "low  $\lambda_3$ " interactions is apparently due to divergences of the kernels. As stated earlier, the pure  $\gamma^5 \gamma^{\mu}$  ( $\lambda_3 = 0$ ) interaction has an additional power of momentum in the numerator of the  $\pi$  kernel. This extra power of momentum does not appear in the pure  $\gamma^5$  ( $\lambda_3 = 1$ ) kernel. With the high mass regularization of  $3M$  or  $4M$ , the divergence is very sensitive to  $\lambda$ . What we must find is an  $M_R$  with

Figure 5. The four relativistic deuteron wave functions for  $\lambda_3 = 1$ .  
The small circles are values of Reid's u and w shown for  
comparison.

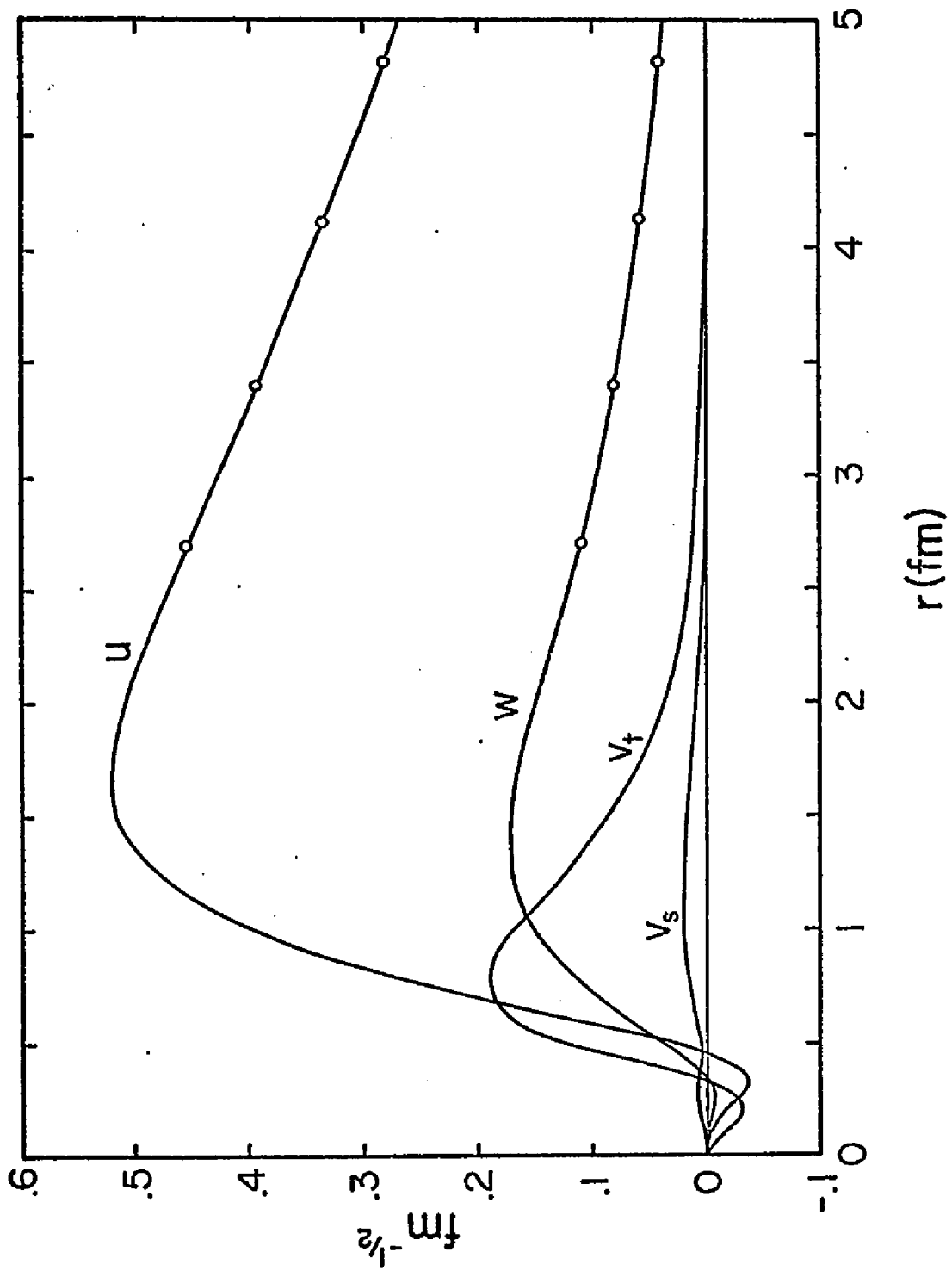


Figure 6. The four relativistic deuteron wave functions for  $\lambda_3 = .9$ .

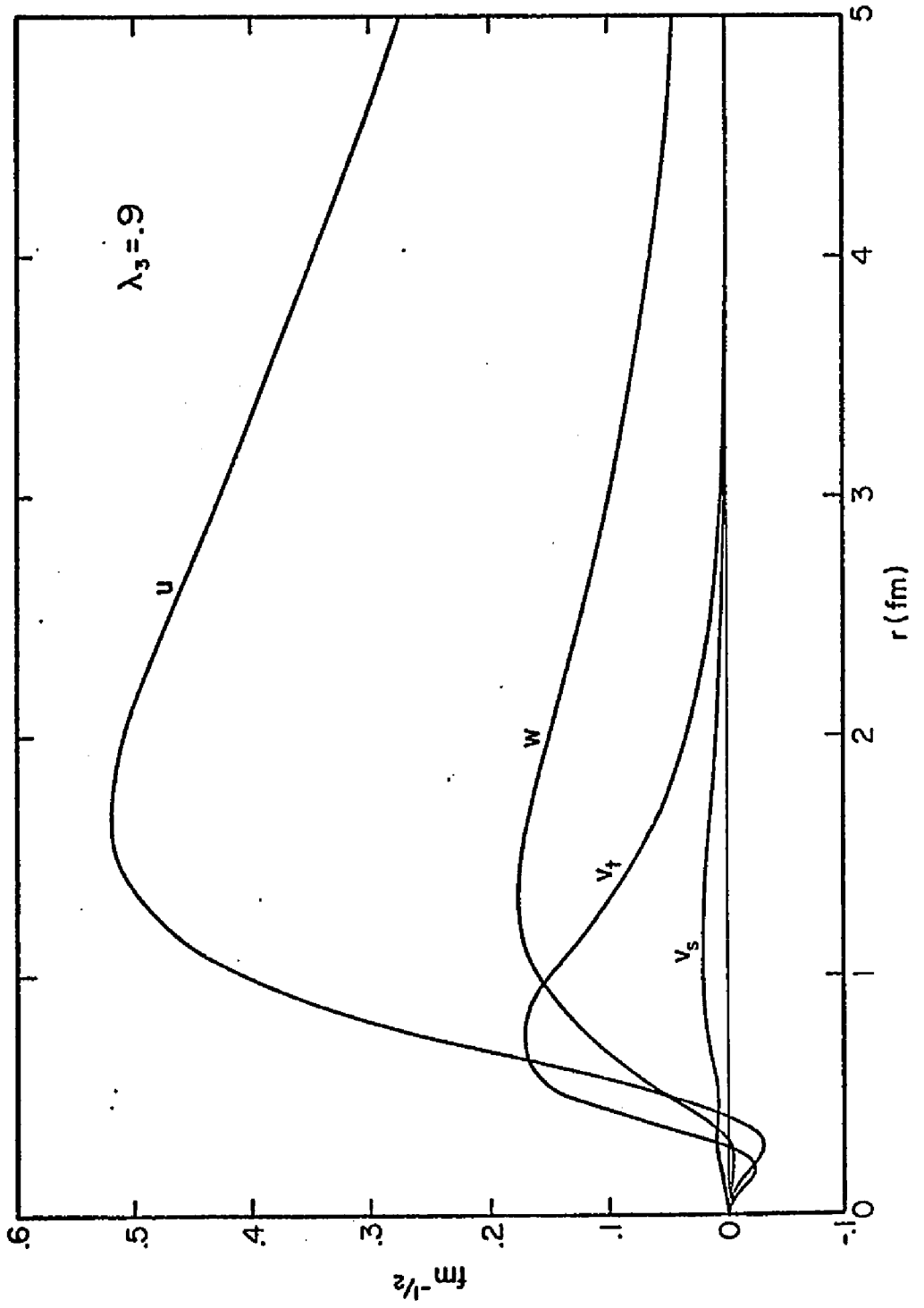


Figure 7. The four relativistic deuteron wave functions for  $\lambda_3 = .6$ .

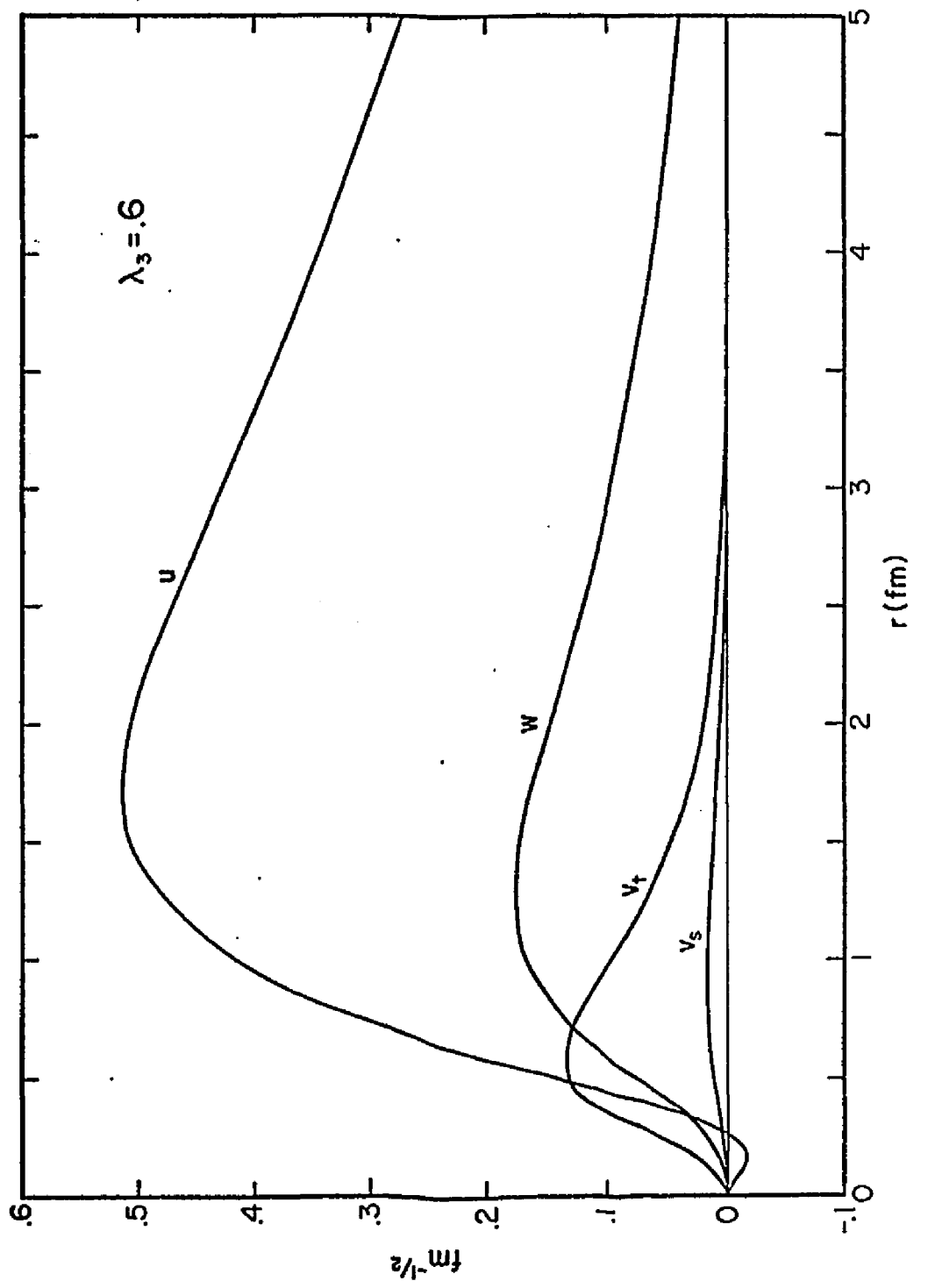
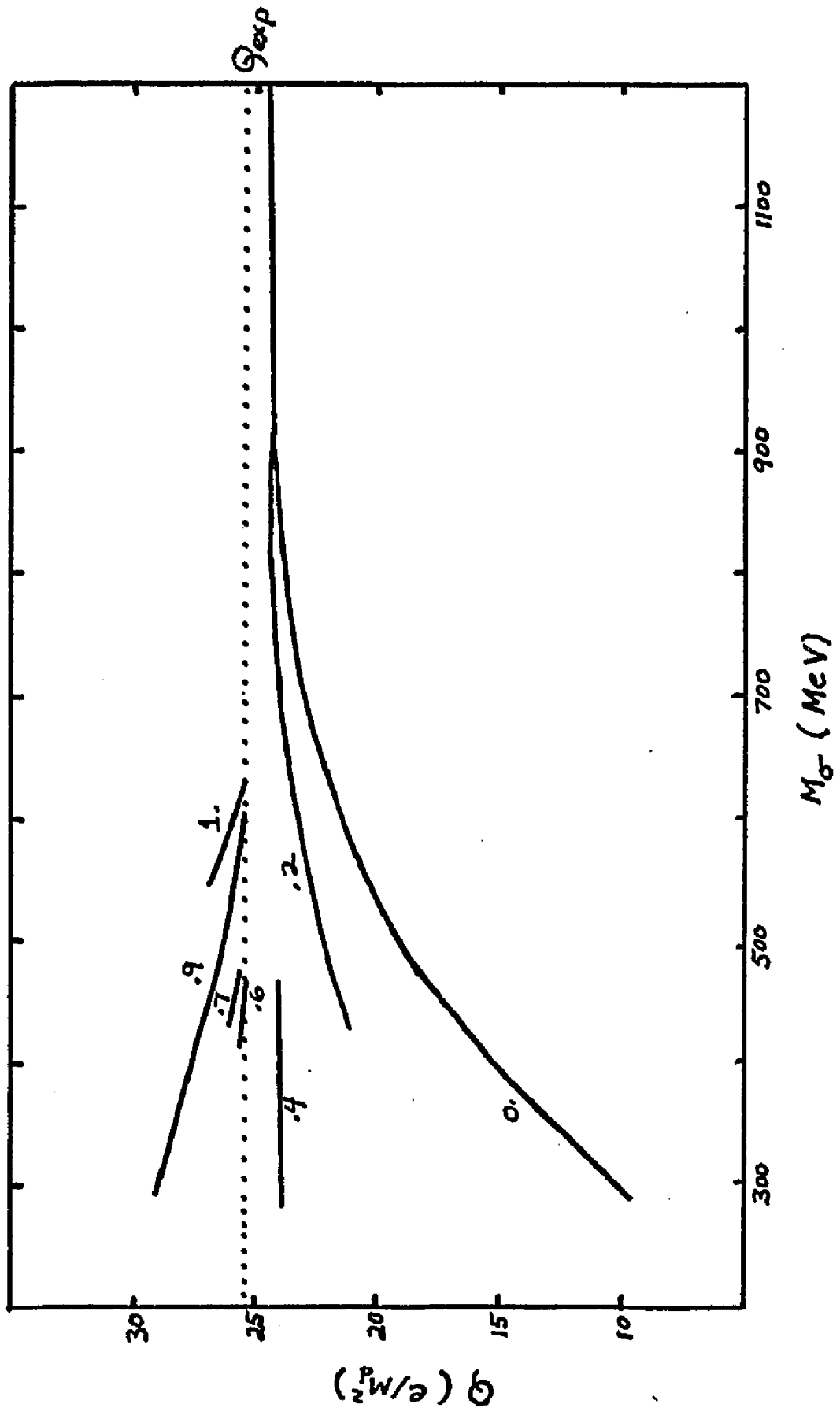


Figure 8. The quadrupole moment of the deuteron,  $Q$ , versus the sigma mass for fixed values of  $\lambda_3$  as indicated on each curve. The dotted line is the experimental value for  $Q$ .



a value such that all of the kernels momentum dependence is virtually insensitive to  $\lambda$ , varying only the sigma meson's coupling constant and mass. Once that is found, solutions will exist for all  $\lambda$ . This value of  $M_R$  has not yet been found. An alternative, that was found but not included in this discussion, is to raise  $g^2/4\pi$  to obtain additional solutions.

#### Solution for Low Mass Regularization (Case II)

For this case, the form of the regularization was taken from equation 17. Since the  $M_R$  chosen for this case is the omega meson mass,  $M_\omega = 784$  MeV, this low mass regularization can be thought of as a form factor.

The choice of  $M_R = M_\omega$  is a natural one. The sigma meson, a representation of the  $2\pi$  continuum, can be thought of as coupling to the rho meson, a  $2\pi$  resonance. By coupling, it is meant that the sigma form factor mass be the rho mass,  $m_\rho$ . Similarly, the  $3\pi$  continuum which couples to the pion, while not of the right quantum numbers to be a real meson, could be roughly approximated by a peaking in the vicinity of the omega mass. Because the sigma is phenomenological and  $m_\rho$  is approximately equal to  $m_\omega$ , the choice of  $M_R = M_\omega$  was made.

The literature contains several papers which use a number of values for form factor masses. Recently, a calculation by W. Nutt

and B. Loiseau quoted a form factor mass very near that of  $M_\omega$ .<sup>17</sup>

Another example of form factor mass choices can be found in reference 18; form factor masses quoted there are 450, 650, and 850 MeV.

Interactions using the low mass regularization are denoted by  $\lambda_\omega$  and solutions were found for  $\lambda_\omega = 1, .8, \text{ and } 0$ . The data for the  $\lambda_\omega$  interactions along with the  $\lambda_4$  and  $\lambda_3$  interactions appears in table 1. Figures 9, 10, and 11 illustrate the position space wave functions for  $\lambda_\omega$  interactions. Notice that for  $\lambda_\omega = 1$ , there are no oscillations, and for  $\lambda_\omega = 0$ ,  $v_t$  is mostly negative. In fact,  $u$  and  $w$  in the  $\lambda_\omega = 1$  interaction resemble very strongly the Reid Soft Core (RSC) wave functions. Indeed, as is indicated in Section V,  $\lambda_\omega = 1$  gives the same result as RSC (for  $v_t = v_s = 0$  everywhere). The  $\lambda_\omega = 0$  interaction with a negative  $v_t$  is in agreement with the predictions of the semi-relativistic treatment of Gross; for a pure  $\gamma^5 \gamma^\mu$  ( $\lambda = 0$ ) interaction, the short range behavior is dominated by the sigma, not by the pion.

Figure 12 shows the quadrupole moment versus the sigma mass for the  $\lambda_\omega$  interactions. Again, solutions were restricted to only a few values of  $\lambda_\omega$ .

Figure 13 illustrates the s state wave functions  $u$  for  $\lambda_3 = 1, .9, \text{ and } .6$ . It is shown there that the higher values of  $\lambda_3$

Figure 9. The four relativistic deuteron wave functions for  $\lambda_\omega = 1$ .

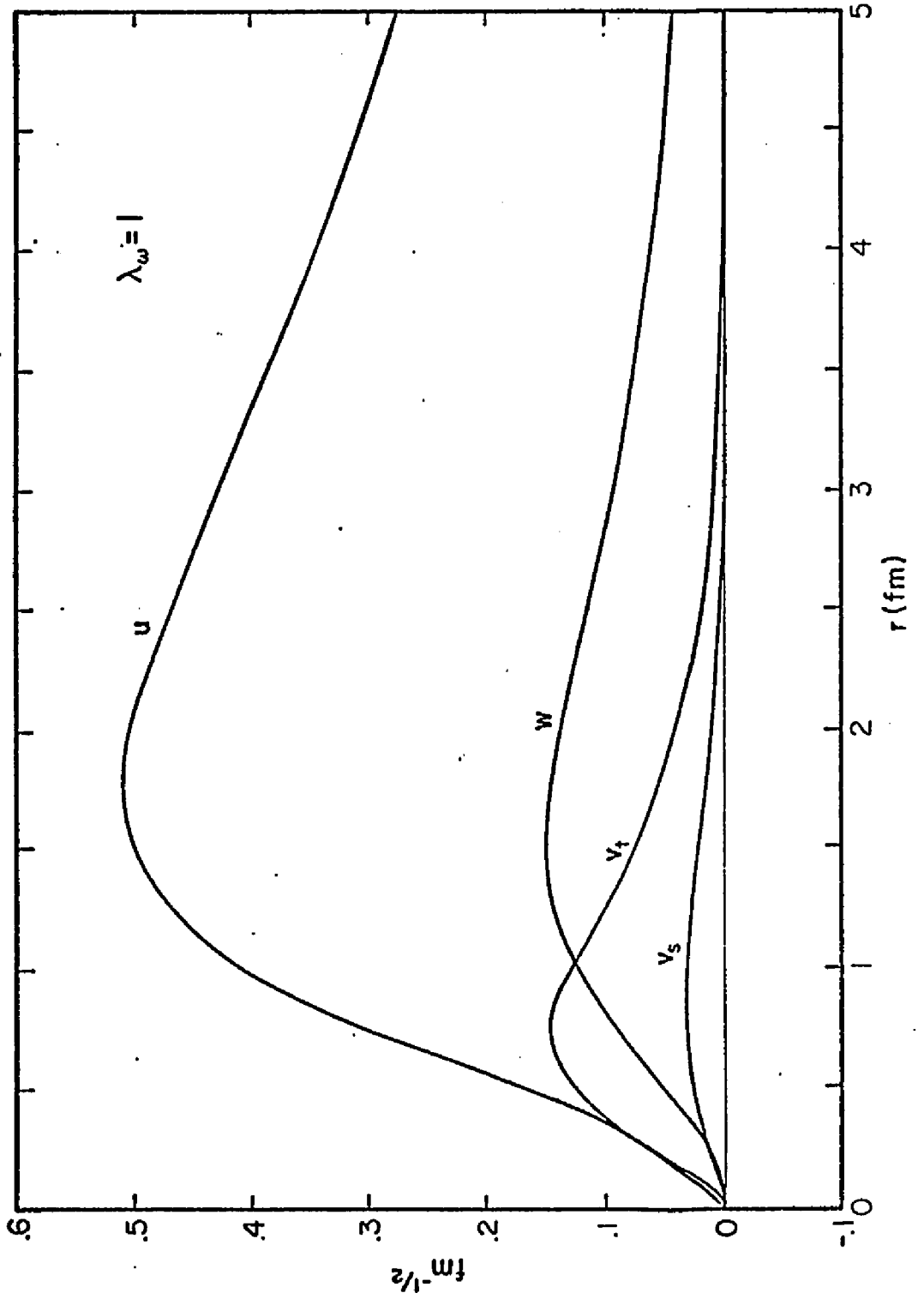


Figure 10. The four relativistic deuteron wave functions for  $\lambda_\omega = .8$ .

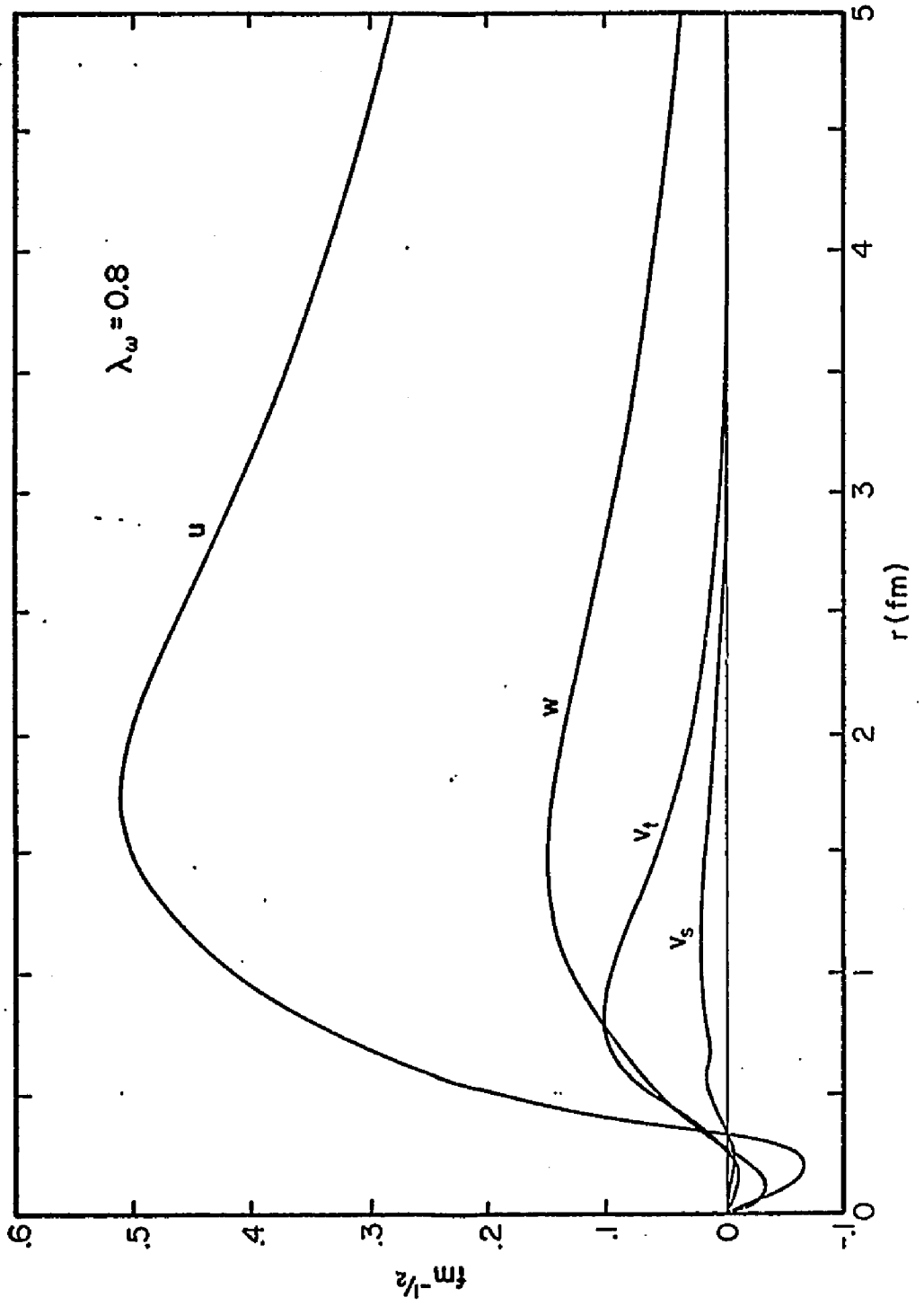


Figure 11. The four relativistic deuteron wave functions for  $\lambda_\omega = 0$ .

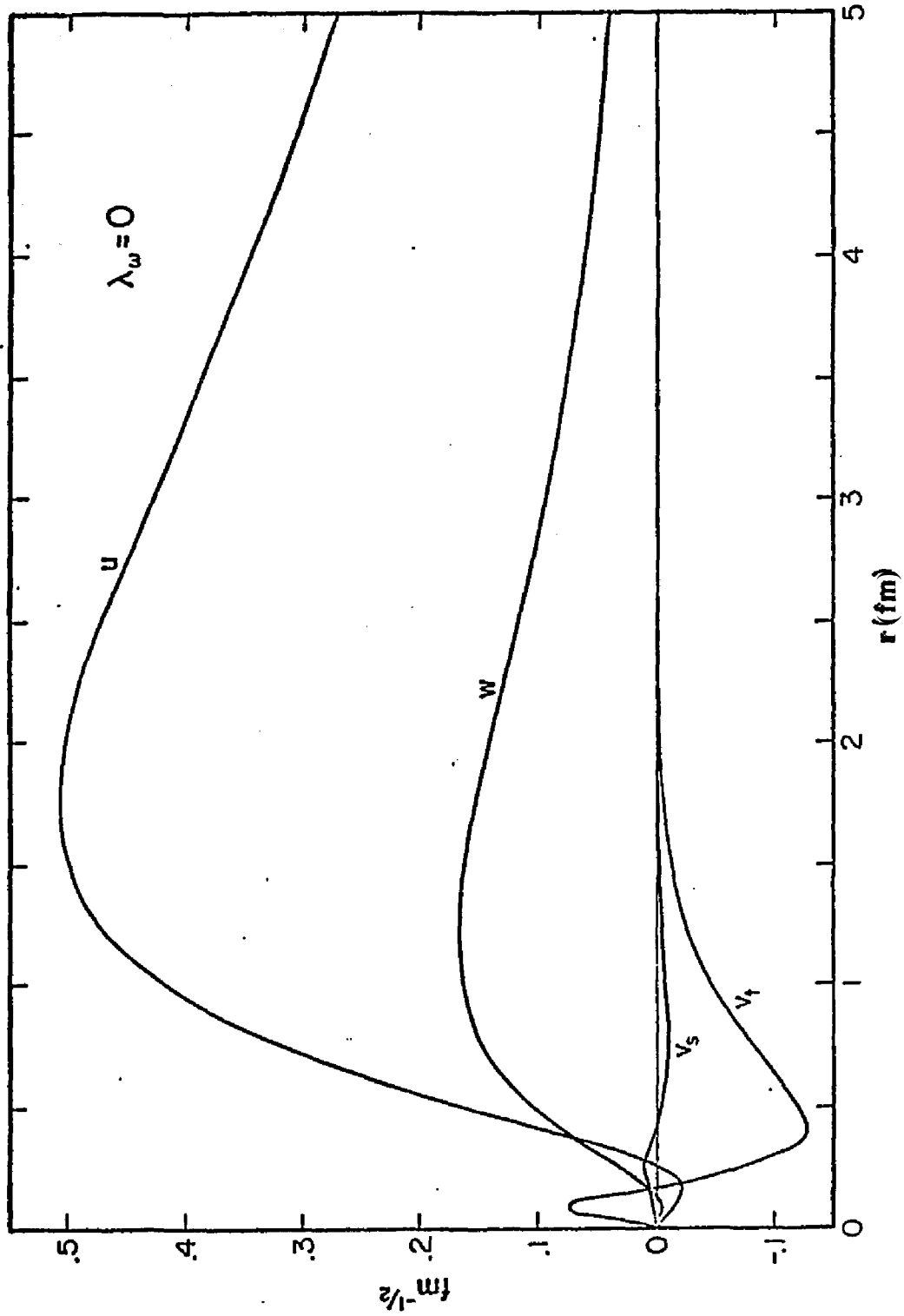


Figure 12. The quadrupole moment of the deuteron,  $Q$ , versus the sigma mass for fixed values of  $\lambda_\omega$  as indicated on each curve.

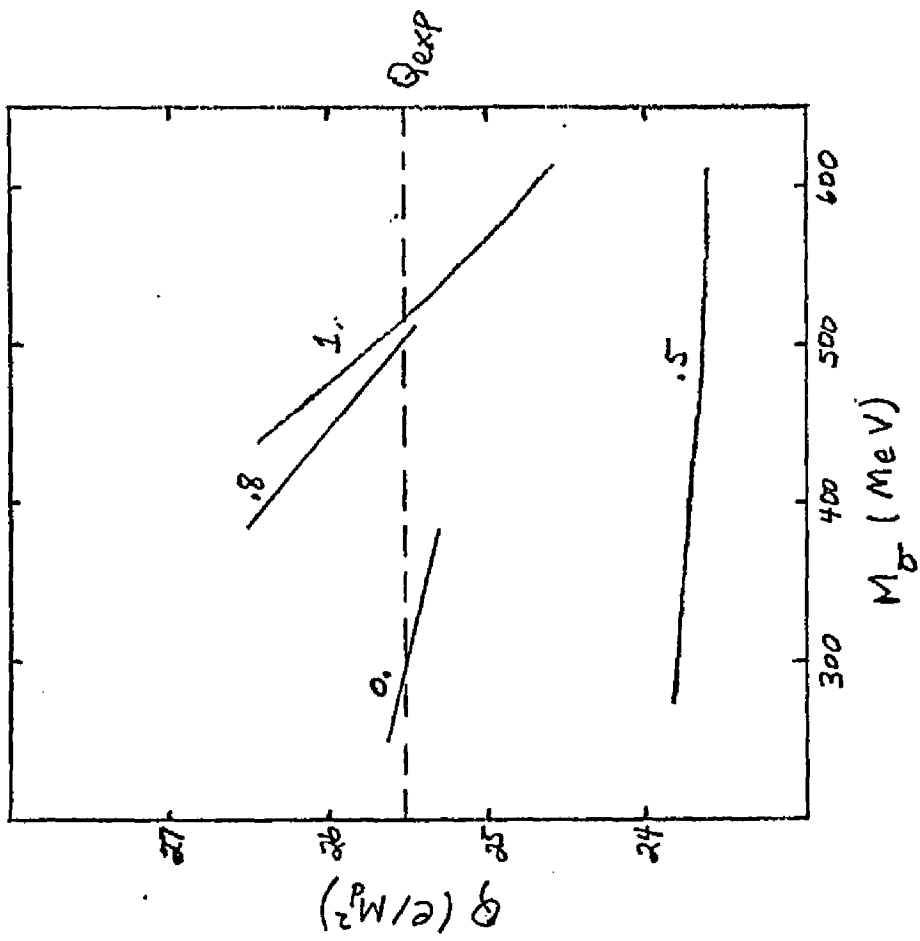
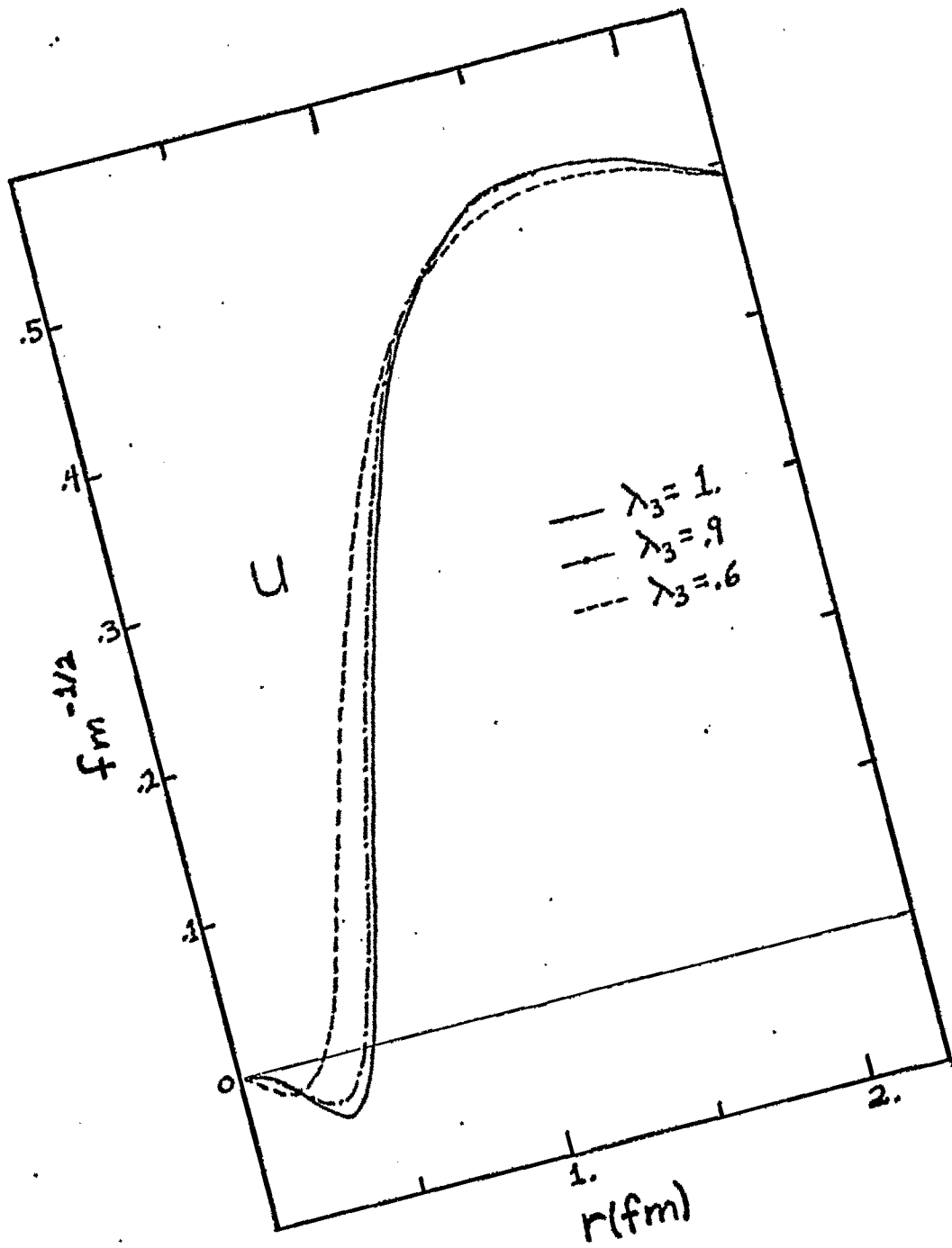


Figure 13. The short range structure of  $u$  for  $\lambda_3 = 1, .9, \text{ and } .6$ .



force the wave function further away from the origin; an indication of repulsion. Hence  $\lambda_3 = .6$  exhibits a softer core than does  $\lambda_3 = 1$ . This behavior of  $u$  is consistent with semi-relativistic predictions.

Further wave function dynamics are illustrated in figure 14. There,  $v_t$  is shown for  $\lambda_\omega = 1, .8, \text{ and } 0$ . The behavior of  $v_t$  for these values of  $\lambda_\omega$  is again consistent with semi-relativistic predictions. For  $\lambda_\omega = 1$  (pure  $\gamma^5$ ), the pion dominates the structure of  $v_t$ . Hence, its long range shape. For  $\lambda_\omega = 0$  (pure  $\gamma^5 \gamma^4$ ), the sigma meson of shorter range dominates  $v_t$ 's structure. The overall sign of  $v_t$  for  $\lambda_\omega = 0$  can partially be explained by Gross' semi-relativistic off-diagonal potentials. The  $\lambda_\omega = .8$  case is part of a transition, then, from pure pion dominance to pure sigma dominance.

The momentum space wave functions displayed in figures 15 through 20 are obtained from the invariant amplitudes F, G, H, and I through the formulae 12a-d. The dimensionless coefficients,  $C_{ji}$ , appearing in equation 38a, which generate F, G, H, and I, are listed in tables 2 through 8.

The invariant amplitudes F, G, H, and I are shown in momentum space for all the  $\lambda_4, \lambda_3, \text{ and } \lambda_\omega$  interactions discussed above in figures 21 through 28. Recall that  $\lambda_4$  and  $\lambda_3$  have equivalent properties.

Figure 14. Overall view of  $v_t$  for  $\lambda\omega = 1, .8, \text{ and } 0.$

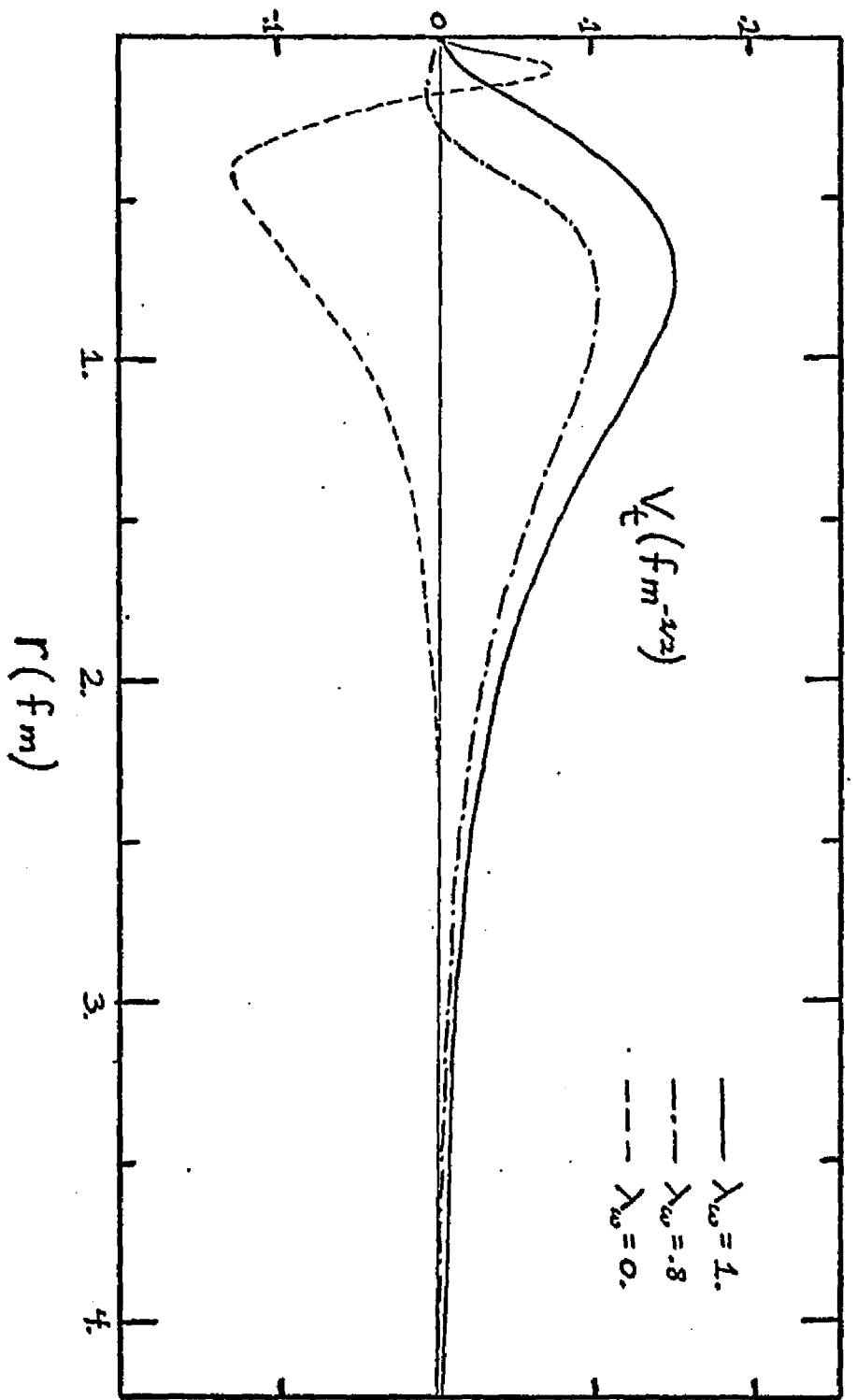


Figure 15. The momentum space S state wave functions,  $u$ , for  $\lambda_3 = 1$ , .9, and .6. The right most curves are to be read from the right scale.

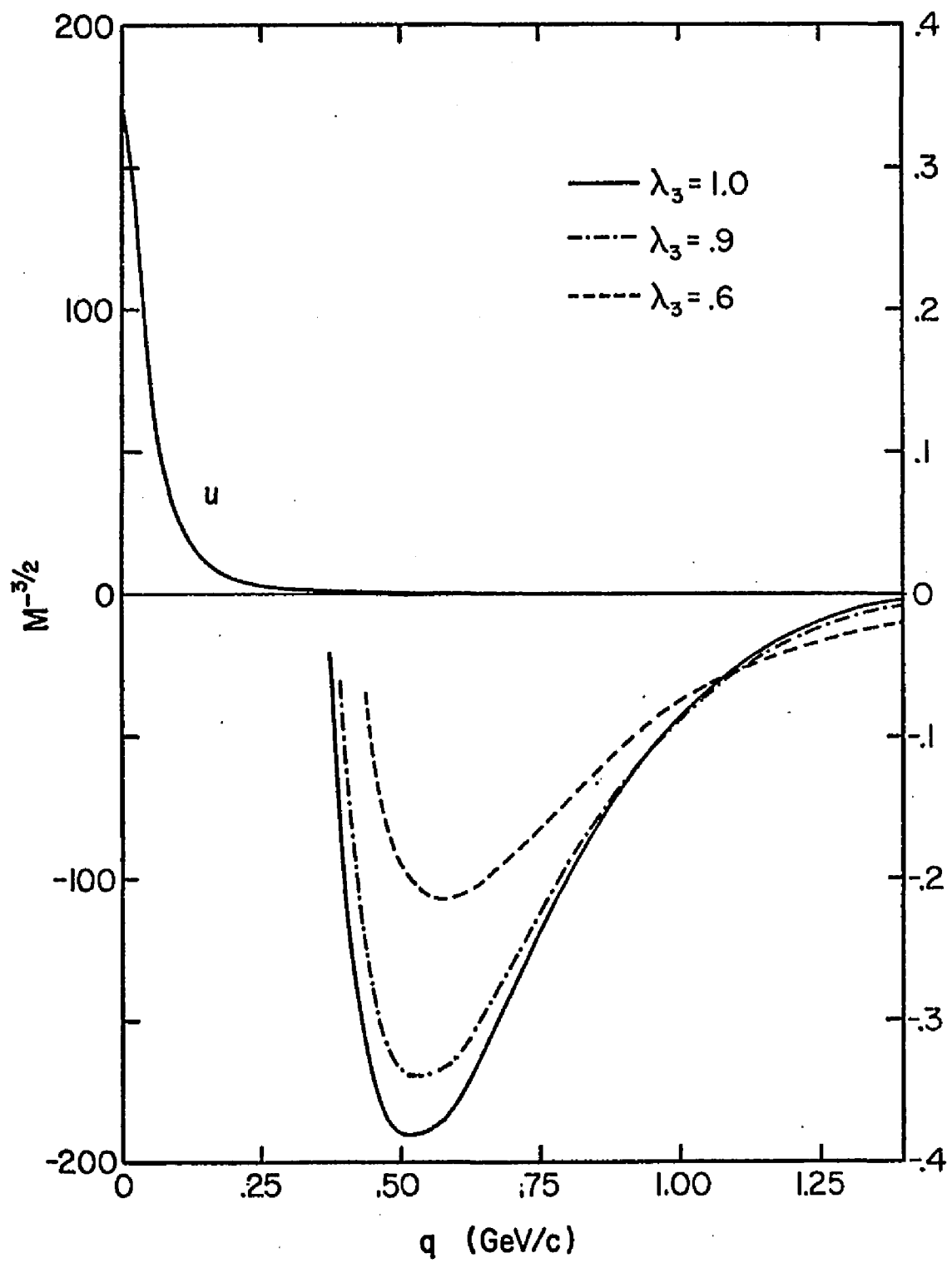


Figure 16. The momentum space D state wave functions,  $w$ , for  
 $\lambda_3 = 1, .9, \text{ and } .6.$

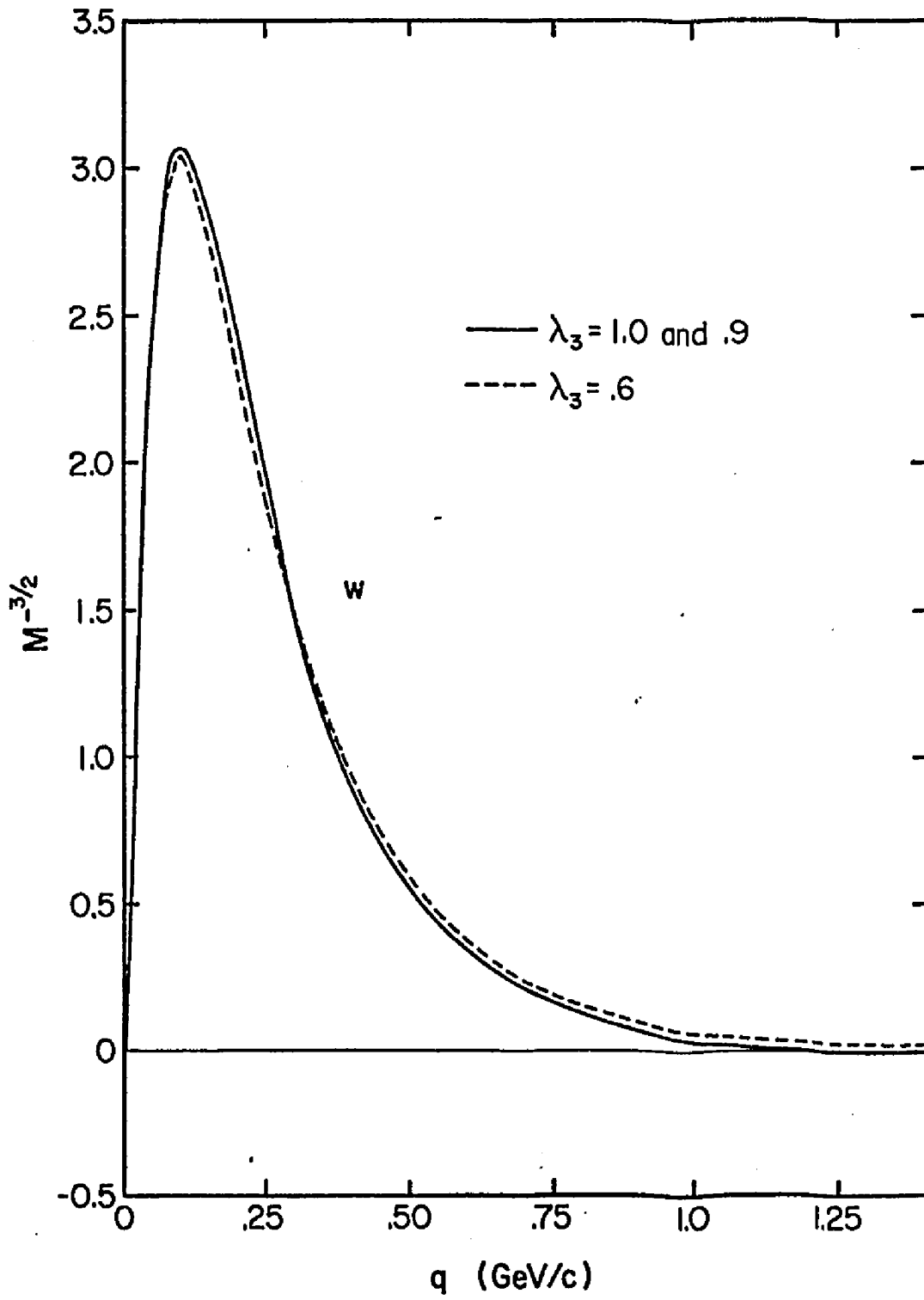


Figure 17. The momentum space P state wave functions,  $v_t$  and  $v_s$ ,  
for  $\lambda_3 = 1, .9, \text{ and } .6$ .

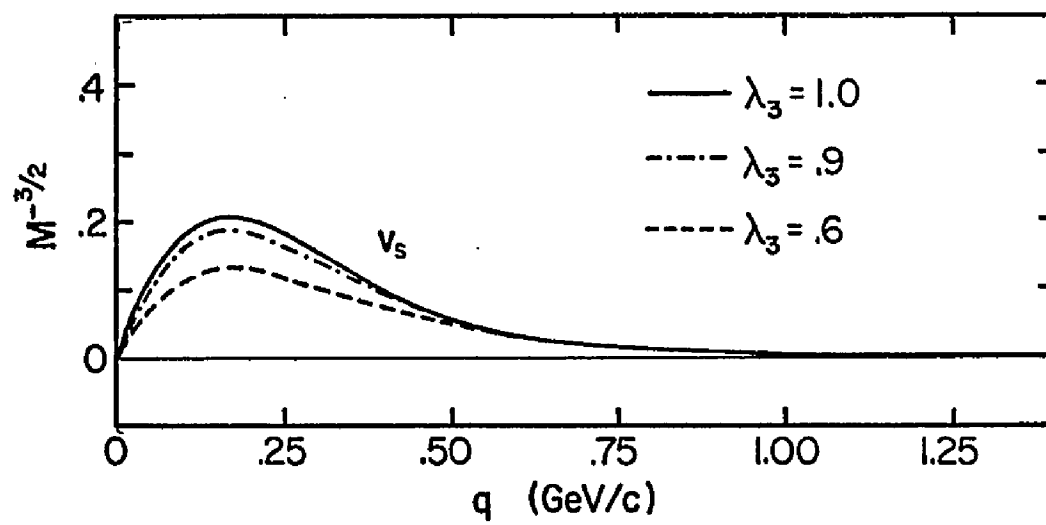
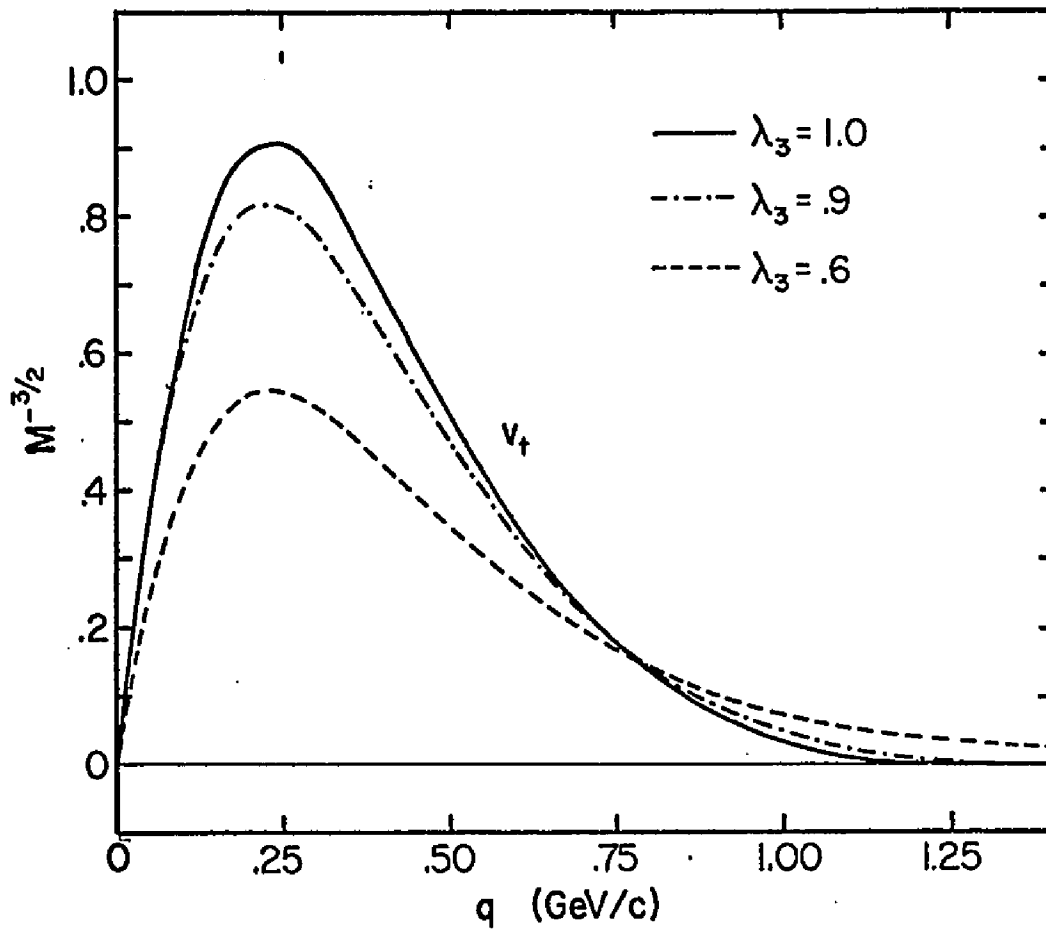


Figure 18. The momentum space S state wave functions,  $u$ , for  $\lambda_{\omega} = 1, .8, \text{ and } 0$ . The right most curves are to be read from the right scale.

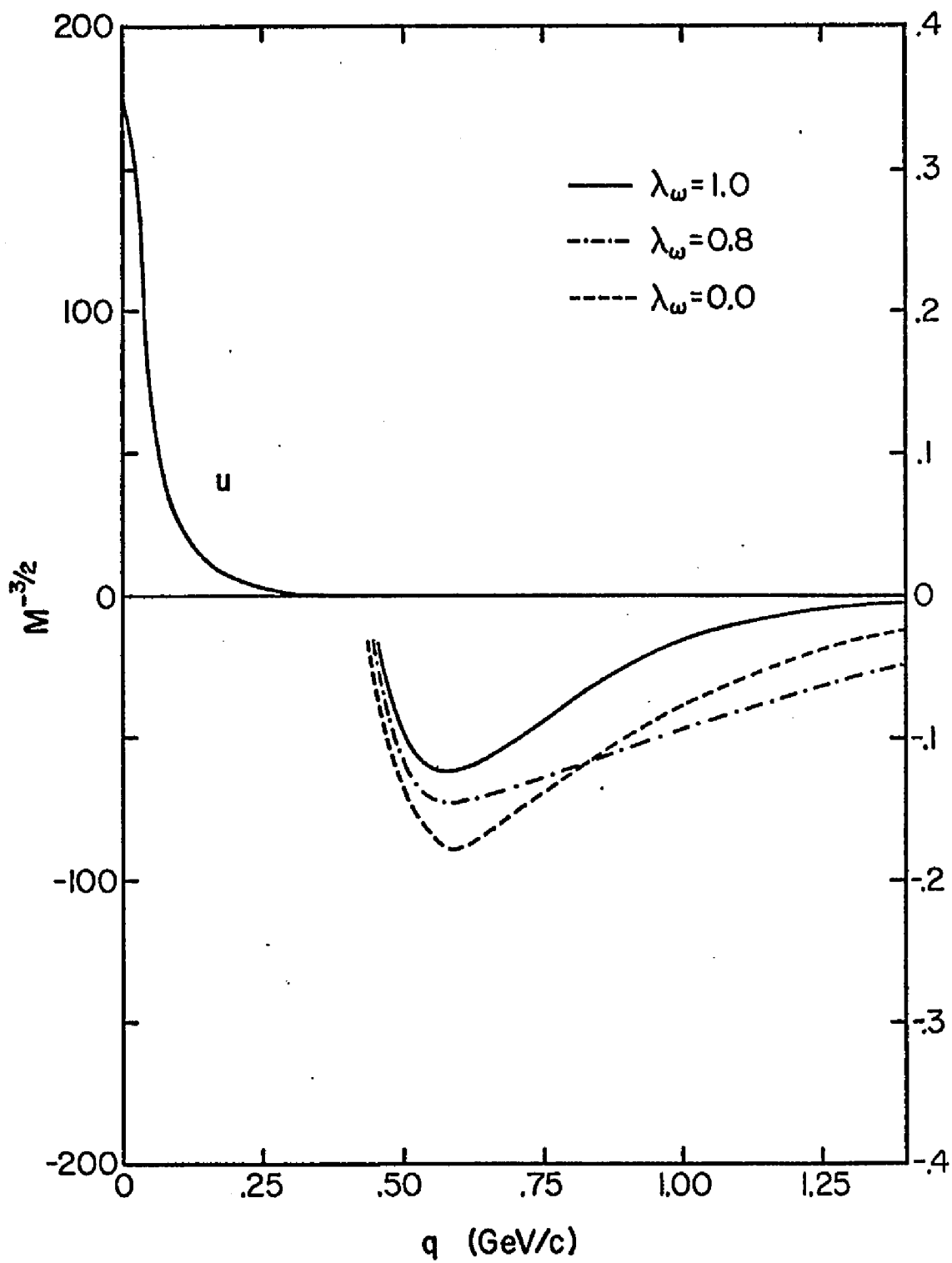


Figure 19. The momentum space D state wave functions,  $w$ , for  
 $\lambda_\omega = 1, .8, \text{ and } 0.$

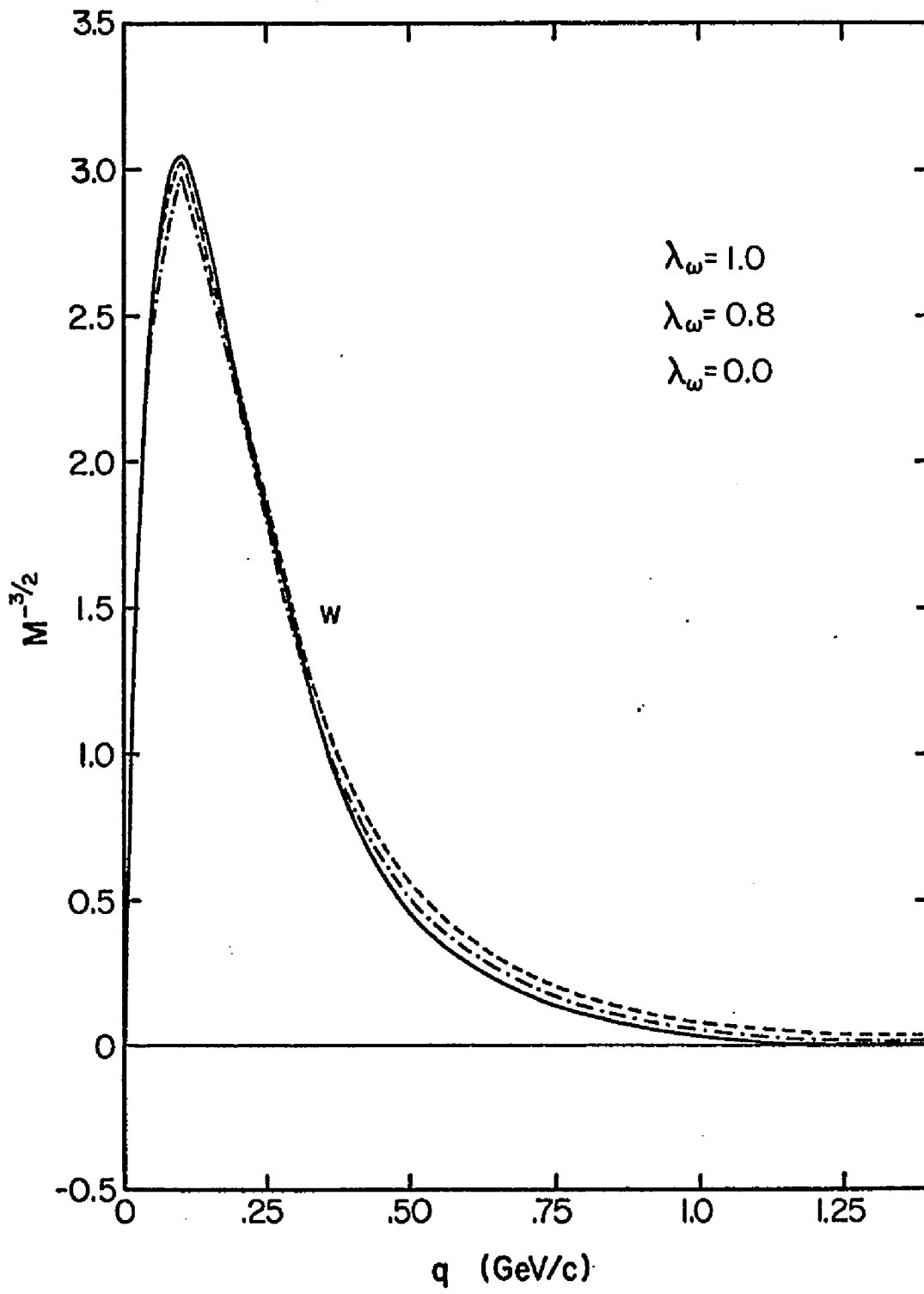


Figure 20. The momentum space P state wave functions,  $v_t$  and  $v_s$ ,  
for  $\lambda_\omega = 1, .8, \text{ and } 0$ .

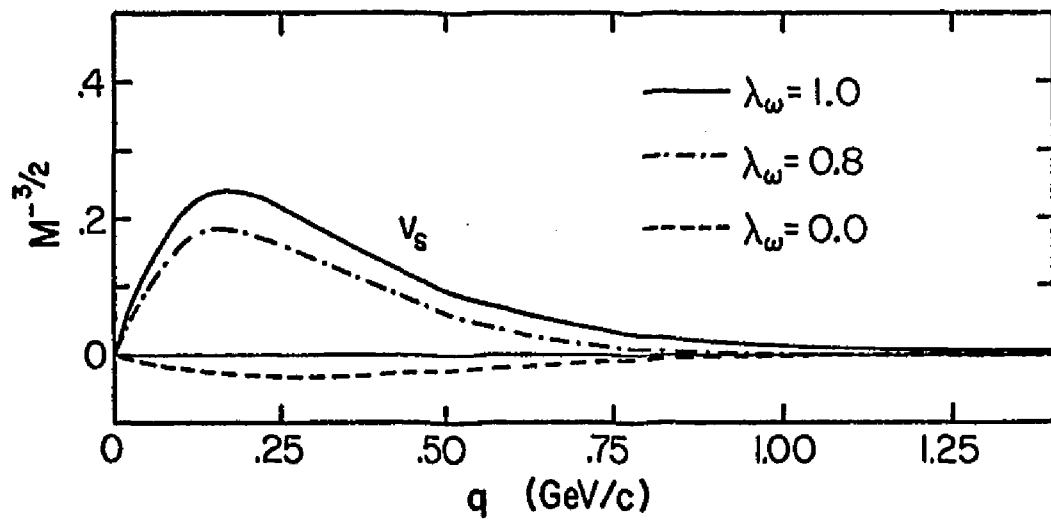
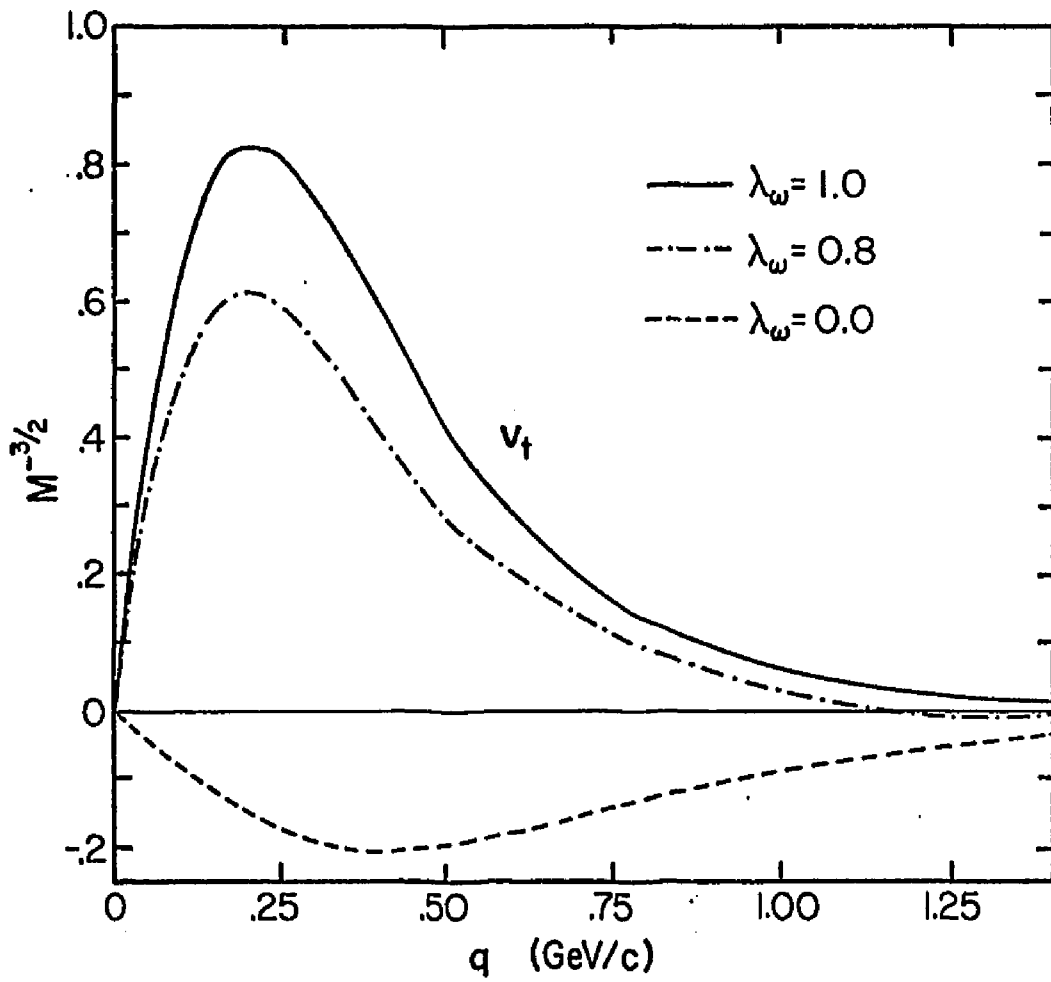


TABLE 2

THE NORMALIZED DIMENSIONLESS COEFFICIENTS  
 $C_{ji}$  FOR THE  $\lambda_4 = 1$  INTERACTION

	$F_1 = F$	$F_2 = G$	$F_3 = H$	$F_4 = I$
$C_{j1}$	3.1666	53.6432	50.8629	8.056
$C_{j2}$	- .7390	- 5.2345	- 4.7053	-3.5277
$C_{j3}$	- .8966	- .87935	- 1.5899	- .0666
$C_{j4}$	.4515	1.3489	.9734	.4001
$C_{j5}$	.2869	.0109	.1317	- .0787
$C_{j6}$	- .2025	- .1405	- .0855	- .0565
$C_{j7}$	- .02435	.0189	.0088	.0016

TABLE 3

THE NORMALIZED DIMENSIONLESS COEFFICIENTS  
 $C_{ji}$  FOR THE  $\lambda_3 = 1$  INTERACTION

	$F_1 = F$	$F_2 = G$	$F_3 = H$	$F_4 = I$
$C_{j1}$	3.1638	53.6549	50.8360	8.0522
$C_{j2}$	- .7303	- 5.2288	- 4.6802	-3.5238
$C_{j3}$	- .9047	- .8883	- 1.6009	- .0687
$C_{j4}$	.4525	1.3527	.9733	.40025
$C_{j5}$	.29146	.0114	.1342	- .0785
$C_{j6}$	- .2055	- .1416	- .0859	.0566
$C_{j7}$	- .0256	.0179	.0071	.0019

TABLE 4

THE NORMALIZED DIMENSIONLESS COEFFICIENTS  
 $C_{ji}$  FOR THE  $\lambda_3 = .9$  INTERACTION

	$F_1 = F$	$F_2 = G$	$F_3 = H$	$F_4 = I$
$C_{j1}$	3.0045	53.3690	45.7736	9.3906
$C_{j2}$	- .5920	- 5.1909	- 4.4830	-3.2431
$C_{j3}$	- .8135	- .6324	- 1.1731	- .04615
$C_{j4}$	.3763	1.1804	.8016	.3535
$C_{j5}$	.2682	- .0335	.0746	- .0753
$C_{j6}$	- .1936	- .0744	- .0448	- .0370
$C_{j7}$	- .0202	.0057	- .0024	.0047

TABLE 5

THE NORMALIZED DIMENSIONLESS COEFFICIENTS  
 $C_{ji}$  FOR THE  $\lambda_3 = .6$  INTERACTION

	$F_1 = F$	$F_2 = G$	$F_3 = H$	$F_4 = I$
$C_{j1}$	2.5164	52.5196	30.6370	13.8877
$C_{j2}$	- .1720	- 5.1178	- 3.7358	- 2.5853
$C_{j3}$	- .5578	.2156	- .0414	.0956
$C_{j4}$	.1979	.5025	.2507	.1604
$C_{j5}$	.1136	.0197	.0131	- .0205
$C_{j6}$	- .0803	.0315	.0248	.0028
$C_{j7}$	- .0028	- .00355	- .0123	.0011

TABLE 6

THE NORMALIZED DIMENSIONLESS COEFFICIENTS  
 $C_{ji}$  FOR THE  $\lambda_{\omega} = 1$  INTERACTION

	$F_1 = F$	$F_2 = G$	$F_3 = H$	$F_4 = I$
$C_{j1}$	3.2194	51.9382	47.0125	4.2773
$C_{j2}$	-1.1355	- 3.1421	- 2.7044	-1.7328
$C_{j3}$	- .1699	- .3757	- .8708	- .2560
$C_{j4}$	.1006	.3373	.1552	.08025
$C_{j5}$	.0924	.2030	.1760	.0203
$C_{j6}$	- .0143	.0288	.0454	- .0102
$C_{j7}$	- .0163	.0002	.0037	- .00945

TABLE 7

THE NORMALIZED DIMENSIONLESS COEFFICIENTS  
 $C_{ji}$  FOR THE  $\lambda_w = .8$  INTERACTION

	$F_1 = F$	$F_2 = G$	$F_3 = H$	$F_4 = I$
$C_{j1}$	2.6585	50.3991	34.8232	8.4459
$C_{j2}$	- .1102	- 2.8823	- 1.0785	-2.0986
$C_{j3}$	-1.2123	- .4381	- 1.07415	.2391
$C_{j4}$	.9026	.6467	.2679	- .0601
$C_{j5}$	- .1471	- .0056	.1165	- .0010
$C_{j6}$	- .2971	.0890	.0209	.0548
$C_{j7}$	.4113	.0052	.04765	- .0686

TABLE 8

THE NORMALIZED DIMENSIONLESS COEFFICIENTS  
 $C_{ji}$  FOR THE  $\lambda_{\omega} = 0$  INTERACTION

	$F_1 = F$	$F_2 = G$	$F_3 = H$	$F_4 = I$
$C_{j1}$	.6863	50.0865	-8.1706	26.0757
$C_{j2}$	2.9132	- 1.6461	4.14465	- 1.8845
$C_{j3}$	-2.3009	- .8044	-1.0354	.1686
$C_{j4}$	.5689	.3365	- .1785	.1167
$C_{j5}$	.2855	.2640	.1847	.0117
$C_{j6}$	- .2858	- .0757	- .0508	.04485
$C_{j7}$	.1229	.0631	.0380	- .0013

Figure 21. The dimensionless momentum space invariant amplitude,  $F$ ,  
for  $\lambda_3 = 1, .9, \text{ and } .6$ .

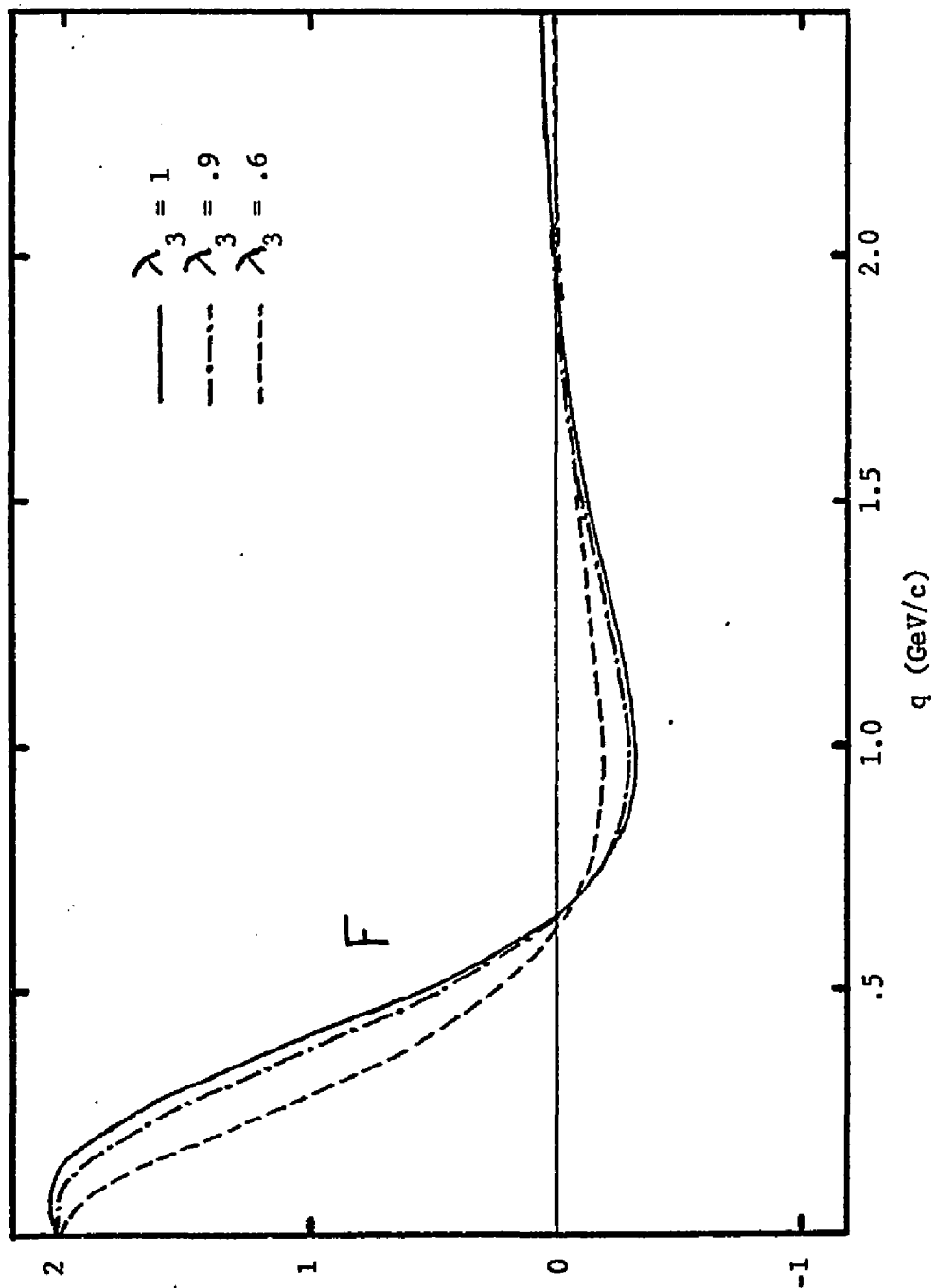


Figure 22. The dimensionless momentum space invariant amplitude,  $G$ , for  $\lambda_3 = 1, .9, \text{ and } .6$ . The right most curves are to be read from the right scale.

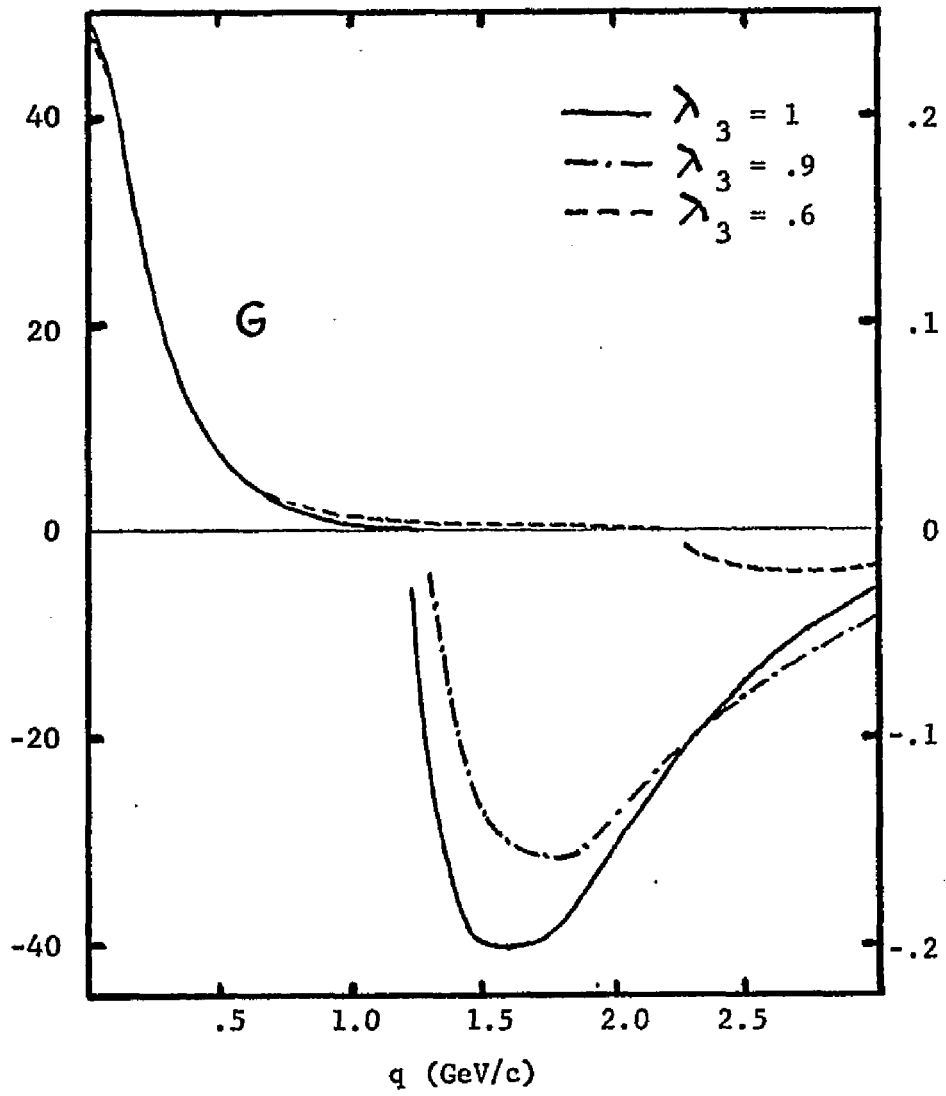


Figure 23. The dimensionless momentum space invariant amplitude,  $H$ ,  
for  $\lambda_3 = 1, .9, \text{ and } .6$ .

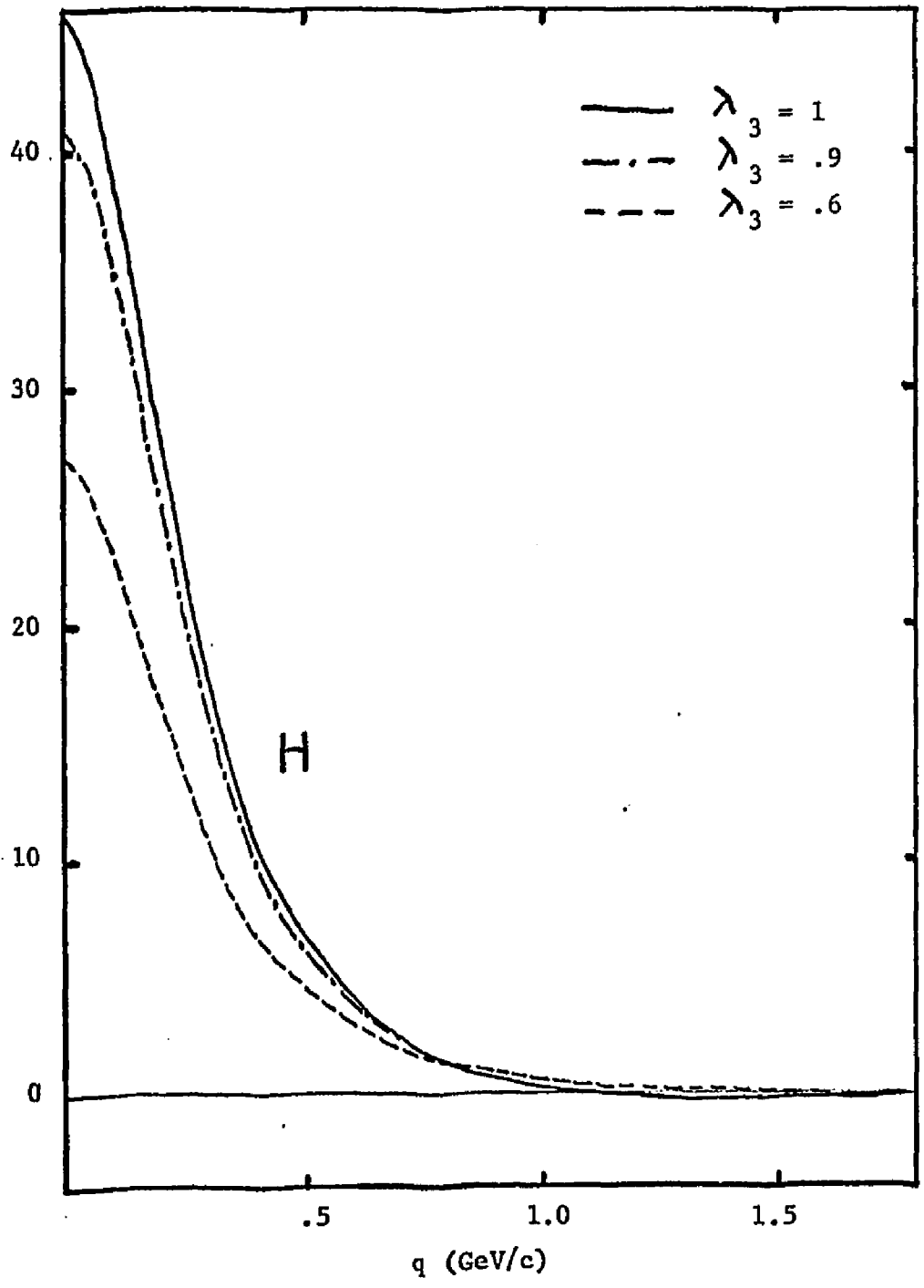


Figure 24. The dimensionless momentum space invariant amplitude,  $I$ ,  
for  $\lambda_3 = 1, .9, \text{ and } .6$ .

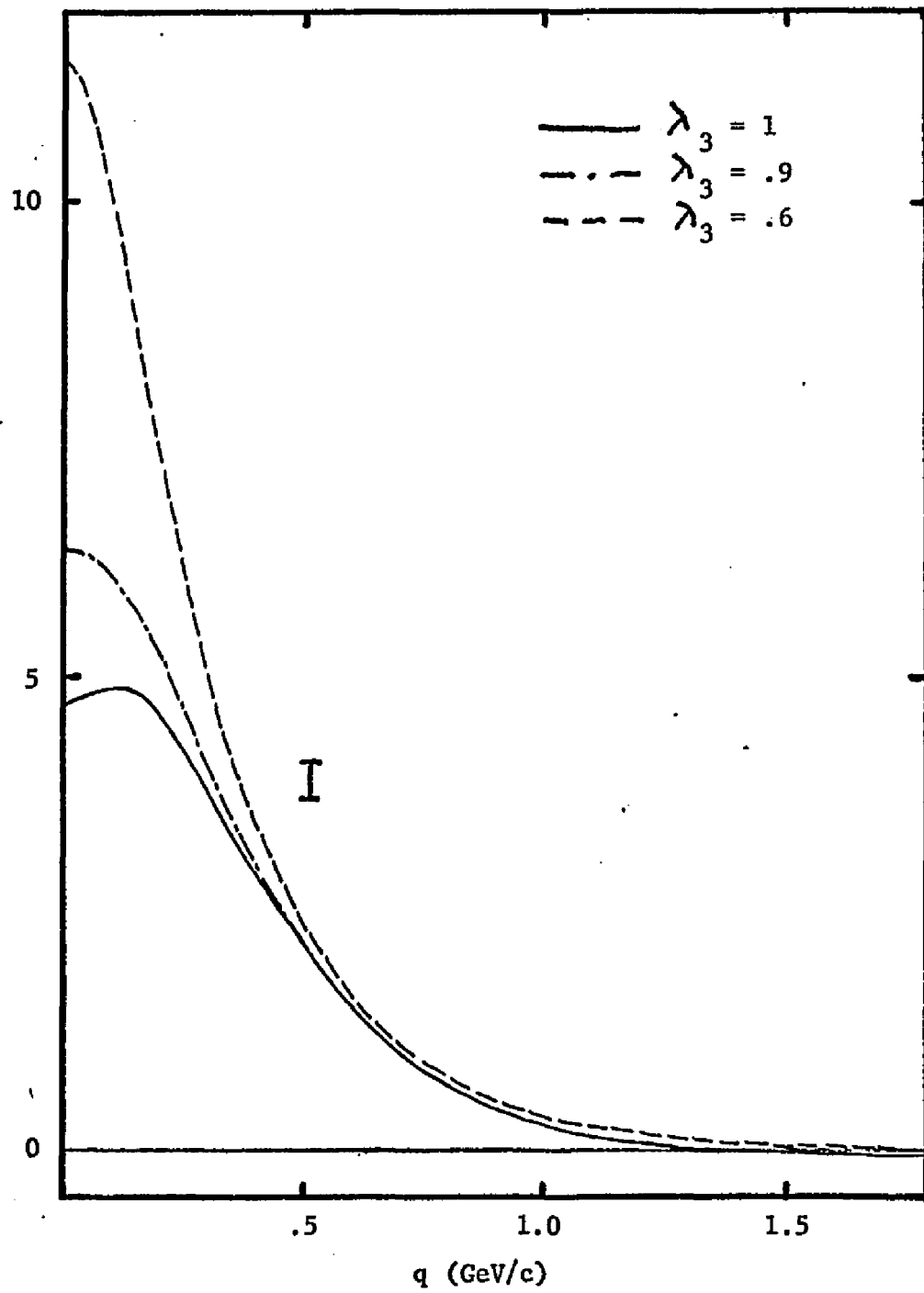


Figure 25. The dimensionless momentum space invariant amplitude,  $F$ ,  
for  $\lambda_\omega = 1, .8, \text{ and } 0$ .

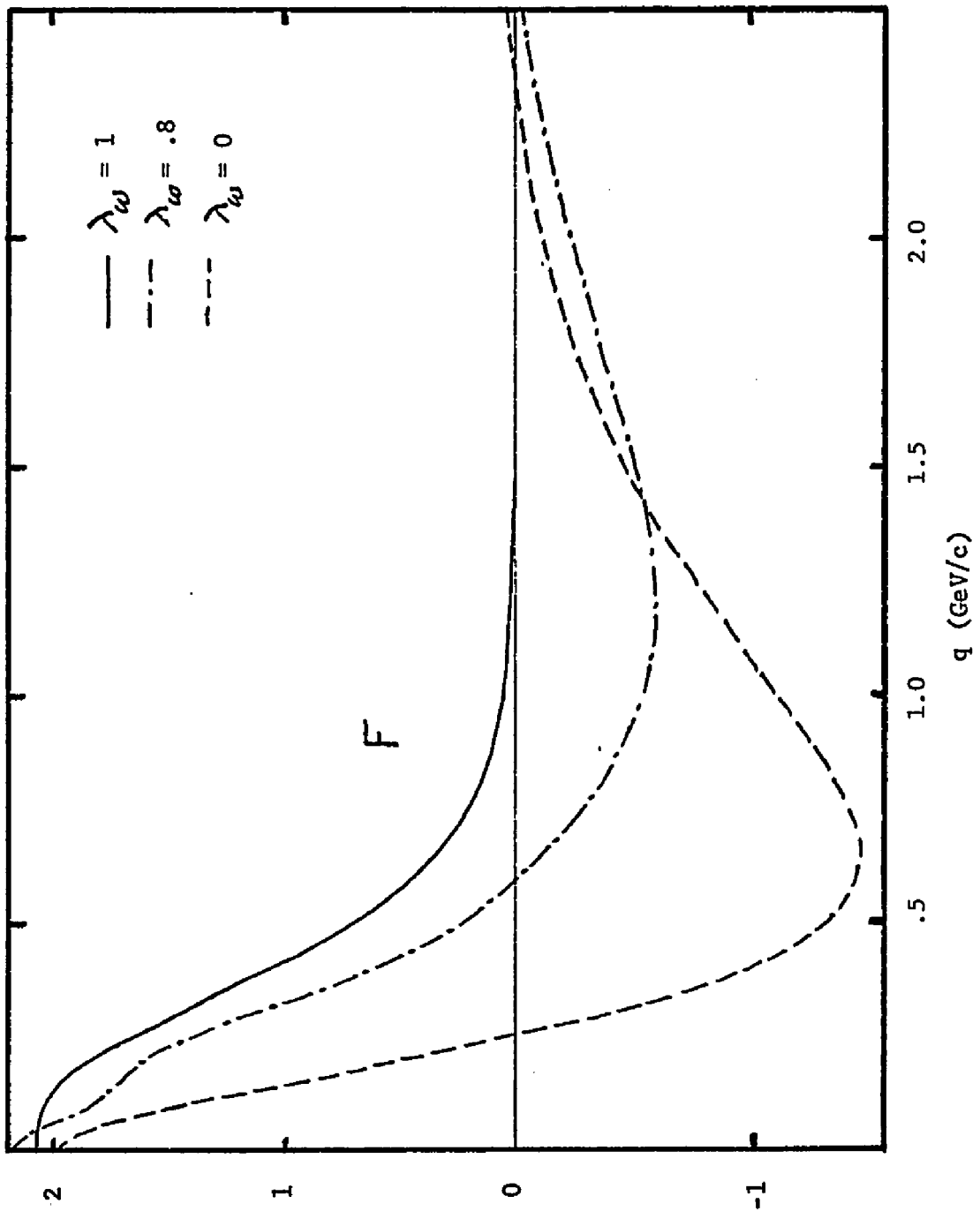


Figure 26. The dimensionless momentum space invariant amplitude,  $G$ , for  $\lambda_\omega = 1, .8, \text{ and } 0$ . The right most curve is to be read from the right scale.

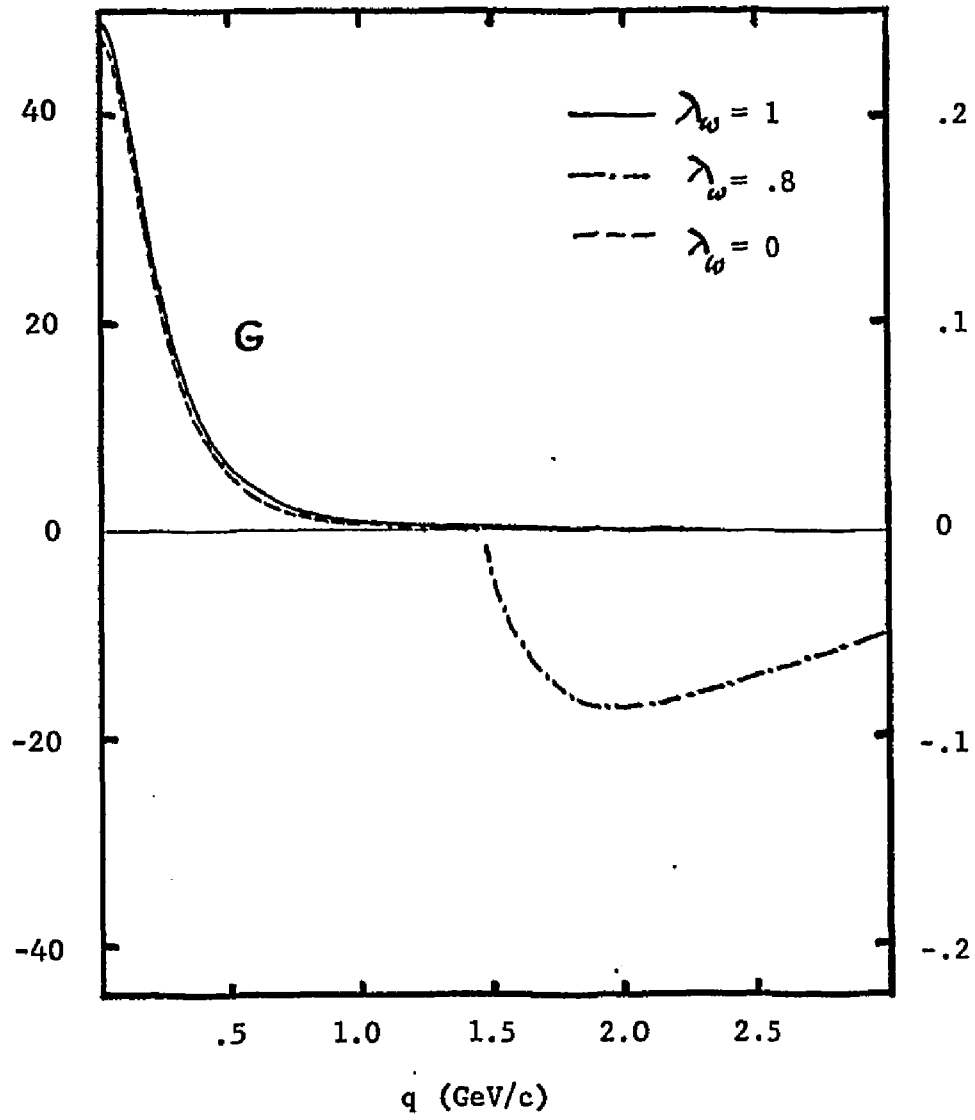


Figure 27. The dimensionless momentum space invariant amplitude,  $H$ ,  
for  $\lambda_\omega = 1, .8, \text{ and } 0$ .

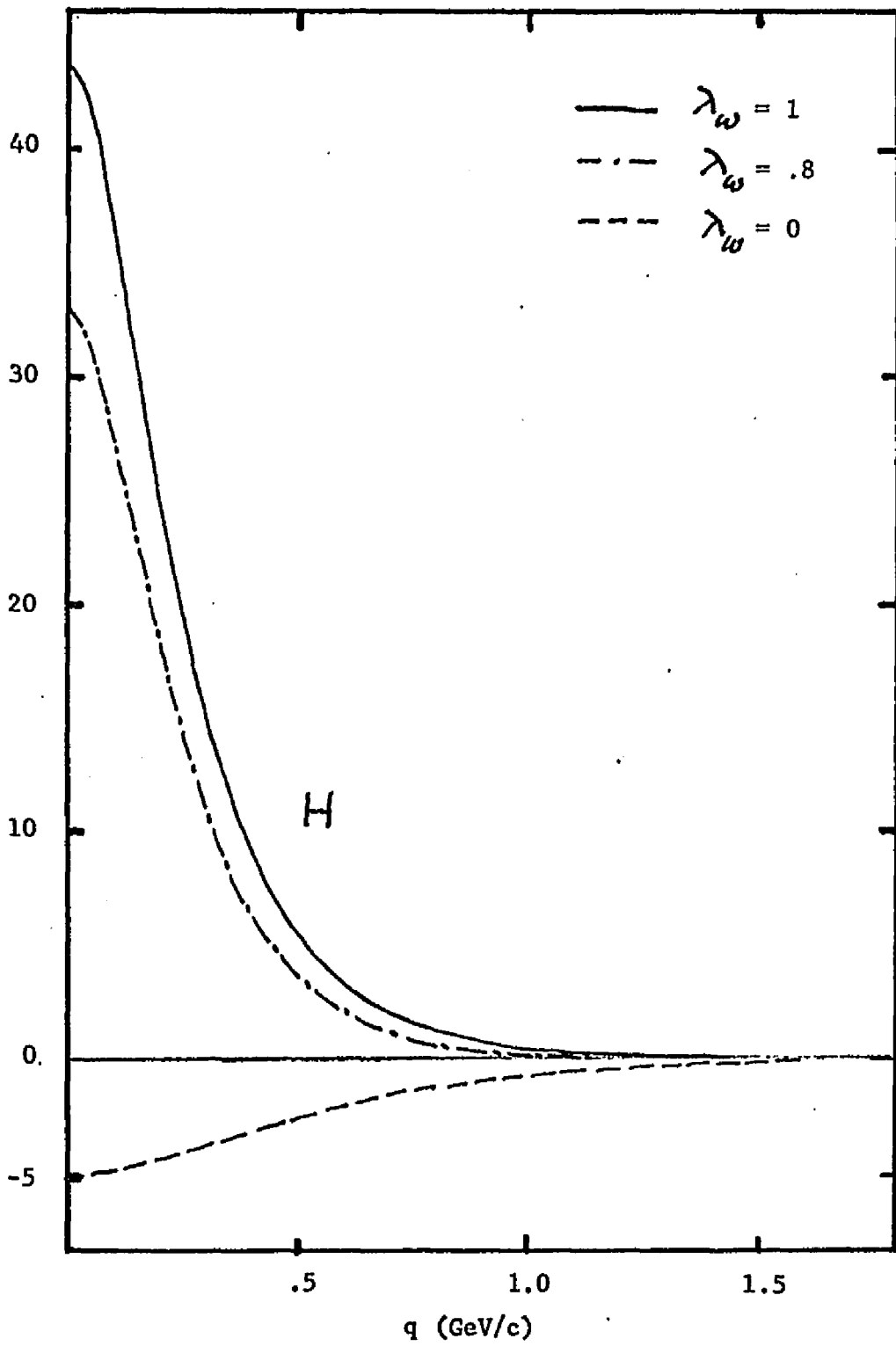
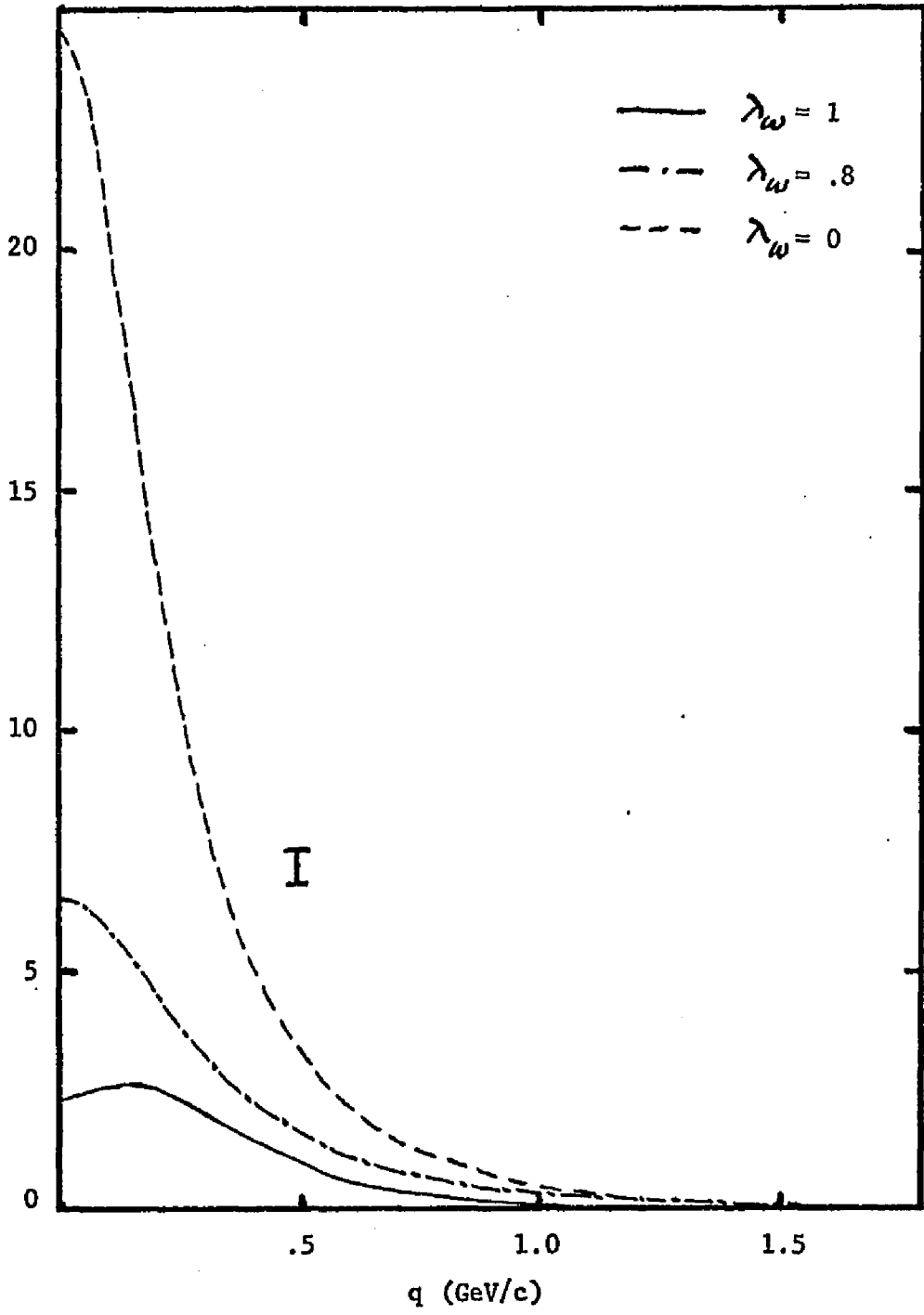


Figure 28. The dimensionless momentum space invariant amplitude,  $I$ ,  
for  $\lambda_w = 1, .8, \text{ and } 0$ .



## V. N-d SCATTERING AT 180°

There have been and are many attempts to explain the "hump" in the N-d scattering differential cross section data in the backward direction. Although the data has been around for many years, difficulties in reproducing the data are still present. Indeed, non-relativistic calculations of the one nucleon exchange (ONE) diagram (see figure 29) fall short in describing the data adequately<sup>19</sup> and hence other exchange mechanisms were folded in, such as the  $N^*$ .

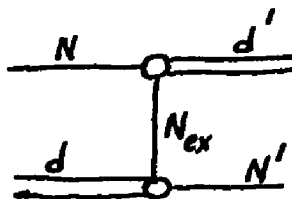


Figure 29

Although the  $N^*$  contributes a great deal to N-d scattering, its role as a deuteron constituent is not clear.<sup>20</sup>

In this chapter, we show the results of calculating the ONE diagram relativistically.<sup>21</sup> This idea is not a new one,<sup>22,23</sup> but the deuteron wave functions we use are new ( $\lambda_3$  and  $\lambda_\omega$  interactions).

The calculated differential cross section at 180° using our relativistic technique is

$$\frac{d\sigma}{d\Omega}_{CM} \Big|_{180^\circ} = \frac{1}{3} \left( \frac{D_0 M}{D_0 + E} \right)^2 \left\{ |M(1, \frac{1}{2}; 1, \frac{1}{2})|^2 + |M(1, -\frac{1}{2}; 1, -\frac{1}{2})|^2 + |M(0, -\frac{1}{2}; 0, \frac{1}{2})|^2 + 2 |M(1, -\frac{1}{2}; 0, \frac{1}{2})|^2 \right\} \quad (40)$$

where

$$M(1, \frac{1}{2}; 1, \frac{1}{2}) = -2 \left[ \theta \left( u - \frac{w}{\sqrt{2}} \right)^2 - 2\sqrt{3} \Lambda \left( u - \frac{w}{\sqrt{2}} \right) \frac{v_t}{\sqrt{2}} + 3M_d \frac{v_s^2}{2} \right]$$

$$M(1, \frac{1}{2}; 1, -\frac{1}{2}) = 0$$

$$M(1, \frac{1}{2}; 0, \frac{1}{2}) = -\sqrt{2} \left[ \theta \left( u + \sqrt{2}w \right) \left( u - \frac{w}{\sqrt{2}} \right) - \sqrt{3} \Lambda \left( u + \sqrt{2}w \right) \frac{v_t}{\sqrt{2}} \right. \\ \left. + \sqrt{3} \Lambda \left( u - \frac{w}{\sqrt{2}} \right) v_s - 3M_d \frac{v_s v_t}{\sqrt{2}} \right]$$

$$M(0, \frac{1}{2}; 0, \frac{1}{2}) = - \left[ \theta \left( u + \sqrt{2}w \right)^2 + 2\sqrt{3} \Lambda \left( u + \sqrt{2}w \right) v_s + 3M_d v_s^2 \right]$$

$$E_p = \sqrt{M^2 + p^2}$$

$$E_d = \sqrt{M_d^2 + p^2}$$

$$p = |\vec{p}_{cm}| =$$

$$Q = \frac{p}{M_d} (E_d - E_p)$$

$$\theta = 2 \sqrt{M^2 + Q^2} - M_d$$

$$\Lambda = \frac{M_d \theta Q}{M(M_d - \sqrt{M^2 + Q^2})}$$

(41)

and the wave functions  $u$ ,  $w$ ,  $v_t$ , and  $v_s$  have  $Q$  as their arguments.

The results obtained from equation 40 are illustrated in figures 30 and 31. It is clear from these figures that ignoring the deuteron's small component wave functions ( $v_t$ ,  $v_s$ ) in this process is not a good approximation. The P states,  $v_t$  and  $v_s$ , are, in fact, down from  $u$  and  $w$  by a factor  $M^{-1}$ ; however,  $v_t$  and  $v_s$  enter in equation 40 with a factor of  $M$ .

Figure 30. The ONE contribution to the differential cross section for N-d scattering at  $180^\circ$  with and without  $(v_t = v_s = 0)$ , NR, the P states for  $\lambda_3$  wave functions. The experimental data is found in reference 24.

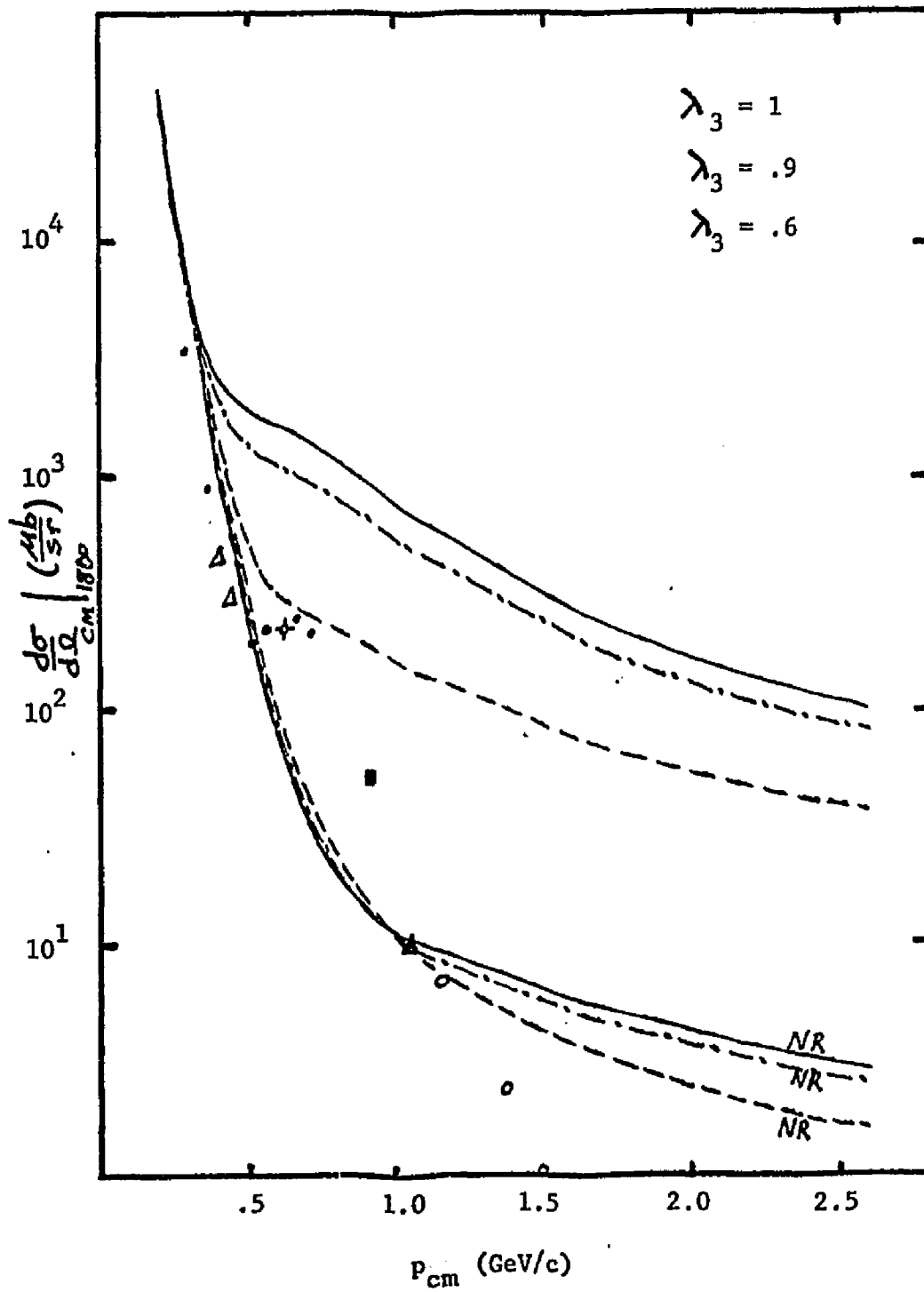
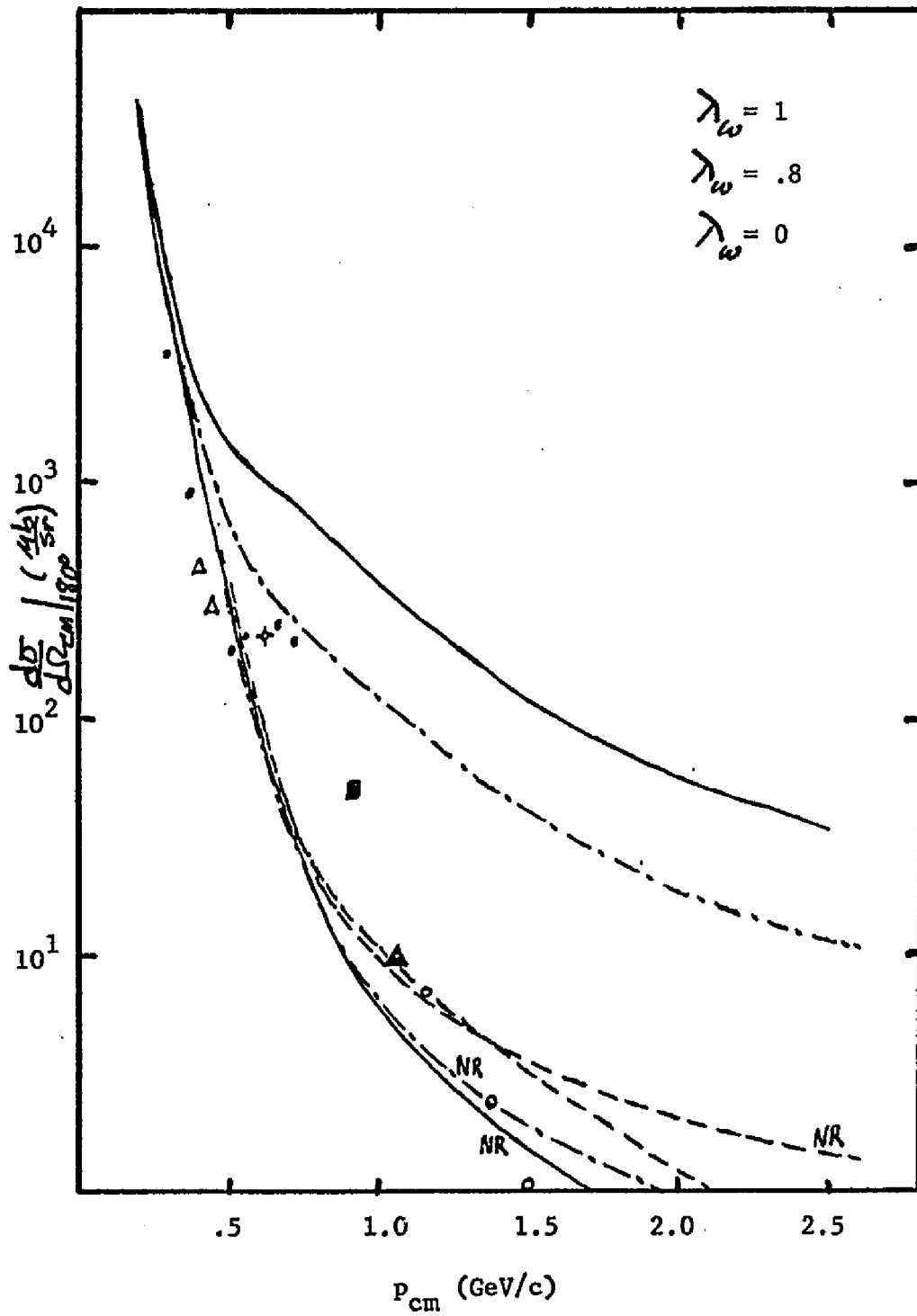


Figure 31. The ONE contribution to the differential cross section for N-d scattering at  $180^\circ$  with and without  $(v_t = v_s = 0)$ , NR, the P states for  $\lambda_w$  wave functions. The experimental data is found in reference 24.



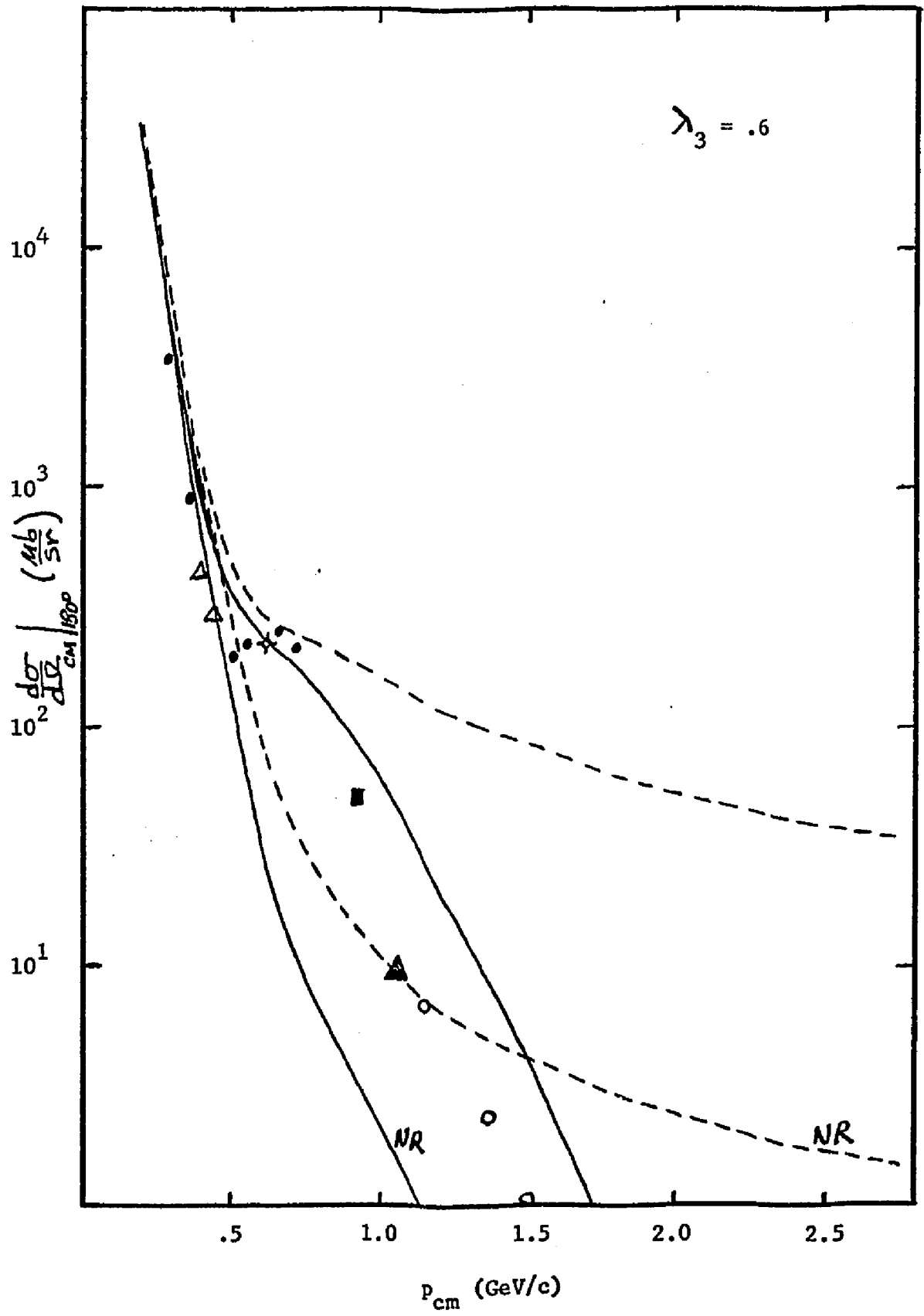
The slow fall off of the relativistic differential cross sections is due to the variable  $Q$ ; <sup>20</sup> as the CM incoming nucleon momentum,  $P_{CM}$ , goes to infinity,  $Q$  goes to a constant value of  $3M/4$ . This fact seems to have gone unnoticed in the literature. The data, on the other hand, falls very fast with  $Q$ .

At low momentum,  $Q$  is approximately  $P_{CM}/2$ . This, however, is a well known result and is apparently used as the argument of the wave functions in much of the literature, <sup>25</sup> even though  $Q$  is defined in the same way as in equation 41. Figure 32 illustrates the differential cross sections for wave functions with an argument of  $Q$  and an argument of  $P_{CM}/2$ . As can be seen from this figure, the difference is dramatic.

An understanding of the effect that the proper variable,  $Q$ , has on the differential cross section may be found when multiple scattering contributions are included.

Furthermore, N-d scattering may furnish an important constraint on the optimum value to be taken for  $\lambda$  in deuteron processes. <sup>4,5</sup>

Figure 32. The ONE contribution to the differential cross section with Q (dashed curves) and P/2 (solid curves) as the arguments of the  $\lambda_3 = .6$  wave functions. The data is the same as in figures 30 and 31.



## VI. SUMMARY

This work has presented several new sets of deuteron wave functions obtained numerically from exact relativistic interactions.<sup>26</sup>

Though the potentials arising from our interactions are purely attractive in the non-relativistic limit, we conclude that the repulsion is due to the relativistic structure of our equation.

The D state probabilities for all the solutions obtained ranged from 5 percent to 6.4 percent, and with the total P state probabilities ranging from .6 percent to 2.8 percent, it was shown that the enhancements obtained from N-d scattering were widely varying and were due mainly to the amount of P state present.

A further demonstration of our relativistic techniques was found in Appendix D. Here, calculations were performed for Hydrogen-like atoms.

Our relativistic technique, the wave functions obtained from the technique, and the contribution that the combination gives to, at least, N-d scattering and pionic disintegration of the deuteron, suggests, perhaps, a new and exciting realm of inquiry.

**APPENDIX**

## APPENDIX A

This appendix contains a description and a list of all the identities used in performing the  $d\phi_k$  and  $dZ$  integrations. Also contained here are definitions used for Second Regularization.

 $d\phi_k$  Integration

To integrate  $\int d\phi_k K^\mu$ , there are only two 4-vectors that contribute,  $q^\mu$  and  $W^\mu$ . Hence a linear combination of  $q^\mu$  and  $W^\mu$  expresses the result

$$\frac{1}{2\pi} \int d\phi_k K^\mu = a q^\mu + b W^\mu \quad (\text{A.1})$$

The coefficients  $a$  and  $b$ , being composed of inner products of 4-vectors, are written

$$a = \frac{k \cdot W q \cdot W - W^2 k \cdot q}{(q \cdot W)^2 - W^2 q^2} \quad (\text{A.2a})$$

$$b = \frac{q \cdot W k \cdot q - q^2 k \cdot W}{(q \cdot W)^2 - W^2 q^2} \quad (\text{A.2b})$$

Similarly we have

$$\frac{1}{2\pi} \int d\phi_k K^\mu K^\nu = c q^\mu q^\nu + d q^\mu W^\nu + e W^\mu W^\nu \quad (\text{A.3})$$

where

$$c = \frac{w \cdot k}{w^2} a - \frac{w \cdot g}{w^2} d \quad (\text{A.4a})$$

$$d = \frac{3}{2} a^2 - \frac{1}{2} \frac{[(k \cdot w)^2 - k^2 w^2]}{(g \cdot w)^2 - w^2 g^2} \quad (\text{A.4b})$$

$$e = \frac{(g \cdot w)^2 - w^2 g^2}{3 w^2} - \frac{1}{3} \frac{(k \cdot w)^2 - k^2 w^2}{w^2} \quad (\text{A.4c})$$

We specialize now to the center of mass of the two nucleons, thereby constraining our coefficients a, b, c, d, and e to be

$$a = \frac{|\vec{k}|}{|\vec{g}|} P_1(z)$$

$$b = \frac{k_0}{M_d} - \frac{g_0}{M_d} a$$

$$c = \frac{k_0 - g_0}{M_d} d$$

$$d = \frac{|\vec{k}|^2}{|\vec{g}|^2} P_2(z)$$

$$e = \frac{|\vec{k}|}{3} [P_2(z) - P_0(z)]$$

$$z = \hat{k} \cdot \hat{g}$$

(A.5)

$P_0(Z)$ ,  $P_1(Z)$ , and  $P_2(Z)$  are Legendre Polynomials of the first kind and our metric is such that  $q^2 = q_0^2 - |\vec{q}|^2$

Thus, using these integration identities,<sup>27</sup> we construct further identities:

$$\frac{1}{2\pi} \int d\phi_k K \cdot \xi = a g \cdot \xi$$

$$\frac{1}{2\pi} \int d\phi_k K = a g + b \psi$$

$$\frac{1}{2\pi} \int d\phi_k \left(\frac{\psi}{2} + K + M\right) = M(1+a) + b' \psi$$

$$\frac{1}{2\pi} \int d\phi_k \delta^5 \left(\frac{\psi}{2} + K + M\right) \delta^5 = M(1-a) - b' \psi$$

$$\frac{1}{2\pi} \int d\phi_k \left(\frac{\psi}{2} + K + M\right) K \cdot \xi = M(a+d) g \cdot \xi + c' g \cdot \xi \psi + e \xi$$

$$\frac{1}{2\pi} \int d\phi_k \delta^5 \left(\frac{\psi}{2} + K + M\right) K \cdot \xi \delta^5 = M(a-d) g \cdot \xi - c' g \cdot \xi \psi - e \xi$$

$$\frac{1}{2\pi} \int d\phi_k \delta^5 \left(\frac{\psi}{2} + K + M\right) P \delta^5 = X - 2e$$

$$\frac{1}{2\pi} \int d\phi_k \delta^5 \left(\frac{\psi}{2} + K + M\right) P K \cdot \xi \delta^5 = Y g \cdot \xi$$

$$\frac{1}{2\pi} \int d\phi_k \delta^5 \left(\frac{\psi}{2} + K + M\right) P \delta^5 = 2Md' g \cdot \xi + (c' - b') g \cdot \xi \psi + e \xi$$

(A.6)

where

$$b' = \frac{1}{2} + b - \frac{a}{2}$$

$$\begin{aligned}
 c' &= \frac{a}{2} + c - \frac{d}{2} \\
 d' &= \frac{1}{2} - a + \frac{d}{2} \\
 X &= 2e + (a-1)2M^2 + 2M_d E_g b' \\
 Y &= 2M_d E_g c' - 2M^2(a-d) + 2e \\
 P &= g - k
 \end{aligned}$$

(A.7)

It is also useful to note that:

$$\begin{aligned}
 -\frac{aM_d E_g}{4M} + \frac{M_d E_k}{4M} - \frac{b'M_d^2}{4M} &= 0 \\
 -\frac{dE_g M_d}{2M} - \frac{c'M_d^2}{2M} + \frac{aM_d E_k}{2M} &= 0 \\
 b' &= \frac{E_k - aE_g}{M_d} \\
 c' &= \frac{aE_k - dE_g}{M_d}
 \end{aligned}$$

(A.8)

#### dZ Integration

The Z integration affects the  $P_\ell$ 's and the exchange particle propagators only.

Consider the exchange propagator:

$$\frac{1}{M_{ex}^2 - P^2} = \frac{1}{M_{ex}^2 - (g_0 - k_0) + (\vec{g}_0 - \vec{k})^2} = \frac{1}{M_{ex}^2 + \vec{k}^2 + \vec{g}_0^2 - 2|\vec{g}_0||\vec{k}|z - (E_g - E_k)^2} \quad (A.9)$$

Now using the following theorem<sup>28</sup>:

$$\int_{-1}^1 \frac{P_\ell(z) dz}{y_1 - y_2 z} = \frac{1}{y_2} \int_{-1}^1 \frac{P_\ell(z) dz}{y_1/y_2 - z} = \frac{2}{y_2} Q_\ell\left(\frac{y_1}{y_2}\right) \quad (\text{A.10})$$

where the  $Q_\ell$ 's are the Legendre Polynomials of the second kind with their arguments being  $y_1/y_2$ , we define

$$\begin{aligned} y_1 &= M_{ex}^2 + |\vec{k}|^2 + |\vec{q}|^2 - (E_\phi - E_k)^2 \\ y_2 &= 2|\vec{k}||\vec{q}| \end{aligned} \quad (\text{A.11})$$

Next, we cast equations 30a through 30d in the following symbolic form:

$$\begin{aligned} F_\alpha &= \frac{\lambda}{(2\pi)^2} \left( \frac{3g^2 d^2 k G_{\alpha\beta}^\pi(p_\ell) F_\beta}{2M_\beta E_k (2E_k - M_\beta) (M_\beta^2 - p^2)} + \frac{1}{(2\pi)^2} \left( \frac{g^2 d^2 k G_{\alpha\beta}^\sigma(p_\ell) F_\beta}{2M_\beta E_k (2E_k - M_\beta) (M_\beta^2 - p^2)} \right) \right) \\ &= \frac{\lambda 3g^2}{(2\pi)^2} \left( \frac{k^2 dk dz G_{\alpha\beta}^\pi(p_\ell) F_\beta}{2M_\beta E_k (2E_k - M_\beta) 2kq (\frac{y_1}{y_2} - z)} + \frac{g^2}{(2\pi)^2} \left( \frac{k^2 dk dz G_{\alpha\beta}^\sigma(p_\ell) F_\beta}{2M_\beta E_k (2E_k - M_\beta) 2kq (\frac{y_1}{y_2} - z)} \right) \right) \\ &= \lambda \left( \frac{g^2}{4\pi} \right) \frac{3}{2\pi q} \left( \frac{k dk G_{\alpha\beta}^\pi(p_\ell) F_\beta}{M_\beta E_k (2E_k - M_\beta)} + \left( \frac{g^2}{4\pi} \right) \frac{1}{2\pi q} \left( \frac{k dk G_{\alpha\beta}^\sigma(p_\ell) F_\beta}{M_\beta E_k (2E_k - M_\beta)} \right) \right) \end{aligned} \quad (\text{A.12})$$

Equation A.12 is now identified with equation 31 where A, B,  $\beta$ , D, E,  $\beta'$ , D', X, Y are just a, b, c, d, e,  $b'$ ,  $c'$ ,  $d'$ , X, Y respectively with the  $P_\ell$ 's being replaced by the  $Q_\ell$ 's.

Second Regularization Procedures

Consider

$$Q_\ell(x) = \frac{1}{2} \int_{-1}^1 \frac{P_\ell(x') dx'}{x-x'} \quad ; \quad x' \equiv z$$

$$x = \frac{\mu_{ex}^2 - 2M^2 + 2E_K E_\beta}{2K\beta} \quad (\text{A.13})$$

So,

$$\frac{dQ_\ell(x)}{dx} = -\frac{1}{2} \int_{-1}^1 \frac{P_\ell(x') dx'}{(x-x')^2} = Q_\ell'(x) \quad (\text{A.14})$$

The integral in equation A.14 is precisely the Second Regularization contribution within a factor,  $-(M_R^2 - \mu_{ex}^2)/2K\beta$ .

Therefore, replace  $Q_\ell$  by  $-(M_R^2 - \mu_{ex}^2) Q_\ell' / 2K\beta$ .

We use:

$$P_0(z) = 1$$

$$P_1(z) = z$$

$$P_2(z) = \frac{1}{2} (3z^2 - 1)$$

$$Q_0(x) = \frac{1}{2} \ln \left( \frac{x+1}{x-1} \right)$$

$$Q_1(x) = x Q_0(x) - 1$$

$$Q_2(x) = \frac{3}{2} x^2 Q_0(x) - \frac{1}{2} Q_0(x) - \frac{3}{2} x$$

(A.15)

## APPENDIX B

We list here the deuteron moment formulae used in this work. Without further ado, the non-relativistic electric quadrupole and magnetic dipole moments are well known and are written:

$$Q = \frac{M_d^2 \sqrt{2}}{10} \int_0^\infty r^2 dr \left[ uW - \frac{W^2}{\sqrt{8}} \right] \quad (\text{B.1})$$

$$\mu_d = (F_1 + F_2) \left(1 - \frac{3}{2} P_D\right) + F_1 \frac{3}{4} P_D \quad (\text{B.2})$$

where U and W are the deuteron's S and D state wave functions in position space respectively,  $F_1 = 1$ ,  $F_2 = -.12$ ,  $P_D$  is the D-state probability, and Q (Quadrupole Moment) and  $\mu_d$  (Dipole moment) are measured in units of  $e/M_d^2$  and nuclear magnetons respectively.

The relativistic quadrupole moment<sup>29</sup> in position space is:

$$\begin{aligned} Q = & \frac{M_d^2 \sqrt{2}}{10} \int_0^\infty r^2 dr \left[ uW - \frac{W^2}{\sqrt{8}} + \frac{v_t^2}{\sqrt{8}} - \frac{v_s^2}{\sqrt{8}} \right. \\ & \left. + W\hat{u} + u\hat{W} - \frac{W\hat{W}}{\sqrt{2}} \right] \\ & + M_d^2 [1 + 2F_2] \int_0^\infty dr \left\{ \frac{3}{20M^2} (\sqrt{2} r W u' - \sqrt{2} W u - r W W') \right. \\ & \left. + \frac{r}{6M} \left[ u \left( \frac{\sqrt{3}}{2} v_t + \sqrt{3} v_s \right) - W \left( \frac{2}{5} \sqrt{3} v_t - \frac{\sqrt{3}}{5} v_s \right) \right] \right\} \end{aligned}$$

$$\hat{u} = \frac{1}{2M^2} \left( -\frac{d^2}{dr^2} + MB \right) u$$

$$\hat{w} = \frac{1}{2M^2} \left( -\frac{d^2}{dr^2} + \frac{6}{r^2} + MB \right) w$$

$$w' = \frac{dw}{dr}$$

$$u' = \frac{du}{dr}$$

(B.3)

B is the deuteron's binding energy.

The relativistic magnetic dipole moment<sup>29</sup> in position space

is:

$$\begin{aligned} \mathcal{M}_d = & (F_1 + F_2) \left( 1 - \frac{3}{2} P_D - P_S - \frac{3}{2} P_t \right) - \sqrt{2} F_2 \int_0^\infty dr v_t v_S \\ & + F_2 \left( \frac{3}{4} P_D + \frac{1}{4} P_t - \frac{1}{2} P_S + \Delta \right) \end{aligned}$$

$$\Delta = \int_0^\infty dr \frac{Mr}{\sqrt{3}} \left\{ v_t \left( \frac{u}{\sqrt{2}} - w \right) - v_S \left( u + \frac{w}{\sqrt{2}} \right) \right\}$$

(B.4)

where  $P_t$  and  $P_S$  are the  ${}^3P_1$  and  ${}^1P_1$  state probabilities respectively.

## APPENDIX C

In this appendix, the method used to solve for the invariant amplitudes F, G, H, and I are discussed.

We begin by considering reference 13 for an uncoupled-homogeneous linear integral equation of the form

(C.1)

Where  $G(x,y)$  and  $K(x,y)$  are the kernels and  $\lambda$  is a number to be determined so that equation C.1 can be solved for  $f(x)$  (i.e.,  $\lambda$  is an eigenvalue and  $f(x)$  is the eigenfunction).

The traditional methods used to solve equation C.1 are the Gauss Quadrature techniques which give rise to often large and hard-to-handle  $N$  by  $N$  matrices ( $N$  = number of gaussian points)

(C.2)

$W_j$  are the weight functions and  $i$  and  $j$  cover the same range.

Convergence of the sums in equation C.2, for sufficiently complicated kernels, may require that  $N = 96$ .

Because our kernels are complicated, the quadrature techniques do not appeal to us. So, we follow reference 13 and make a change of variables in equation C.1, yielding

(C.3)

## APPENDIX C

In this appendix, the method used to solve for the invariant amplitudes F, G, H, and I are discussed.

We begin by considering reference 13 for an uncoupled-homogeneous linear integral equation of the form

$$f(x) = \eta \int G(x,y) f(y) dy + \int K(x,y) f(y) dy \quad (C.1)$$

Where  $G(x,y)$  and  $K(x,y)$  are the kernels and  $\eta$  is a number to be determined so that equation C.1 can be solved for  $f(x)$  (i.e.,  $\eta$  is an eigenvalue and  $f(x)$  is the eigenfunction).

The traditional methods used to solve equation C.1 are the Gauss Quadrature techniques which give rise to often large and hard-to-handle  $N$  by  $N$  matrices ( $N$  = number of gaussian points)

$$f(x_i) = \eta \sum_{j=1}^N W_j G(x_i, x_j) f(x_j) + \sum_{j=1}^N W_j K(x_i, x_j) f(x_j) \quad (C.2)$$

$W_j$  are the weight functions and  $i$  and  $j$  cover the same range.

Convergence of the sums in equation C.2, for sufficiently complicated kernels, may require that  $N = 96$ .

Because our kernels are complicated, the quadrature techniques do not appeal to us. So, we follow reference 13 and make a change of variables in equation C.1, yielding

$$\tilde{f}(z) = \eta \left( \tilde{G}(z, z') \tilde{f}(z') \frac{dy}{dz} dz' + \int \tilde{K}(z, z') \tilde{f}(z') \frac{dy}{dz'} dz' \right) \quad (C.3)$$

Now, we expand  $\tilde{f}$  in a power series of Laguerre Polynomials

$$\tilde{f}(z) = e^{-z/2} \sum_{i=0}^n c_i L_i(z)$$

$c_i = \text{coefficients} \quad ; \quad n \ll N$  (C.4)

and use the ortho-normality property of Laguerre Polynomials to re-express equation C.3 as

$$c_i = \sum_{j=0}^n c_j (\eta U_{ji} + V_{ji})$$

$$U_{ji} = \iint \tilde{G}(z, z') e^{-z'/2} L_j(z') e^{-z/2} L_i(z) \frac{dy}{dz'} dz' dz$$

$$V_{ji} = \iint \tilde{K}(z, z') e^{-z'/2} L_j(z') e^{-z/2} L_i(z) \frac{dy}{dz'} dz' dz \quad (C.5)$$

Integrals  $U_{ji}$  and  $V_{ji}$  are calculated to very good accuracy while the equation for the coefficients is an  $n$  by  $n$  matrix and not an  $N$  by  $N$  matrix.

We next extend this procedure to  $s$  coupled channels and define the variable  $z$ . For  $s$  coupled channels ( $s = 4$  in our case), we have

$$f_{\mu}(x) = \eta \left( \sum_{\nu=1}^s G_{\mu\nu}(x, y) f_{\nu}(y) \right) dy + \sum_{\nu=1}^s \left( K_{\mu\nu}(x, y) f_{\nu}(y) \right) dy \quad (C.6)$$

$\mu = 1 \rightarrow s$

Transforming to  $z$  variable gives

$$\tilde{f}_{\mu}(z) = \eta \sum_{\nu=1}^s \left( \tilde{G}_{\mu\nu}(z, z') \tilde{f}_{\nu}(z') \frac{dy}{dz'} dz' \right) + \sum_{\nu=1}^s \left( \tilde{K}_{\mu\nu}(z, z') \tilde{f}_{\nu}(z') \frac{dy}{dz'} dz' \right)$$

and

$$\tilde{f}_{\mu}(z) = e^{-z/2} \sum_i c_{i\mu} L_i(z) \quad (C.7)$$

Hence, the equation to be solved for the coefficients is

$$C_{i\mu} = \sum_{j\nu} C_{j\nu} [\eta U_{i\mu}^{j\nu} + V_{i\mu}^{j\nu}]$$

where

$$U_{i\mu}^{j\nu} = \iint \tilde{G}_{\mu\nu}^{\sim}(z, z') e^{-z'/2} L_i(z) e^{-z/2} L_j(z') \frac{dy}{dz'} dz' dz$$

$$V_{i\mu}^{j\nu} = \iint \tilde{K}_{\mu\nu}^{\sim}(z, z') e^{-z'/2} L_i(z) e^{-z/2} L_j(z') \frac{dy}{dz'} dz' dz \quad (C.8)$$

The dimensions of the coefficient equation is  $(s \times n)$  by  $(s \times n)$  and not  $(S \times N)$  by  $(S \times N)$ .

Applying this coupled channel technique to equation 29.

$$\eta = g\sigma^2/4\pi$$

$\tilde{G}$  = transformed sigma kernel

$\tilde{K}$  = transformed pion kernel

$$z = \frac{1}{.64} \left[ \sinh^{-1} \left( \frac{q}{M_{\pi} + \sqrt{MB}} \right) \right]^2 \quad (C.9)$$

The mapped variable,  $Z$ , optimizes convergence of equations C.7 by transforming the singularities due to the branch points of the Legendre Polynomials of the Second Kind,  $Q_1$ , from the momentum plane to the  $Z$ -plane.

Note: Other exchange potentials, such as rho and omega, can easily be folded into  $\tilde{K}$ .

Hence, the equation to be solved for the coefficients is

where

(C.8)

The dimensions of the coefficient equation is  $(s \times n)$  by  $(s \times n)$  and not  $(S \times N)$  by  $(S \times N)$ .

Applying this coupled channel technique to equation 31.

$G =$  transformed sigma kernel

$K =$  transformed pion kernel

(C.9)

The mapped variable,  $Z$ , optimizes convergence of equations C.7 and C.8 by transforming the singularities due to the branch points of the Legendre Polynomials of the Second Kind,  $Q$ , from the momentum plane to the  $Z$ -plane.

Note: Other exchange potentials, such as rho and omega, can easily be folded into  $K$ .

## APPENDIX D

## Hydrogen-Like Atoms

We show in this appendix that the techniques used to formulate equation 21 for the deuteron can also be applied to hydrogen-like atoms.

Consider the interaction to be composed of a one photon exchange as illustrated in figure 33. Anomalous and multiple exchange contributions are ignored and the photon will be given a mass,  $M \neq 0$ , to facilitate analytic manipulation of the equations. Once the equations are in the form we desire, the limit will be taken as  $M \rightarrow 0$ .

We now display the analytic equation corresponding to figure 33.

$$\Gamma(\beta) = \frac{-ie^2}{(2\pi)^3} \int d^3k \gamma^\mu \left( \frac{W}{2} + K + M_p \right) \left( g_{\mu\nu} + \frac{P_\mu P_\nu}{M^2} \right) \gamma^\nu \left( \frac{W}{2} - K + m_e \right) \Gamma(k)$$

$$\frac{2E_k (E_k + E_k - W)(E_k - E_k + W)(M^2 - P^2)}$$

$\frac{e^2}{4\pi}$  = photon coupling constant

$m_p$  = proton's mass

$m_e$  = electron's mass

$M$  = photon's mass

$P = \beta - k$

$K_0 = E_k - \frac{W}{2}$

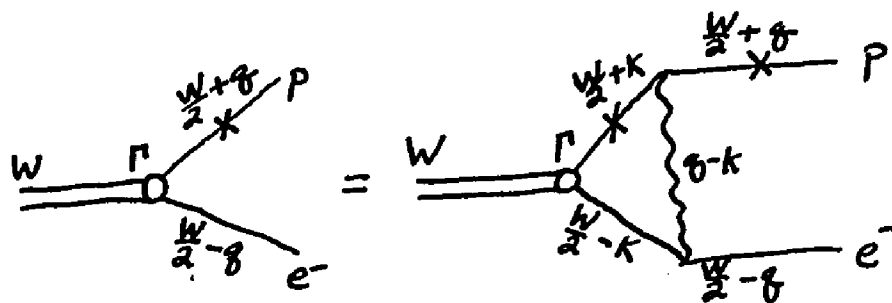


Figure 33

$$E_K = (m_e^2 + \vec{K}^2)^{1/2}$$

$$E_K = (m_p^2 + \vec{K}^2)^{1/2}$$

$$W = m_p + m_e + \epsilon$$

$$\epsilon = \text{binding energy}$$

(D.1)

$\Gamma$  is now the vertex function corresponding to an arbitrary energy level within the atom.

Using the relations

$$\frac{(\frac{W}{2} + K + m_p)}{2m_p} = \sum_{\text{spins}} u_p(\vec{K}) \bar{u}_p(\vec{K})$$

$$\frac{(\frac{W}{2} - K + m_e)}{2m_e} = \frac{1}{2E_K} (\epsilon_K + W - E_K) \sum_{\text{spin}} u_e(-\vec{K}) \bar{u}_e(-\vec{K})$$

$$- \frac{1}{2E_K} (\epsilon_K - W + E_K) \sum_{\text{spin}} v_e(\vec{K}) \bar{v}_e(\vec{K})$$

(D.2)

and defining wave functions  $\phi_+$  and  $\phi_-$  as

$$\phi_+(\vec{K}) = \frac{\bar{u}_p(\vec{K}) \bar{u}_e(-\vec{K}) \Gamma(K)}{E_K - W + E_K}$$

$$\phi_-(\vec{K}) = \frac{\bar{u}_p(\vec{K}) \bar{v}_e(\vec{K}) \Gamma(K)}{E_K + W - E_K}$$

(D.3)

equation D.1 can be written as a set of two coupled equations in  $\phi_+$  and  $\phi_-$ .

$$(\epsilon_{\delta} - W + E_{\delta}) \phi_{+}(\vec{\delta}) = \frac{2m_e e^2}{(2\pi)^3} \int d^3k \frac{[\bar{u}_{\delta}(-\vec{\delta}) \gamma^0 u_{\delta}(-\vec{k}) \phi_{+}(\vec{k}) - \bar{u}_{\delta}(-\vec{\delta}) \gamma^0 u_{\delta}(\vec{k}) \phi_{-}(\vec{k})]}{2\epsilon_k [\mu^2 + (\vec{\delta} - \vec{k})^2]}$$

$$(\epsilon_{\delta} + W - E_{\delta}) \phi_{-}(\vec{\delta}) = \frac{2m_e e^2}{(2\pi)^3} \int d^3k \frac{[\bar{u}_{\delta}(\vec{\delta}) \gamma^0 u_{\delta}(-\vec{k}) \phi_{+}(\vec{k}) - \bar{u}_{\delta}(\vec{\delta}) \gamma^0 u_{\delta}(\vec{k}) \phi_{-}(\vec{k})]}{2\epsilon_k [\mu^2 + (\vec{\delta} - \vec{k})^2]}$$

(D.4)

where we have taken the static limit of the proton and used

$$\bar{u}_{\delta}(\vec{\delta}) \not{P} u_{\delta}(\vec{k}) = 0$$

(D.5)

Next we evaluate the matrix elements of the spinors in D.4, keeping only terms of order  $q/m_e$  compared to the leading term. The result is

$$(\epsilon_{\delta} - W + E_{\delta}) \phi_{+}(\vec{\delta}) = \frac{2m_e e^2}{(2\pi)^3} \int d^3k \frac{[\phi_{+}(\vec{k}) + \frac{\vec{\sigma} \cdot \vec{p}}{2m_e} \phi_{-}(\vec{k})]}{2\epsilon_k (\mu^2 + \vec{p}^2)}$$

$$(\epsilon_{\delta} + W - E_{\delta}) \phi_{-}(\vec{\delta}) = \frac{2m_e e^2}{(2\pi)^3} \int d^3k \frac{[\frac{\vec{\sigma} \cdot \vec{p}}{2m_e} \phi_{+}(\vec{k}) - \phi_{-}(\vec{k})]}{2\epsilon_k (\mu^2 + \vec{p}^2)}$$

(D.6)

Then, transforming equations D.6 to configuration space, we obtain the coupled equations:

$$\left(-\frac{\nabla^2}{2m_e} - \epsilon\right) \phi_{+}(\vec{r}) = \frac{e^2}{4\pi} \frac{e^{-\mu r}}{r} \phi_{+}(r) + \frac{ie^2}{4\pi} \frac{\vec{\sigma} \cdot \nabla}{2m_e} \left(\frac{e^{-\mu r}}{r}\right) \phi_{-}(\vec{r})$$

$$2m_e \phi_{-}(\vec{r}) = \frac{ie^2}{4\pi} \frac{\vec{\sigma} \cdot \nabla}{2m_e} \left(\frac{e^{-\mu r}}{r}\right) \phi_{+}(\vec{r}) - \frac{e^2}{4\pi} \frac{e^{-\mu r}}{r} \phi_{-}(\vec{r})$$

(D.7)

It is clear from D.7 that  $\phi_-$  is smaller than  $\phi_+$  by one order of  $m_e^{-1}$ .

Finally, uncoupling equations D.7 and keeping terms to the lowest order of  $m_e^{-1}$ , we obtain

$$\left(-\frac{\nabla^2}{2m_e} - \epsilon\right) \phi_+(\vec{r}) = \frac{e^2}{4\pi} \frac{e^{-M r}}{r} \phi_+(\vec{r}) \quad (\text{D.8})$$

$\phi_+(\vec{r})$  is identified to be the Schrodinger wave function of an electron moving in a shielded Coulomb Potential. (The limit as  $M \rightarrow 0$  gives the standard unshielded Coulomb Potential.)

For positronium, equal mass case, we obtain

$$\left(-\frac{\nabla^2}{m} - \epsilon\right) \phi_+(\vec{\rho}) = \frac{e^2}{4\pi} \frac{2}{\rho} \phi_+(\vec{\rho})$$

$$\rho = |\vec{\rho}| = 2|\vec{r}|$$

(D.9)

Evaluating the matrix elements of the spinors to next order in  $q/m_e$ , equation D.4 gives

$$\frac{(\epsilon_0 - W + \epsilon_0)}{(\epsilon_0 + m_e)^{1/2}} \phi_+(\vec{\delta}) = \frac{e^2}{(4\pi)^3} \left( \frac{d^3 k (\epsilon_k + m_e)^{1/2}}{2\epsilon_k (M^2 + \vec{p}^2)} \left[ \phi_+(\vec{k}) + \frac{\vec{\sigma} \cdot \vec{\delta} \vec{\sigma} \cdot \vec{k}}{(\epsilon_k + m_e)(\epsilon_0 + m_e)} \phi_+(\vec{k}) - \frac{\vec{\sigma} \cdot \vec{k} \phi_-(\vec{k})}{(\epsilon_k + m_e)} + \frac{\vec{\sigma} \cdot \vec{\delta} \phi_-(\vec{k})}{\epsilon_0 + m_e} \right] \right)$$

$$\frac{(\epsilon_0 + W - \epsilon_0)}{(\epsilon_0 + m_e)^{1/2}} \phi_-(\vec{\delta}) = \frac{e^2}{(4\pi)^3} \left( \frac{d^3 k (\epsilon_k + m_e)^{1/2}}{2\epsilon_k (M^2 + \vec{p}^2)} \left[ \frac{\vec{\sigma} \cdot \vec{\delta} \phi_+(\vec{k})}{\epsilon_0 + m_e} - \frac{\vec{\sigma} \cdot \vec{k} \phi_+(\vec{k})}{\epsilon_k + m_e} - \phi_-(\vec{k}) - \frac{\vec{\sigma} \cdot \vec{\delta} \vec{\sigma} \cdot \vec{k} \phi_-(\vec{k})}{(\epsilon_k + m_e)(\epsilon_0 + m_e)} \right] \right)$$

(D.10)

Upon Fourier Transforming equations D.10, we obtain

$$\frac{2E_r(E_r - W + E_r)}{E_r + m_e} \mathbb{H}_+^{\pm}(\vec{r}) = \frac{e^2}{4\pi} \left[ \frac{e^{-\mu r}}{r} - \frac{\vec{\sigma} \cdot \vec{\nabla}}{4m_e^2} \left( \frac{e^{-\mu r}}{r} \right) \vec{\sigma} \cdot \vec{\nabla} - \frac{e^{-\mu r}}{r} \nabla^2 \right] \mathbb{H}_+^{\pm}(\vec{r}) \\ + \frac{ie^2}{4\pi(2m_e)} \vec{\sigma} \cdot \vec{\nabla} \left( \frac{e^{-\mu r}}{r} \right) \mathbb{H}_+^{\pm}(\vec{r})$$

$$\frac{2E_r(E_r + W - E_r)}{E_r + m_e} \mathbb{H}_-^{\pm}(\vec{r}) = \frac{ie^2}{4\pi(2m_e)} \vec{\sigma} \cdot \vec{\nabla} \left( \frac{e^{-\mu r}}{r} \right) \mathbb{H}_-^{\pm}(\vec{r}) \\ - \frac{e^2}{4\pi} \left[ \frac{e^{-\mu r}}{r} - \frac{\vec{\sigma} \cdot \vec{\nabla}}{4m_e^2} \left( \frac{e^{-\mu r}}{r} \right) \vec{\sigma} \cdot \vec{\nabla} - \frac{1}{4m_e^2} \frac{e^{-\mu r}}{r} \nabla^2 \right] \mathbb{H}_-^{\pm}(\vec{r})$$

(D.11)

Now, keeping all orders of  $m_e^{-1}$  up to and including orders of  $m_e^{-2}$ , we obtain the Pauli Equation.<sup>30</sup>

$$(H_0 + H^1) \mathbb{H}_\pm(\vec{r}) = \epsilon \mathbb{H}_\pm(\vec{r})$$

$$H_0 = -\frac{\nabla^2}{2m_e} + V$$

$$V = -\frac{e^2}{4\pi} \frac{e^{-\mu r}}{r} \quad \lim_{\mu \rightarrow 0} -\frac{e^2}{4\pi} \frac{1}{r}$$

$$H^1 = -\frac{(\epsilon - V)^2}{2m_e} - \frac{1}{4m_e^2} \frac{\partial V}{\partial r} \left( \frac{\partial}{\partial r} - \frac{2}{r} \vec{L} \cdot \vec{S} \right)$$

(D.12)

where  $\vec{L}$  and  $\vec{S}$  are the total angular momentum and total spin vectors respectively, and

$$\mathbb{H}_\pm(\vec{k}) = \frac{(\epsilon_k + m_e)^{1/2}}{2\epsilon_k} \phi_\pm(\vec{k})$$

(D.13)

Finally, considering all orders of  $q/m_e$ , equation D.4 gives,

in momentum space, the Dirac Theory of the electron:

$$(\not{\beta} - m_e + \delta^0 V(\vec{q})) \Psi(\vec{q}) = 0$$

$$\not{\beta} = E\gamma^0 - \vec{\gamma} \cdot \vec{q}$$

$$E = m_e + \epsilon$$

$$\Psi(\vec{q}) = \begin{pmatrix} \Psi_+(\vec{q}) \\ \Psi_-(\vec{q}) \end{pmatrix}$$

(D.14)

where  $\Psi_+$  and  $\Psi_-$  are the positive and negative energy wave functions expressed in terms of  $\phi_+$  and  $\phi_-$  as:

$$\Psi_+(\vec{k}) = \frac{(\epsilon_k + m_e)^{1/2}}{2\epsilon_k} \left[ \phi_+(\vec{k}) - \frac{\vec{\sigma} \cdot \vec{k}}{\epsilon_k + m_e} \phi_-(\vec{k}) \right]$$

$$\Psi_-(\vec{k}) = \frac{(\epsilon_k + m_e)^{1/2}}{2\epsilon_k} \left[ \frac{\vec{\sigma} \cdot \vec{k}}{\epsilon_k + m_e} \phi_+(\vec{k}) + \phi_-(\vec{k}) \right]$$

(D.15)

and  $V(q)$  is the momentum space Coulomb Potential and  $\vec{\sigma}$ , of course, are the Pauli Matrices.

The above derivations of the Schrodinger, Pauli and Dirac Equations from our relativistic prescription is not surprising since Gross<sup>10</sup> has shown that this relativistic prescription can be used to derive the Grotch-Yennie Equation.

## REFERENCES

1. F. Gross, Phys. Rev. D 10, 223 (1974).
2. R. Reid, Ann. Phys. (N.Y.) 50, 411 (1968).
3. J. Hornstein and F. Gross, Phys. Lett. 47B3, 205 (1973).
4. E. Delacroix and F. Gross, in preparation.
5. W. Buck, F. Gross and E. A. Remler, in preparation.
6. Throughout this manuscript, we use the notation of J. Bjorken and S. Drell, "Relativistic Quantum Mechanics."
7. R. Blankenbecler and L. F. Cook, Phys. Rev. 119, 1745 (1960).
8. J. Hornstein, Ph.D. thesis, unpublished.
9. E. E. Salpeter and H. A. Bethe, Phys. Rev. 84, 1232 (1951).
10. F. Gross, Phys. Rev. 186, 5 (1969) 1448-1462.
11. E. A. Remler, Nucl. Phys. B42, 56 (1972).
12. Models that omit the important two pion exchange potential invariably find it necessary to include a sigma exchange which is viewed in part as a pole approximation to this potential. Among the authors who use the sigma are: T. Ueda and A. E. S. Green, Phys. Rev. 174, 1304 (1968); G. Schierholz, Nucl. Phys. B7, 483 (1968); B40, 335 (1972); M. H. Partovi and E. L. Lomon, Phys. Rev. D2, 1999 (1970); K. Holinde, K. Erkelenz and R. Alzetta, Nucl. Phys. A. 194, 161 (1972); also private communication from F. Gross and N. Bewtra.

13. Y. A. Chao and A. D. Jackson, Nucl. Phys. A 215, 157 (1973).
14. W. Buck and F. Gross, submitted for publication.
15. D. D. Bradshaw, Proceedings of the International Conference on Few Body Problems in Nuclear and Particle Physics (Québec, Canada), 691 (1974).
16. J. P. Vary, Phys. Rev. C 7, 521 (1973).
17. W. Nutt and B. Loiseau, Nucl. Phys. B104 (1976) 98-110.
18. K. Holinde and R. Machleidt, preprint title "OBEP Plus  $\Delta$  - Resonance: Description of Two-Nucleon Data, Nuclear Matter and Neutron Matter."
19. A. K. Kerman and L. S. Kisslinger, Phys. Rev. 180 (1969) 1483.  
J. S. Sharma, V. S. Bhasin, and A. N. Mitra, Nucl. Phys. B35 (1971) 466.
20. J. V. Noble and H. J. Weber, Phys. Lett. 50B (1974) 233.
21. F. Gross, Proceedings of the International Conference on Few Body Problems in Nuclear and Particle Physics (Delhi, India) (1976).
22. See reference 11 as well as E. A. Remler, Nucl. Phys. B42 (1972) 69; E. A. Remler and R. A. Miller, Ann. Phys. 82 (1974) 189.
23. S. Moroiika and T. Ueda, Proceedings of the International Conference on Few Body Problems in Nuclear and Particle Physics (Delhi, India) (1976).

24. ● J. C. Alder et al., Phys. Rev. C, 6, 2010 (1972);  
▲ G. Igo et al., Nucl. Phys., 195 A, 33 (1972);  
✦ N. E. Booth et al., Phys. Rev. D, 4, 1261 (1971);  
■ G. W. Bennett et al., Phys. Rev. 19, 387 (1967);  
▲ E. Coleman et al., Phys. Rev., 164, 1655 (1967);  
○ L. Dubal et al., Phys. Rev., D9, 597 (1974).
25. For example, see reference 19.
26. This thesis is being prepared for publication.
27. N. Bewtra, Ph.D. thesis, Cornell University, unpublished.
28. M. Abramowitz and I. Segun, Handbook of Mathematical Functions  
(Dover Press), pp. 334, 335.
29. C. Carlson and F. Gross, private communication.
30. H. A. Bethe and E. E. Salpeter, Quantum Mechanics of One- and  
Two-Electron Atoms (Springer-Verlag, Berlin, 1957).
31. See reference 10 and H. Grotch and D. R. Yennie, Rev. of Mod.  
Phys. V41, 2 (1969) 350-374.